Experimental Investigation of Void Fraction During Horizontal Flow in Smaller Diameter Refrigeration Applications

D. A. Yashar, T. A. Newell, and J. C. Chato

ACRC TR-141 July 1998

For additional information:

Air Conditioning and Refrigeration Center
University of Illinois
Mechanical & Industrial Engineering Dept.
1206 West Green Street
Urbana, IL 61801

(217) 333-3115

Prepared as part of ACRC Project 74
Experimental Investigation of Void Fraction
During Refrigerant Condensation and Evaporation
T. A. Newell and J. C. Chato, Principal Investigators

The Air Conditioning and Refrigeration Center was founded in 1988 with a grant from the estate of Richard W. Kritzer, the founder of Peerless of America Inc. A State of Illinois Technology Challenge Grant helped build the laboratory facilities. The ACRC receives continuing support from the Richard W. Kritzer Endowment and the National Science Foundation. The following organizations have also become sponsors of the Center.

Amana Refrigeration, Inc.
Brazeway, Inc.
Carrier Corporation
Caterpillar, Inc.
Copeland Corporation
Dayton Thermal Products
Delphi Harrison Thermal Systems
Eaton Corporation
Ford Motor Company
Frigidaire Company
General Electric Company
Hill PHOENIX
Hydro Aluminum Adrian, Inc.
Indiana Tube Corporation
Lennox International, Inc.
Modine Manufacturing Co.
Peerless of America, Inc.
The Trane Company
Whirlpool Corporation
York International, Inc.

For additional information:

Air Conditioning & Refrigeration Center
Mechanical & Industrial Engineering Dept.
University of Illinois
1206 West Green Street
Urbana IL 61801

217 333 3115

Abstract

EXPERIMENTAL INVESTIGATION OF VOID FRACTION DURING HORIZONTAL FLOW IN SMALLER DIAMETER REFRIGERATION APPLICATIONS

David Anthony Yashar
Department of Mechanical and Industrial Engineering
University of Illinois at Urbana-Champaign, 1998
Ty Newell and John Chato, Advisors

Void fractions were determined for Refrigerants 134a and 410A evaporating inside three different tubes during horizontal flow. These tubes are as follows: a smooth 4.26 mm i.d. tube, a 7.25 mm axially grooved tube, and a 7.26 mm 18° helically grooved tube. Tests that encompass a range of mass fluxes of 75 - 700 $\frac{kg}{m^2 s}$, inlet qualities of 0.10 - 0.80, and heat fluxes of 0 - 10 $\frac{kW}{m^2}$ were performed at a temperature of 5° C. The experimental apparatus and procedures are described. The predictions of several existing correlations are compared to the data, and recommendations as to which correlations are best suited for particular applications are given. Also, adjustments to these correlations are recommended for special geometries, and for simplicity of use.

Table of Contents

List of Tables

List of Figures

Nomenclature

D_i	Tube inside diameter	
F_1	Premoli correlation variable	Equation 2.18
F_2	Premoli correlation variable	Equation 2.19
F_{td}	Modified Froude number of Taitel and Dukler	
Fr	Froude number	Equation 2.29
Ft	Froude Rate	Equation 2.22
$F(X_{tt})$	Function of Lockhart-Martinelli parameter	Equation 2.14
G	Mass flux	
g_c	gravitational constant	
i.d.	inner diameter	
K	Smith's Entrainment Ratio	
K_H	Hughmark correction factor	Table 2.3
$\dot{m}_l$	mass flow rate of liquid phase	
$\dot{m}_v$	mass flow rate of vapor phase	
P	Pressure	
Re_L	Liquid Reynolds number	$=\frac{GD_i}{\mu_l}$
Re_α	Reynolds number as defined by Hughmark	Equation 2.28
S	Slip ratio	Equation 2.2
V	Velocity	
V_l	Velocity of liquid phase	
V_v	Velocity of vapor phase	
W_{e_L}	Liquid Weber number	Equation 2.20
x	Quality	
x_s	Static Quality	

X_{tt}	Lockhart-Martinelli correlating parameter	Equation 2.9
y	Premoli Correlation Variable	Equation 2.17
y_L	Hughmark liquid volume fraction	Equation 2.30
Z	Hughmark correlation parameter	Equation 2.27
α	Void fraction	
β	Volumetric quality	$=\frac{1}{1+\left(\frac{1-x}{x}\right)\left(\frac{\rho_v}{\rho_l}\right)}$
μ_l	Liquid viscosity	
μ_v	Vapor viscosity	
ρ_l	Liquid density	
ρ_v	Vapor density	
σ	Surface tension	

Chapter 1
Introduction

Studies of void fraction are numerous in the technical literature. These studies include experimental efforts to measure the void fraction of certain fluids, analytical efforts to model two-phase fluid processes and a combination of the two. Most investigators have collected void fraction data for a bounded set of fluids under a range of operating conditions that were suitable for the application they were studying.

The work described herein represents an effort to evaluate these correlations based on experimental data for refrigeration applications. In Chapter 2, background information and existing literature is reviewed. This includes a detailed review of existing void fraction correlations. Chapter 3 presents the experimental facility that was used in this study. In chapter 4, the experimental methods used to collect and verify void fraction data are described. The experimental void fraction data from this investigation is presented, reviewed, and compared to the existing correlations in Chapter 5, for the 4.26 mm smooth tube, Chapter 6, for the 7.25 mm axially grooved tube, and Chapter 7, for the 7.26 mm 18° helically grooved tube. Chapter 8 presents the conclusions and recommendations of this investigation.

Chapter 2
Literature Review

The study of two phase fluid mechanics has been of interest for quite some time. One of the most important parameters in two phase flow is void fraction. Knowledge of void fraction is of great importance because it influences heat transfer and pressure drop, and also allows a system's mass inventory to be calculated. Many researchers have studied void fraction and derived correlations to predict void fraction. Rice [1987] gives a description of many of these models, and has classified them into the following four categories: homogeneous, slip-ratio, Lockhart-Martinelli, and mass flux dependent. This literature review gives an overview of 11 of these correlations and some of the assumptions and their intended usage.

2.1 Homogeneous

The homogeneous model is the simplest model. This model assumes that liquid and vapor are a homogeneous mixture traveling at the same velocity. The relationship between void fraction, a, mass quality, x, liquid density, ρ_l, and vapor density, ρ_v, is shown below.

$$\alpha = \frac{1}{1+\left(\frac{1-x}{x}\right)\left(\frac{\rho v}{\rho l}\right)} = \frac{1}{1+\left(\frac{1-x}{x}\right)P.I.1} \qquad (2.1)$$

The term $P.I._1$ is termed property index 1.

2.2 Slip-Ratio

The basis for the slip-ratio correlations is the assumption that the liquid and vapor phases are separated into streams that are traveling with different velocities, V_v and V_l, the vapor and liquid velocities. The ratio of these velocities is termed the slip-ratio.

$$S = \frac{Vv}{Vl} \qquad (2.2)$$

The void fraction equation is then

$$\alpha = \frac{1}{1+\left(\frac{1-x}{x}\right)\left(\frac{\rho v}{\rho l}\right)\bullet S} \tag{2.3}$$

2.2.1 Zivi Correlation

Zivi [1964] derived his void fraction correlation by applying the principle of minimum entropy production to two phase flow. Zivi formulated the rate of energy dissipation in terms of the void fraction, from which he determined the void fraction that minimized the dissipation. To do this, Zivi assumed that the flow pattern was purely annular with no liquid entrained in the vapor core and that energy dissipation due to wall friction was negligible. Using these assumptions, he derived his slip ratio to be

$$S = \left(\frac{\rho v}{\rho l}\right)^{-1/3} \tag{2.4}$$

and his correlation for void fraction is then

$$\alpha = \frac{1}{1+\left(\frac{1-x}{x}\right)\left(\frac{\rho v}{\rho l}\right)^{2/3}} \tag{2.5}$$

Zivi compared his correlation to data taken by Martinelli and Nelson [1948], Larson [1957], and Maurer [1960] in addition to his own data. He found that his correlation formed a lower bound for the data and that the homogeneous model formed an upper bound. He also noted that as the pressure increased, the limit for his curve is the homogeneous curve. Zivi realized that liquid entrainment was an important factor in determining void fraction, and stated that the amount of liquid entrainment was the determining factor in interpolating between the two curves.

2.2.2 Rigot Correlation

The Rigot correlation is the simplest slip-ratio based correlation, in which he suggests using a constant slip-ratio value of S=2 for his intended application.

2.2.3 Ahrens Correlation

Ahrens [1983] used the steam/water data of Thom [1963] which was suitably generalized by the property index 2.

$$P.I.2 = \left(\frac{\mu l}{\mu v}\right)^{0.2}\left(\frac{\rho v}{\rho l}\right) = \left(\frac{\mu l}{\mu v}\right)^{0.2} \bullet P.I.1 \qquad (2.6)$$

Ahrens defined his slip-ratio in terms of the property index 2. Table 2.1 shows the relation between the independent variable $P.I._2$ and the slip-ratio S.

$P.I._2$	S
0.00116	6.45
0.0154	2.48
0.0375	1.92
0.0878	1.57
0.187	1.35
0.466	1.15
1.0	1

Table 2.1 Ahrens slip-ratio vs. property index 2

2.2.4 Smith Correlation

Smith [1969] assumed a homogeneous mixture core and a purely liquid annulus for his model. He also assumed that the homogeneous mixture in the center behaves as a single fluid with variable density and that thermal equilibrium exists. His model was based on equal velocity heads of the center and the annulus. His relation defines the slip-ratio in terms of the density ratio, the mass quality, and a parameter termed the entrainment ratio. This entrainment ratio, K, is the mass of water flowing in homogeneous mixture divided by the total mass of water flowing. The expression for Smith's slip-ratio is given below.

$$S = K + (1-K)\left\{\frac{\left(\frac{\rho l}{\rho v}\right) + K\left[\frac{1-x}{x}\right]}{1 + K\left[\frac{1-x}{x}\right]}\right\}^{1/2} \qquad (2.7)$$

Smith compared his correlation to the data taken by Rouhani and Becker [1963]; Haywood, Knights, Middleton and Thom [1961]; and Anderson and Mantzouranis [1960] at different values of K. Through these comparisons, he determined that a value of K=0.4 was suitable. It should be noted that the three data sets were taken by different methods, which added confidence to this value in that it did not include a systematic error common to a particular method.

2.2.5 Levy Correlation

Levy[1960] developed his correlation out of equations governing the slip effects in the forced circulation of water. His correlation was derived from a momentum exchange model which assumes equal friction and head losses of the two phases. Levy's correlation is given below.

$$x = \frac{\alpha(1-2\alpha) + \alpha\sqrt{(1-2\alpha)^2 + \alpha\left[2\left(\frac{\rho l}{\rho v}\right)(1-\alpha)^2 + \alpha(1-2\alpha)\right]}}{\left[2\left(\frac{\rho l}{\rho v}\right)(1-\alpha)^2 + \alpha(1-2\alpha)\right]} \qquad (2.8)$$

Levy correlation was shown to have fairly good agreement for steam at high pressures and high qualities. Other conditions showed great deviation from experimental data.

2.3 Lockhart-Martinelli

Early work by Lockhart and Martinelli [1949] presented two-phase, two-component flow in terms of a new parameter, the Lockhart-Martinelli parameter, shown below.

$$Xtt = \left(\frac{1-x}{x}\right)^{0.9}\left(\frac{\rho v}{\rho l}\right)^{0.5}\left(\frac{\mu l}{\mu v}\right)^{0.1} \qquad (2.9)$$

There are two assumptions in which the Lockhart-Martinelli analysis was based. The first assumption is that the static pressure for both phases must be equal regardless of flow pattern, which is a valid assumption in the absence of a radial pressure gradient. The other assumption infers that the flow pattern does not change along the length of the tube, which eliminates the possibility of "slug flow".

2.3.1 Wallis and Domanski Correlations

Wallis [1969] correlated the data af Lockhart and Martinelli as a function of the Lockhart-Martinelli parameter. This correlation is shown below.

$$\alpha = \left(1 + X_{tt}^{0.8}\right)^{-0.378} \tag{2.10}$$

Wallis stated that the Lockhart-Martinelli parameter balances frictional shear stress versus pressure drop. Therefore, he realized that as the frictional component of pressure drop decreases in proportion to the other terms, this would lead to increasing error.

Domanski and Didion [1983] refined the Wallis correlation by adding a condition that it would only hold for X_{tt} less than or equal to 10. For $10 < X_{tt} < 189$, the following correlation should hold.

$$\alpha = 0.823 - 0.157 \ln(X_{tt}) \tag{2.11}$$

For the conditions examined in the study and the companion studies of Wilson [1998], Graham [1998], and Kopke [1998], X_{tt} was always less than 10.

2.3.2 Baroczy Correlation

Baroczy [1965] developed a correlation which involves the Lockhart-Martinelli parameter and the property index 2. Baroczy used liquid-mercury/nitrogen and air/water data to determine liquid fraction (1-α) as a function of the Lockhart-Martinelli parameter and the property index 2. His correlation is presented in the form of a table shown in Table 2.2.

	X_{tt}										
P.I.2	0.01	0.04	0.1	0.2	0.5	1	3	5	10	30	100
	Liquid Fraction (1-α)										
0.00002				0.0012	0.009	0.068	0.17	0.22	0.30	0.47	0.71
0.0001			0.0015	0.0054	0.030	0.104	0.23	0.29	0.38	0.57	0.79
0.0004		0.0022	0.0072	0.180	0.066	0.142	0.28	0.35	0.45	0.67	0.85
0.001	0.0018	0.0066	0.0170	0.0345	0.091	0.170	0.32	0.40	0.50	0.72	0.88
0.004	0.0043	0.0165	0.0370	0.0650	0.134	0.222	0.39	0.48	0.58	0.80	0.92
0.01	0.0050	0.0210	0.0475	0.0840	0.165	0.262	0.44	0.53	0.63	0.84	0.94
0.04	0.0056	0.0250	0.0590	0.1050	0.215	0.330	0.53	0.63	0.72	0.90	0.96
0.1	0.0058	0.0268	0.0640	0.1170	0.242	0.380	0.60	0.70	0.78	0.92	0.98
1	0.0060	0.0280	0.0720	0.1400	0.320	.500	0.75	0.85	0.90	0.94	0.99

Table 2.2 Baroczy Correlation

2.4 Mass Flux Dependent

This last set of correlations predict void fraction as a function of mass flux in addition to the other properties of the two phase flow.

2.4.1 Tandon Correlation

Tandon [1985] developed his model in the same manner as Zivi [1964], but his analysis was much more involved. Like Zivi, he assumed the flow to be an axisymmetric, with a liquid annulus and vapor core with no liquid entrainment. He also assumed that the flow is steady, one dimensional, turbulent in the core and annulus, and that there is no significant radial pressure gradient. The correlation of Tandon predicts void fraction as a function of the liquid Reynolds number and the Lockhart-Martinelli parameter. This correlation is shown below

$$\alpha = 1 - 1.928\frac{Re_L^{-0.315}}{F(X_{tt})} + 0.9293\frac{Re_L^{-0.63}}{F(X_{tt})^2} \quad \text{for } 50<Re_L<1125 \quad (2.12)$$

$$\alpha = 1 - 0.38\frac{Re_L^{-0.088}}{F(X_{tt})} + 0.0361\frac{Re_L^{-0.176}}{F(X_{tt})^2} \quad \text{for } Re_L>1125 \quad (2.13)$$

where

$$F(X_{tt}) = 0.015\left(\frac{1}{X_{tt}} + \frac{2.85}{X_{tt}^{0.476}}\right) \tag{2.14}$$

and

$$Re_L = \frac{GD_i}{\mu_l} \tag{2.15}$$

Tandon compared his model to those of Zivi, Wallis and Smith. He found that his model was more accurate than those of Zivi and Wallis, but stated that Smith's correlation was just as accurate.

2.4.2 Premoli Correlation

Premoli [1971] developed a mass flux dependent correlation that takes the form of the slip-ratio correlations described in section 2.2. His correlation was developed for upward flow in a vertical channel under adiabatic conditions. He developed his correlation by comparing slip-ratio and governing parameters and then optimized the correlation with the objective on minimizing density calculation errors. Premoli's equation takes the following form:

$$S = 1 + F_1\left(\frac{y}{1 + F_{2y}} - F_{2y}\right)^{1/2} \tag{2.16}$$

where

$$y = \frac{\beta}{1-\beta} \tag{2.17}$$

$$F_1 = 1.578 \bullet Re_L^{-0.19}\left(\frac{\rho_l}{\rho_v}\right)^{0.22} \tag{2.18}$$

$$F_2 = 0.0273 \bullet We_L Re_L^{-0.51}\left(\frac{\rho_l}{\rho_v}\right)^{-0.08} \tag{2.19}$$

and

$$WeL = \frac{G^2 Di}{\sigma \rho l g c} \tag{2.20}$$

$$\beta = \frac{1}{1 + \left(\frac{1-x}{x}\right)\left(\frac{\rho v}{\rho l}\right)} \tag{2.21}$$

and the liquid Reynolds number is as shown in equation 2.15.

2.4.3 Graham Correlation

Graham [1998] examined the refrigerants R134a and R410A condensing in a horizontal smooth tube. His correlation is based on the work of Hurlburt and Newell [1997] who found that a transition between stratified and annular flow can be indicated by a Froude rate parameter. Similar to the Froude number which is a ratio of kinetic to gravitational potential energy, the Froude rate parameter is defined as a ratio of the vapor's power due to its kinetic energy to the power required to pump liquid from the bottom of the tube to the top of the tube.

$$Ft = \left(\frac{mv Vv^2}{ml g D}\right)^{1/2} \tag{2.22}$$

On a two phase basis the Froude rate parameter becomes

$$Ft = \left(\frac{x^3 G^2}{\rho v^2 g D(1-x)}\right)^{1/2} \tag{2.23}$$

Graham correlated his data and that of Sacks [1975] to within 10% with the following relationship

$$\alpha = 1 - \exp\left(-1 - 0.3\ln(Ft) - 0.0328(\ln(Ft))^2\right) \quad \text{for } Ft>0.01032 \tag{2.24}$$

$$\alpha = 0 \quad \text{for } Ft<0.01032 \tag{2.25}$$

2.4.4 Hughmark Correlation

Hughmark [1962] developed a correlation for void fraction which he based on the work of Bankoff [1960]. The model proposed by Bankoff was one in which the mixture flows as a suspension of bubbles in the liquid and that the bubble concentration was greatest at the center of the pipe, decreasing monotonically in the radial direction vanishing at the pipe wall. Bankoff also assumed that the liquid and vapor velocity at any radial position were equal, with the average velocity of the vapor being greater because it is concentrated in regions of higher velocity. The Hughmark correlation is shown below.

$$\alpha = \frac{KH}{1+\left(\frac{1-x}{x}\right)\left(\frac{\rho v}{\rho l}\right)} \tag{2.26}$$

where K_H is a function of the parameter Z as shown in Table 2.3:

Z	K_H
1.3	0.185
1.5	0.225
2.0	0.325
3.0	0.49
4.0	0.605
5.0	0.675
6.0	0.72
8.0	0.767
10	0.78
15	0.808
20	0.83
40	0.88
70	0.93
130	0.98

Table 2.3 Z vs. K_H for Hughmark correlation

and Z is found through the following relations:

$$Z = \frac{Re\alpha^{1/6} Fr^{1/8}}{yl^{1/4}} \tag{2.27}$$

$$Re\alpha = \frac{DiG}{\mu l + \alpha(\mu v - \mu l)} \tag{2.28}$$

$$Fr = \frac{1}{gcDi}\left(\frac{Gx}{\beta \rho v}\right)^2 \tag{2.29}$$

$$yl = \frac{1}{1+\left(\frac{x}{1-x}\right)\left(\frac{\rho l}{\rho v}\right)} = 1 - \beta \tag{2.30}$$

Unfortunately, Hughmark's correlation must be solved in an iterative manner in which a value for the void fraction must be initially guessed to solve for the liquid Reynolds number, the Froude number, and y_l; from which the void fraction can be evaluated. These steps must be repeated until convergence on the value of the void fraction is met.

Chapter 3
Experimental Facility

The facility used to perform this investigation will be described in this chapter. The facility is located in the Mechanical Engineering Laboratory at the University of Illinois at Urbana-Champaign. Wattelet [1989] designed and built the evaporator loop to study two-phase refrigerant-side evaporative flow regimes, heat transfer and pressure drop. The facility has been extensively documented in Wattelet [1990], Panek [1991], Christoffersen [1993], and De Guzman [1997]. A brief summary of the main features as well as modifications made to the facility will be outlined.

3.1 Experimental Test Facility

The experimental test facility is a system composed of four major components. These components are a refrigerant loop, a chiller loop, a horizontal tube test section, and a data acquisition system. This section a brief description of these components will be provided.

3.1.1 Refrigerant Loop

The purpose of the refrigerant loop is to deliver the working fluid to the test section at the desired conditions. The conditions controlled during the experiment were saturation temperature, mass flow rate, and inlet quality. A diagram of the test section is provided as Figure 3.1.

A MicroPump™ three-gear, variable speed, magnetic coupled pump in used to draw fluid from the condenser and provide the necessary flow through the refrigerant loop. The flow rate is controlled via the use of the pump's variable speed controller as well as a refrigerant bypass line. The bypass line is a section of pipe controlled by a needle valve that circumvents the pump. The bypass line is used to divert refrigerant from the high pressure side of the pump to the low pressure side without passing through the loop. Greater accuracy could be obtained in mass flow rate by fine tuning the bypass line needle valve after the pump is set to a speed which is near the desired speed. The main motivation for using this system is that a magnetic coupled gear pump would allow for the testing of pure refrigerants, whereas a compressor would require the working fluid be mixed with oil.

After the gear pump, the fluid passes through a MicroMotion™ mass flow meter. This flow meter provides real time measurements while maintaining an accuracy of +/- 0.1%. After the fluid passes through the mass flow meter, it continues to the preheater section where the desired inlet quality to the test section is controlled. The preheater is a

three pass, horizontal, serpentine copper annulus with a 7/8" outside diameter and a 3/8" inside diameter. The annular configuration was used to reduce the charge needed in the refrigerant loop. Wrapped around the outer tube of the preheater are a series of Kapton™ strip heaters manufactured by Minco to provide heat input into the preheater. These heaters were controlled by four on/off switches and a 115 Volt Variac. Controlling the switches and the variac output allowed the proper amount of heat to be transfered to the refrigerant to obtain a desired quality.

Once the refrigerant passed through the preheater, it continued on to the test section or the test section bypass line and then to the condenser which will be discussed in a later section.

3.1.2 Chiller System

In order to condense the two phase refrigerant exiting the test section, it must undergo heat rejection. This was accomplished by way of a chiller system that consists of an antifreeze loop and an R502 loop. Figure 3.2 provides a diagram of the chiller system. The R502 loop consists of a compressor, a heat exchanger to condense the R502 cooled with waste water, two expansion valves in parallel (one for high capacity requirements and one for lower capacity requirements), and a heat exchanger to chill the antifreeze loop. Immediately after the antifreeze exits the heat exchanger with the R502 loop, it collects in a storage tank that is monitored by a thermocouple. A set point temperature for the storage tank is controlled through a chiller control panel. The chiller system would run until the set point was obtained in the storage tank, after which it would cycle on and off to keep the tank to within +/- 2.0°F of the set point.

The antifreeze loop consists of 5 components: pumps, a heat exchanger connected to the refrigerant loop, a false load heater, another heat exchanger connected to the R502 loop, and a storage tank. The working fluid in the antifreeze loop is a 50/50 mixture of ethylene glycol (antifreeze) and water. First, the antifreeze goes through the heat exchanger with the R502 loop to reject heat. The antifreeze then collects in a storage tank whose purpose was described earlier. Next, it passes through the pumps to circulate the flow through the loop. The antifreeze is then passed through a counterflow, helical heat exchanger that is connected to the refrigerant loop. This heat exchanger acts as a condenser for the refrigerant loop. Finally, the antifreeze passes through the false load heater. The purpose of the false load heater is to add extra heat into the antifreeze loop. Since the chiller system cycles on and off when the set point temperature is met, maintaining steady state conditions would be impossible. With the false load heater, an artificially low set point temperature can be established and the false load heater can be used to add the extra heat needed to prevent the system from reaching the set point.

3.1.3 Test Section

Three different test sections were used in this investigation: A 4.26 mm i.d. smooth tube, a 7.25 mm base diameter axially grooved tube, and a 7.25 mm base diameter 18° helically grooved tube. These tube geometries were chosen to represent common geometries that are currently used in evaporators. A companion study by Wilson [1998] examined a 6.2 mm i.d. smooth tube, a 8.89 mm base diameter axially grooved tube, and a 8.93 mm base diameter 18° helically grooved tube.

The smooth tube is an ordinary copper tube with an inner diameter of 4.26 mm and an outer diameter of 6.35 mm. The grooved tubes are more of interest. A diagram of these tubes are shown in Figure 3.3. Both the axially grooved and helically grooved tubes have 50 fins carved around the perimeter of the tube. The fins on the axially grooved tube are parallel to the centerline of the tube, while those on the helically grooved tube are rifled down the tube at an angle of 18° from the centerline of the tube. Dimensions for the fins and tubes are shown in Figure 3.3.

The test section is made from a segment of any of the above tubes. A representation of the test section is shown in Figure 3.4. Two pressure taps are separated by 48" along the tube. Just ahead of the downstream pressure tap is a void fraction tap. Four stations of thermocouples are laid out along the length of the tube; station 1 at 6" from the upstream pressure tap, station 2 at 18", station 3 at 30", and station 4 at 42". The entire length of the tube between pressure taps is wrapped in Minco™ heater strips to provide heat input into the test section. Just outside of each pressure tap is a Hoke™ 7100 series ball valve. These two ball valves are connected with a four bar linkage configuration so that each valve is in the same position as the other valve at all times (both open or both closed).

The pressure taps and the void fraction tap are brass pieces that were designed specially for these experiments. The void fraction tap is shown in Figure 3.5. It was manufactured from 1/2" stock brass rod, and its dimensions are provided in the diagram. The tube is inserted into this piece where it is soldered into place. Then a 1/16" hole is drilled into the tube through the existing hole in the piece. The 1/2" length of brass is left on this piece to allow a size 6 ferrule connection to be made here. A Hoke™ 7100 series valve is then connected to this junction. The 7/32" diameter section is left on this piece to minimize the amount of space in the connection by extending all the way up to the ball in the ball valve. At the opposite end of the ball valve is the valve insert shown in figure 3.6. Similar to the void fraction tap, the valve insert also extends inside the ball valve all the way to the ball to minimize the amount of volume. The valve insert allows a Refrigerant Research 1917 Receiver tank to be attached to it via a size 6 ferrule compression fitting.

The pressure taps are shown in Figure 3.7 with their dimensions. They are very similar to the void fraction tap, yet a little simpler. Once again, the tube is inserted through the large hole and soldered into place. Then a 1/16" hole is drilled into the tube. The 1/8" diameter piece on these taps allows for a size 4 ferrule connection. The pressure tap has a Hoke valve to isolate the test section from the pressure transducer when void fraction measurements are made.

The thermocouples that are attached to the tubes are shown in Figures 3.8 and Figure 3.9. The smooth tubes have a thicker wall than the grooved tubes and therefore may have the thermocouples attached in the following manner. A groove is carved along the wall of the tube, parallel to its axis using a Dremel™ cutoff wheel. The thermocouple wires are then placed into this groove and the thermocouple bead is soldered into the corner of the groove. Since the axially and helically grooved tubes have a much thinner wall, it was not feasible to attempt to carve a groove on the outside of the tube. Instead a copper coupling with four slots cut through it was placed around the tube and soldered into place. Here the thermocouple wires were placed into the slot on the coupling and the bead was soldered into the corner of the coupling. On all of the test sections and at all four thermocouple stations, the thermocouples were placed at 90° from each other reading the outer wall temperature at the top, bottom, left, and right sides of the tubes.

3.2 Data Acquisition System

The data acquisition system was used to control and monitor the apparatus during operation and to record all relevant measurements when test conditions have been set. The data acquisition system consists of the following components: a Macintosh II computer, four Strawberry Tree™ data acquisition boards, six Strawberry Tree™ terminal panels, and a data acquisition program called Analog Connection Workbench™.

The interfaces between the thermocouple outputs and the Strawberry Tree™ data acquisition boards were four T-21 terminal panels with aluminum, isothermal plates. Other sensors, such as pressure, power, and flow rate transducers, provided signals to the data acquisition boards through T-51 terminal panels. Finally, the false load output signal was relayed to the main logic controller by a T-51 terminal panel.

Terminal panels were linked to the data acquisition boards via a 50 pin ribbon connector. The data acquisition boards consisted of two 8 channel boards with analog output capability, model numbers ACM2-16-8A and ACM2-12-8A. In the model numbers, 16 and 12 denote bit precision. In addition, there were two 16 channel data acquisition boards: ACM2-16-16. In total, the system had the capability of accepting 48 analog inputs and providing 4 analog outputs. Typically, data was sampled as 1 Hz for the data acquisition configuration that was chosen.

Along with the hardware, Strawberry Tree™ provided software to run the data acquisition system. This icon driven program displayed and recorded signals from the data acquisition hardware. In the program, computation was done using calculation blocks which stored the necessary calibration curves. In terms of control, the false load heater was manually controlled through the continual adjustment of one of the calculation blocks. Once flow conditions satisfied test requirements, the data was logged to disk in a tab-delimited file.

3.3 Instrumentation

This section will describe the various measurement devices used in the experimental apparatus. These devices include flow meters, power transducers, thermocouples, and pressure transducers.

3.3.1 Mass Flow Measurements

A Coriolis-type mass flow meter manufactured by Micro-Motion™ was used to measure the mass flow rate of the working fluid circulating through the refrigerant loop. This flow meter, model D-12, featured two small orifices located at the inlet and outlet which help dampen oscillations in the flow.

3.3.2 Power Measurements

Three Ohio Semitronics™ Watt transducers were used in the experimental facility. The first transducer, model PC5-49D292, measured the heat input at the test section. The next transducer, model PC5-50-D292, measured the power controlled by the four preheater switches. The last transducer, model PC5-010D, monitored the power input provided by the Variac controller. All three devices were tested at the factory at an uncertainty of 0.2% of the full scale reading.

3.3.3 Pressure Measurements

Four pressure transducers were installed on the refrigerant loop to monitor system performance and provide a secondary check on the saturation temperature. An absolute BEC strain-gage type pressure transducer took measurements at the inlet to the preheater. The output of this preheater pressure transducer, range of 0-300 psia (0-2100 kPa), was used to determine the amount of subcooling in the liquid. Another pressure transducer, same as the preheater transducer, was used to measure the pressure at the inlet to the test section. For two phase flow, this inlet pressure measurement determined the amount of subcooling available at the test section entrance. The last absolute pressure transducer, manufactured by Sentra™ with a range of 0-1000 psia (0-6900 kPa), measured the

pressure at the inlet of the gear pump. These pressure measurements are used to determine the amount of subcooling at the pump entrance. If there is insufficient subcooling, the pump does not operate at maximum efficiency. Finally, in order to determine the pressure drop across the test section, a Sensotec™ differential pressure transducer with a range of 0-5 psi (0-35 kPa) was used. All four devices were calibrated using a dead weight tester with an uncertainty of 0.3% of the full scale reading.

3.3.4 Temperature Measurements

Temperature measurements were utilized to determine surface and bulk fluid temperatures. For the surface temperatures, the thermocouple beads were attached to the test section as described in section 3.1. To determine bulk fluid temperatures, thermocouples protected by a stainless steel sheath were extended into the refrigerant flow. These probes were held in place with ferrule compression fittings and were located at the following locations: the inlet of the pump, before the preheater, the entrance of the test section, and at the exit of the test section. At the inlet to the pump and preheater, the temperature measurement was used to determine the amount of subcooling and the refrigerant's enthalpy. At the test section entrance and exit, the temperature measurements were compared to the pressure measurements as a check on saturation temperature.

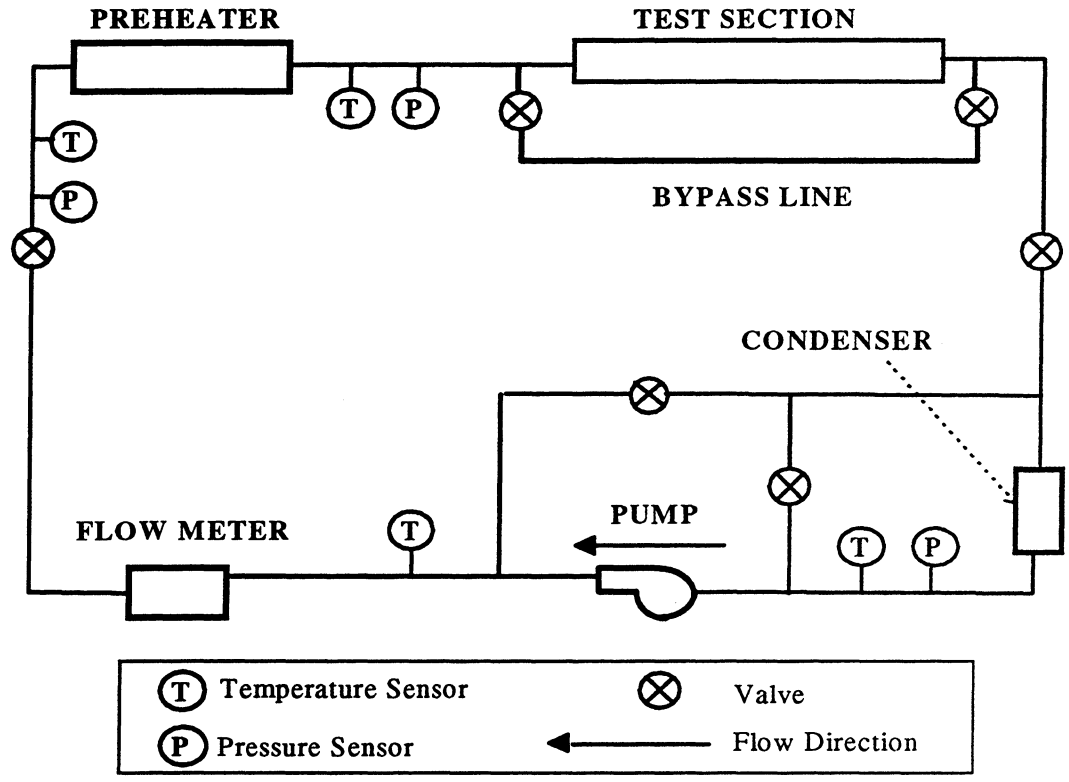

Figure 3.1 Schematic of refrigerant loop

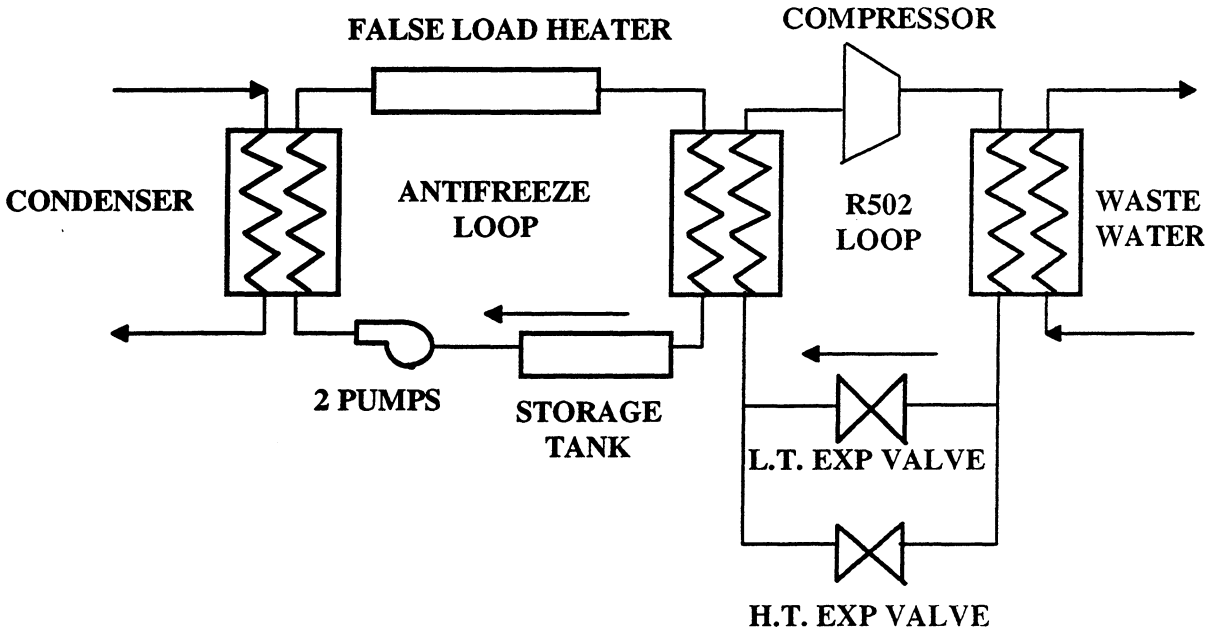

Figure 3.2 Chiller system

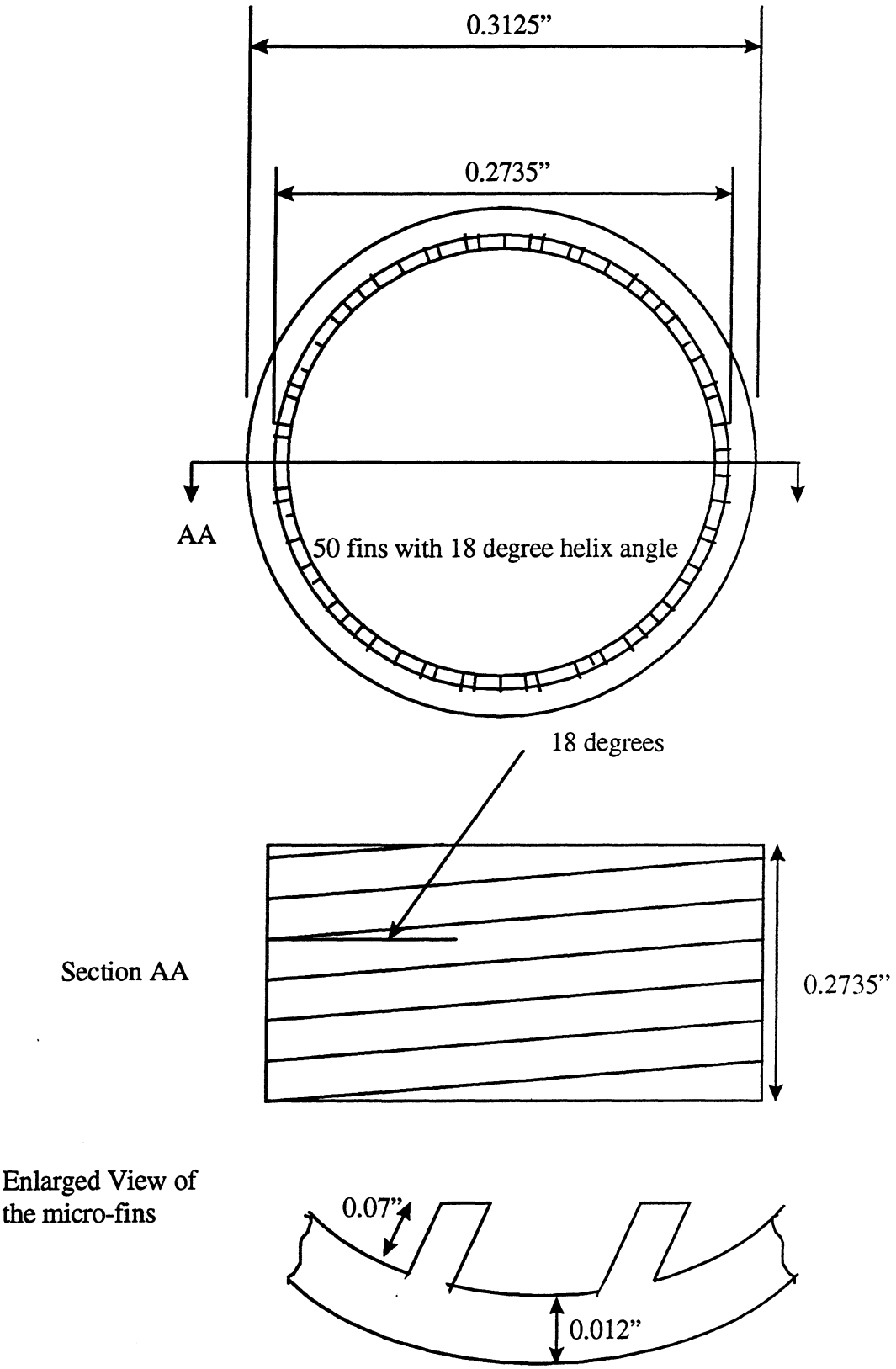

Figure 3.3 Micro-fin tube dimensions and features for 8.93 mm inner diameter micro-finned test section

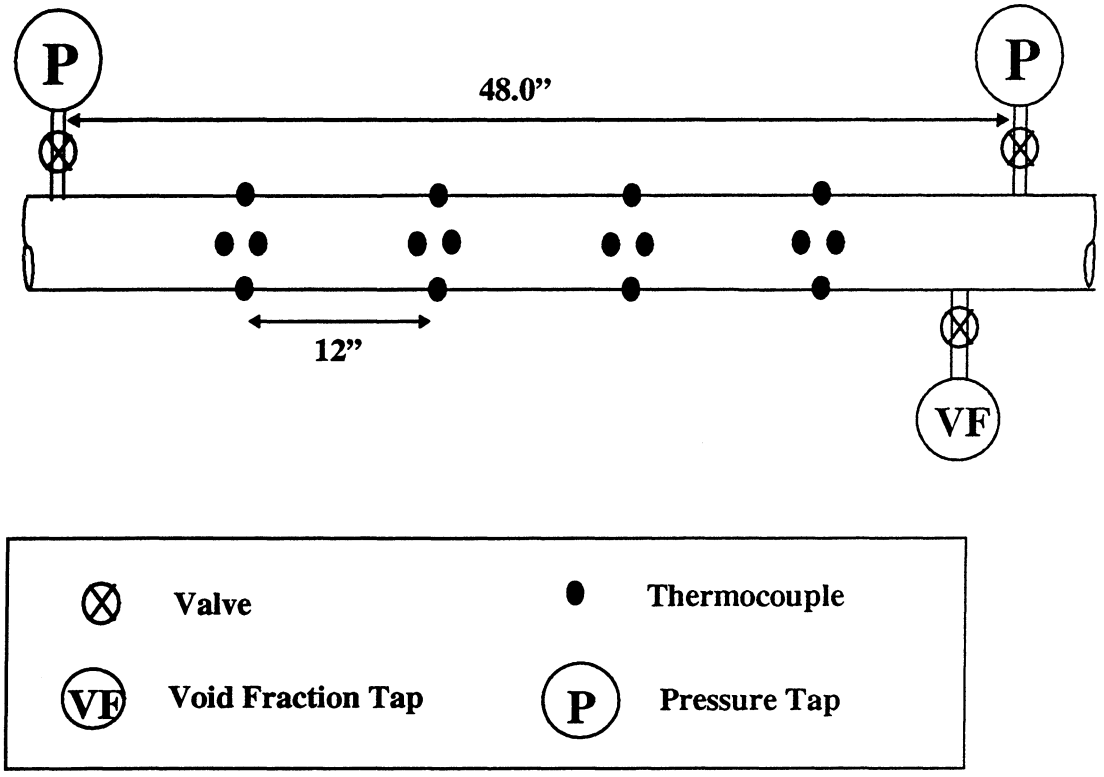

Figure 3.4 Test section dimensions and features

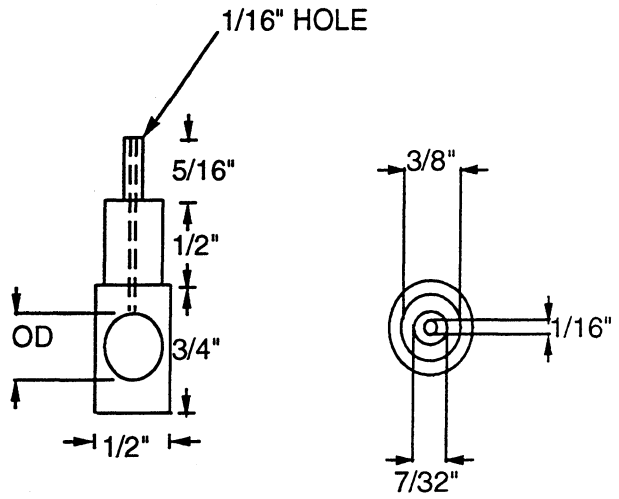

Figure 3.5 Void fraction tap where OD is the outside diameter of the test section the tap will fit on to.

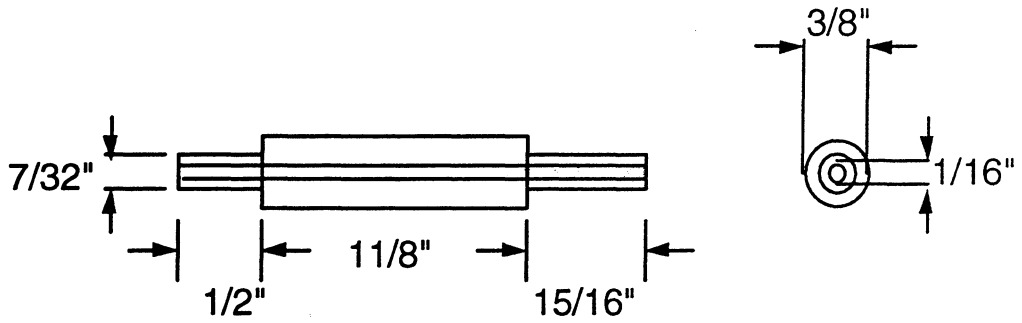

Figure 3.6 Valve Insert

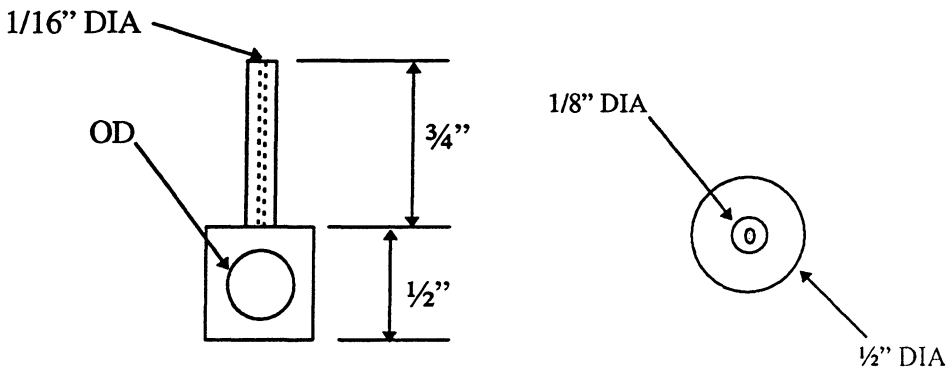

Figure 3.7 Pressure tap where OD is the outside diameter of the test section the tap will fit on to

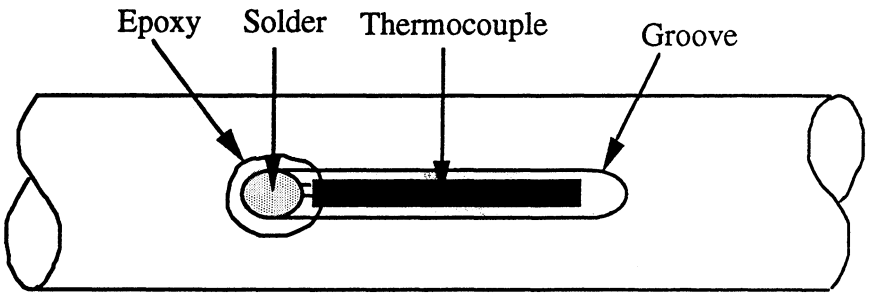

Figure 3.8 Thermocouple placement in thick walled tubes

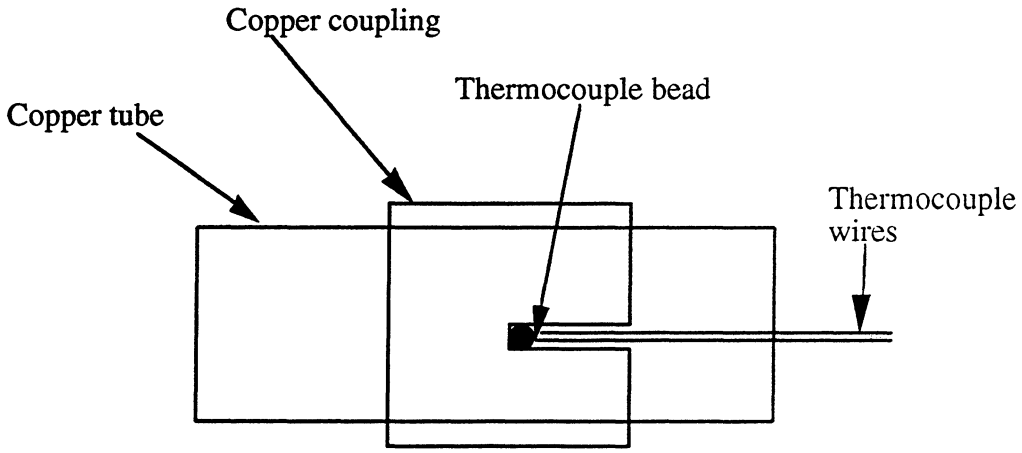

Figure 3.9 Thermocouple placement in thin walled tubes

Chapter 4
Experimental Procedure

The operational procedure for the evaporator loop have been extensively discussed in Wattelet [1990], Panek [1991], Christoffersen [1993], and De Guzman [1997]; therefore only the operational procedure for the void fraction measurements will be outlined here. The operation of the experimental facility is explained in two parts. First, there are a few tests needed for the preparation of the test section prior to the experimental data acquisition. These tests are performed only once after each test section is installed onto the apparatus. Next, the steps taken to measure the void fraction will be outlined. Second, the void fraction measurement procedure is discussed.

4.1 System Preparation

The system preparation comprises three steps. First, the test section must be installed and checked for leaks. The volume of the test section is then determined.

The installation of the test section is rather straightforward. The test section is connected at both ends to the ball valves which isolate the section from the rest of the system. Pressure sensor lines are connected to pressure taps. A ball valve is used to isolate the pressure tap lines and sensors from the test section. Finally, the ball valve and void fraction insert are connected to the void fraction tap.

After the test section is connected to the apparatus and is leak proof, the volume of the test section is determined. First, the pressure taps are closed and the test section is closed off from the rest of the apparatus. The pressure taps are closed due to the fact that the pressure tap lines have a volume that is comparable to that of the test section and would induce a large error to the calculations. Next, the test section is evacuated with a vacuum pump. A refrigerant receiver tank, approximately 1 liter, is filled with a mass of a known gas. The receiver tank is then connected to the test section via the void fraction tap. The valve between them is opened and vapor is allowed to flow from the tank to the test section. After approximately 1 minute, the pressure is assumed to be equal in the test section and the tank. The pressure is read from the receiver tank pressure guage and the temperature in the test section is found from averaging the 16 thermocouples along the test section. The valve is then closed and the refrigerant receiver is weighed again to determine the amount of mass that has left the tank for the test section. By knowing the gas, the mass of vapor inside the test section, and the pressure inside the test section, the volume is determined. These tests are performed with two refrigerants, R22 and R134a, as well as nitrogen. Since the density of nitrogen is much less than that of these refrigerants, extra

precision scale is needed to weigh the tank. Each of the gases is used 3 to 4 times at different pressures, giving 9 to 12 measurements for the volume. The measurements are then averaged to yield the value of the volume that was used in the calculations. An example of the test section volume measurements are provided in table 4.1

4.2 Void Fraction Measurements

The operation of the apparatus to achieve desired mass flux, inlet quality, and saturation temperature have been extensively outlined in Wattelet [1990], Panek [1991], Christoffersen [1993], and De Guzman [1997], therefore these procedures will not be discussed here. Only the procedures performed to measure the void fraction will be discussed in this section.

Once the desired conditions are met (mass flux, inlet quality, saturation temperature, and test section heat flux) and the operational data has been logged, the void fraction may be measured in the following manner. First, the pressure taps are closed to isolate the pressure tap lines from the test section. Then, the valves at the inlet and outlet of the test section are simultaneously closed using the linkage that connects them. This traps the refrigerant in the test section, taking a snapshot of the amount of refrigerant in the test section at a given set of operating conditions. Once the test section is closed off from the rest of the loop, the bypass line is immediately opened to allow the refrigerant to continue to circulate through the loop. Also, if this particular test involves heat addition into the test section, two people must be present to trap the refrigerant, one person to perform the aforementioned duties and one person to shut off the test section heaters. Because the refrigerant is stagnant in the test section, the test section can get very hot if the heaters are not shut off fast enough.

An evacuated refrigerant receiver tank is weighed, packed in a bucket of ice, and connected to the void fraction tap. The valves between the test section and the receiver tank are then opened to allow the refrigerant to migrate from the test section to the receiver tank. The test section heaters are then turned on to vaporize and superheat all of the refrigerant in the test section to approximately 30°C. When this is achieved, the test section temperature is then found from averaging the test section thermocouple readings, and the pressure in the test section is assumed to be the same as that of the receiver tank and is also recorded. The valve to the test section is then closed. Before closing the valve on the receiver tank, the void fraction insert piece is heated with a heat gun to minimize the amount of refrigerant that is lost in this piece. Then the valve on the tank is closed and the tank is removed from the test section. The tank is then heated and dried off to eliminate condensate on the outside of the tank. It is then weighed.

The total amount of refrigerant that was trapped in the test section is then determined by summing the refrigerant left in the test section and the refrigerant in the receiver tank. The refrigerant in the receiver tank is determined by taking the difference in the mass of the tank before and after the refrigerant is extracted. This mass makes up the bulk of the mass that was in the test section. The amount of refrigerant left in the test section is determined from the temperature and pressure in the test section just before it is closed off from the receiver tank, in conjunction with the test section volume. The mass left in the test section generally is on the order of 0.5% of the total mass in the section during operation.

Now that the amount of refrigerant in the test section is known, it is used to calculate a "static quality" in the following manner. The static quality is to be distinguished from the quality of refrigerant flowing in the loop. The local quality at a point inside a refrigeration system component refers to the ratio of vapor mass flow rate to total refrigerant mass flow rate. When the section is valved off, the static quality refers to the mass of vapor in the section to the total mass of refrigerant in the section. The difference between these qualities is a measure of average velocity difference between the vapor and liquid phases. The specific volume of the refrigerant in the test section is determined by dividing the volume of the test section by the total mass of the refrigerant. The temperature of the refrigerant is known from the tests (5°C for these tests). Engineering Equation Solver is then used to determine X_{st}, the static quality, from the specific volume, the temperature, and the refrigerant. Once the static quality is known, the void fraction is determined from the following relationship:

$$X_{st} = [((1-\alpha)/\alpha)(v_v/v_l) + 1]^{-1}$$

where α=void fraction
v_v=vapor phase specific volume
v_l=liquid phase specific volume

This equation is inverted using Engineering Equation Solver to determine the void fraction for each test. Each void fraction test was taken at least two times to ensure repeatability and accuracy. If the two tests did not show very good agreement, a third test was taken.

Gas	Δm (g)	V_{ts} (m^3)
R134a	1.2	5.15E-3
R134a	0.71	4.77E-3
R134a	0.92	5.02E-3
R22	1.5	5.48E-3
R22	1.3	5.35E-3

Table 4.1 Sample Calculations of Test Section Volume

Chapter 5
Smooth Tube Results

This chapter discusses the results of the 4.26 mm i.d. smooth tube. The results will be examined for both R134a and R410A, the effect of heat addition into the tube, the effect of varying the quality of the fluid in the test section, and the mass flux of the fluid passing through the test section. The data will then be compared to the predictions of 10 different correlations.

5.1 Void Fraction Results

This section examines the effects of refrigerant, heat addition, mass flux, and diameter on void fraction using the mass quality as the basis of comparison.

5.1.1 Effect of Refrigerant on Void Fraction

All tests were performed with two refrigerants, R134a and R410A. Figure 5.1 shows void fraction vs. quality for both R134a and R410A. It is easily seen from this graph that R410A consistently has a lower void fraction than R134a at any given quality. This was expected because R410A has a vapor density approximately twice that of R134a, while their liquid densities are relatively similar. Being that the vapor density to liquid density ratio of R410A is much greater than that of R134a, at a given mass quality, the denser vapor of R410A should take up a much smaller volume than R134a.

5.1.2 Effect of Heat Flux on Void Fraction

Figure 5.2 shows void fraction vs. quality for R134a at three different heat fluxes: $0\ \frac{kW}{m^2}$, $3\ \frac{kW}{m^2}$ and $10\ \frac{kW}{m^2}$. It should be noted that the heat flux was used to calculate the average quality of the refrigerant in the test section. The refrigerant R134a was chosen for this plot to demonstrate the effect of heat flux. This plot shows that heat flux has no effect on void fraction. Similar effects are observed with R410A.

5.1.3 Effect of Mass Flux on Void Fraction

The effect of mass flux on void fraction was determined experimentally by running tests at three different mass fluxes: 200 $\frac{kg}{m^2s}$, 500 $\frac{kg}{m^2s}$, and 700 $\frac{kg}{m^2s}$. Figure 5.3 shows void fraction vs. quality for R410A at three different mass fluxes. It is apparent from this plot that for these particular tests that void fraction is independent of mass flux.

5.1.4 Effect of Tube Diameter on Void Fraction

The effects of tube diameter on void fraction was determined by comparing data with that of Wilson [1998]. Wilson performed identical tests on the same apparatus using a test section that had a diameter of 6.12 mm. Figure 5.4 shows void fraction vs. quality for the refrigerant R410A, for both the 4.26 mm tube and the 6.12 mm tube. No major separation of data by diameter is seen on this on this plot indicating that void fraction does not depend on diameter for this particular case.

5.2 Comparison of Data with Correlations

This section compares all of the data taken in this experiment for the 4.26 mm smooth tube with the 10 of the existing correlations. The results are presented in by the same classifications as in Chapter 2: homogeneous, slip-ratio, Lockhart-Martinelli, and mass flux dependent. All of the plots shown in this section have different markers for the two refrigerants. Since the mass flux showed very little influence on the void fraction, it will not be discussed here, with the exception of the mass flux dependent correlations; rather plots with different markers for the three mass fluxes are shown in the appendix.

5.2.1 Homogeneous Correlation

The homogeneous correlation, as presented by Rice [1987], consistently over predicted the void fraction for this data, having an average error of approximately 10% and a maximum error of nearly 18%. Figure 5.5 shows a comparison of the data taken in this experiment with the homogeneous correlation. This plot shows different markers for the two refrigerants. It is noted that there is no noticeable separation of the data sets by refrigerant, which is important for later discussion.

5.2.2 Slip-Ratio Correlations

There are four slip-ratio correlations that are examined in this section. These are the Zivi [1963] correlation, the Rigot [1973] correlation, the Smith [1969] correlation and the Ahrens [1983] correlation.

The first slip-ratio correlation is the Zivi correlation. The comparison of the data for the 4.26 mm smooth tube versus the Zivi correlation is shown in Figure 5.6. The Zivi correlation was fairly accurate for data that had a void fraction greater than approximately 87%. However, it consistently under predicted data that had a void fraction less than 87%. Zivi noted that his correlation should form a lower bound for all data, with the upper bound being the homogeneous correlation, and this proved to be the case. It is noted that as the void fraction gets lower, the error associated with the Zivi correlation gets larger, with the error at the lowest void fraction is as high as 40%. It is also noted that at lower void fractions, the data in this plot is segregated by refrigerant unlike the homogeneous correlation, suggesting that the Zivi slip-ratio of $\left(\frac{\rho l}{\rho v}\right)^{1/3}$ is credited with the associated error.

The second slip-ratio correlation is the Rigot correlation. This correlation uses a constant slip-ratio of 2. Figure 5.7 shows the comparison of the data with the predictions of the Rigot correlation. The Rigot correlation over predicts at higher void fractions and under predicts at lower void fractions. The Rigot correlation had a fairly low average error associated with its predictions of 5%, but the maximum error seen here is slightly greater than 20%.

The third slip-ratio correlation is the Ahrens correlation. The comparison of the data with the Ahrens correlation is shown in Figure 5.8. Similar to the Rigot correlation, the Ahrens correlation over predicts at high void fractions and under predicts at low void fractions. The average error for the Ahrens correlation is less than 5%; but accuracy is lost as the void fraction gets lower and the lower void fractions yield errors of 17%. Ahrens, like Zivi, uses the liquid to vapor density ratio as a main parameter for the determination of the slip-ratio. This plot also shows noticeable segregation by refrigerant at lower void fractions.

The last slip-ratio correlation is the Smith correlation. Figure 5.9 shows the comparison of the data with the Smith correlation. The Smith correlation yielded the best accuracy for the slip-ratio based correlations. The average error for the Smith correlation was less than 4%, with a maximum error less than 15%. The Smith correlation shows

very good agreement for void fraction above 85%, after which it begins to under predict the void fraction. The Smith slip-ratio is mildly dependent on the liquid to vapor density ratio, and it is noted that there is mild separation of the data by refrigerants at low void fraction.

5.2.3 Lockhart-Martinelli Correlations

There are two Lockhart-Martinelli correlations examined in this section. These are the Wallis [1969] correlation and the Baroczy [1965] correlation. After the discussion of these two correlations, a comparison of this data to the Lockhart-Martinelli parameter will be shown.

The first Lockhart-Martinelli correlation is the Wallis correlation. The comparison of this data to the Wallis correlation is shown in Figure 5.10. Overall, the Wallis correlation shows the best agreement with the experimental data having an average error of less than 3% and a maximum error of 10%. All of the data with a void fraction of 84% (corresponding to a L-M parameter of 0.5) or higher had very good agreement with this correlation. For data below 80% (L-M parameter of 0.7), the Wallis correlation over predicts void fraction for R410A and under predicts void fraction for R134a. The trends observed from this plot are such that the R410A data lie approximately 5% below the Wallis prediction, and the R134a data lie approximately 5% above the Wallis prediction.

The other Lockhart-Martinelli correlation is the Baroczy correlation. Figure 5.11 shows this data compared to the Baroczy correlation. The Baroczy correlation consistently under predicted the data resulting in an average error of nearly 8% and a maximum error of nearly 23%. Also, segregation of the data by refrigerant is noticed here.

It is useful to examine the plot of void fraction versus the Lockhart-Martinelli parameter shown in Figure 5.12. It is observed that the experimental data collapses very well for $X_{tt} < 0.5$, but for $X_{tt} > 0.7$ the data is separated by refrigerants. From this it inferred that although the Lockhart-Martinelli parameter may be a good correlating parameter for lower values of X_{tt} in this tube, it is not very accurate for higher values of X_{tt}.

5.2.4 Mass Flux Dependent Correlations

Three mass flux dependent correlations are examined in this section. These are the Tandon [1985] correlation, the Premoli [1971] correlation, and the Hughmark [1962] correlation.

The first of the mass flux dependent correlations is the Tandon correlation. The Tandon correlation is a weak function of mass flux. Figure 5.13 shows the comparison of

the data to the Tandon correlation. The Tandon correlation consistently under predicts the void fraction for all cases. The Tandon correlation yields an average error of 5.5% and a maximum error of nearly 23%. This plot shows that there is segregation by refrigerant. Since the Tandon correlation is mass flux dependent, it is helpful to examine a plot of the data for one refrigerant with different markers for the different mass fluxes. Figure 5.14 shows the data for R134a compared to the Tandon correlation, delimited by mass flux. From this plot, it seems as if a systematic error segregated by mass flux is present for lower void fractions.

The Premoli and Hughmark correlations yield similar results as the Tandon correlation. Plots of the Premoli and Hughmark correlations compared to the data are shown in Figure 5.15 and Figure 5.16 respectively. The Premoli correlation under predicted the void fraction by an average of 5.6%; while the Hughmark was a little less accurate, under predicting the void fraction by an average of 7.6%. The effects of mass flux in these correlations are similar to that of Tandon and are shown in Figure 5.17 and Figure 5.18.

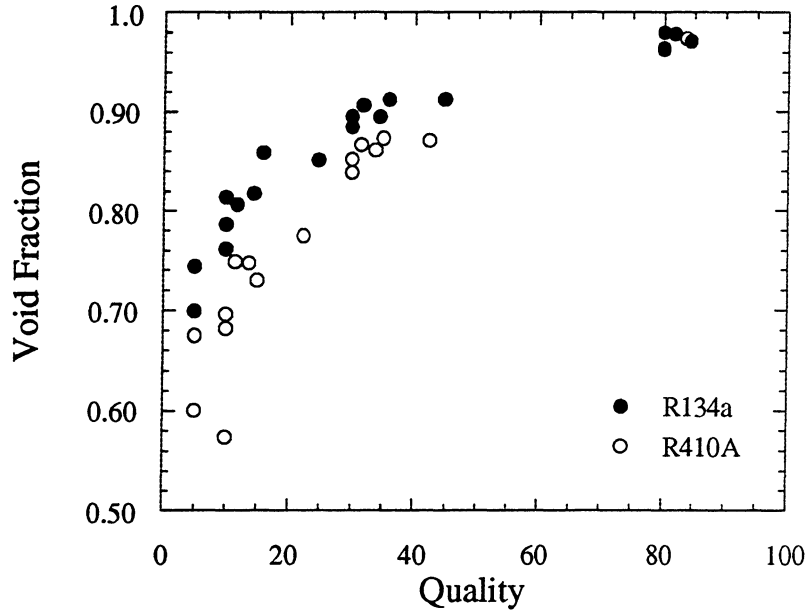

Figure 5.1 Void Fraction vs. Average Quality for R134a and R410A

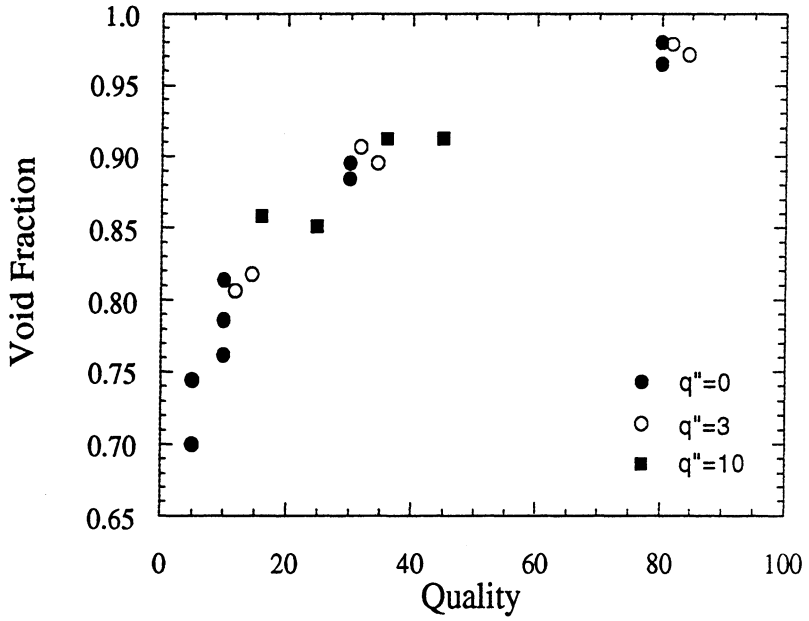

Figure 5.2 Void Fraction vs. Average Quality for R134a to show heat flux effect (heat flux in $\frac{kW}{m^2}$)

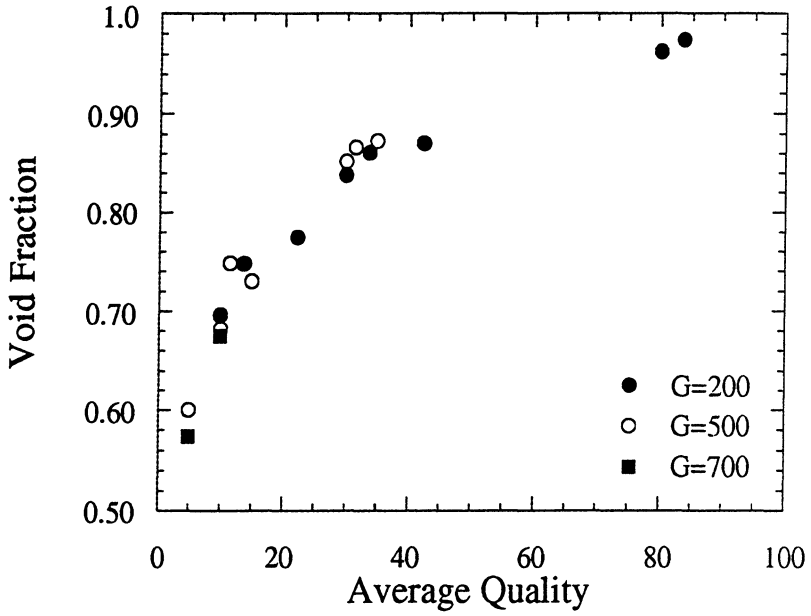

Figure 5.3 Void Fraction vs. Average Quality for R410A to show mass flux effect

(mass flux in $\frac{kg}{m^2 s}$)

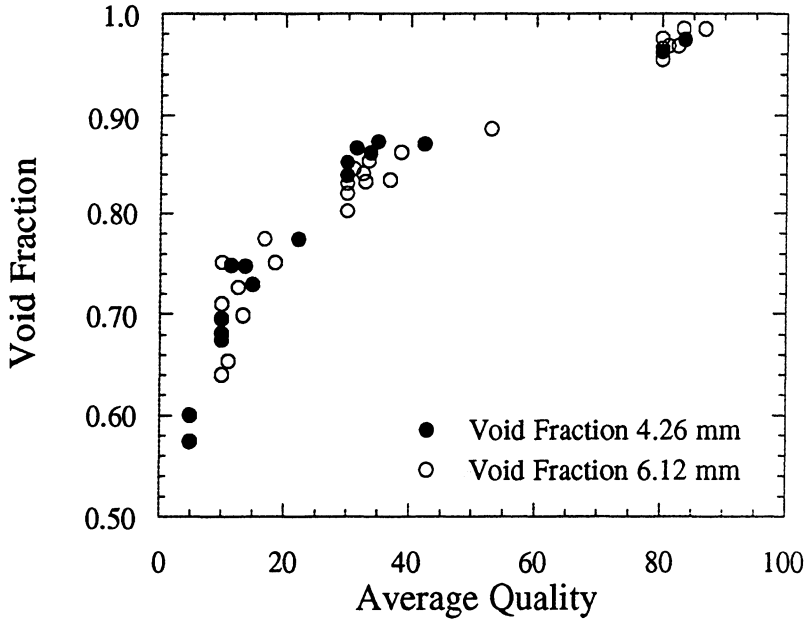

Figure 5.4 Void Fraction vs. Average Quality for R410A to show diameter effect

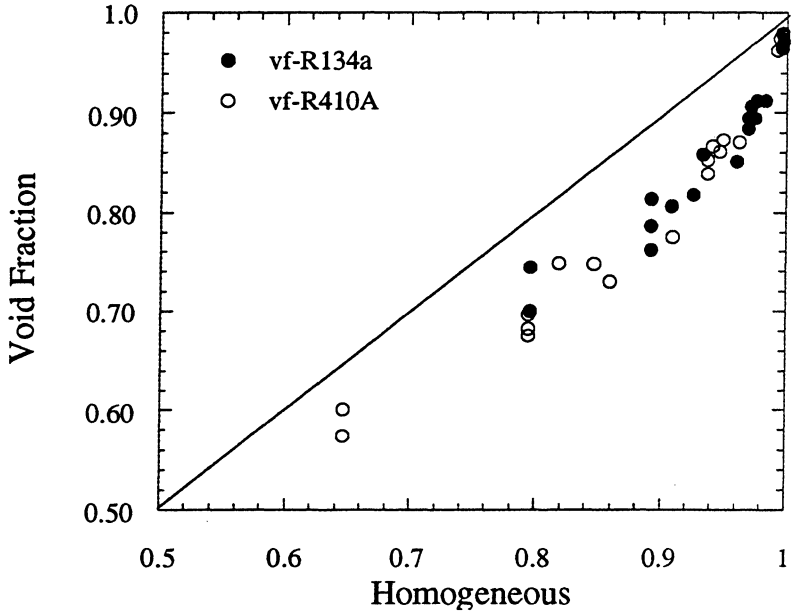

Figure 5.5 Void Fraction vs. Homogeneous correlation

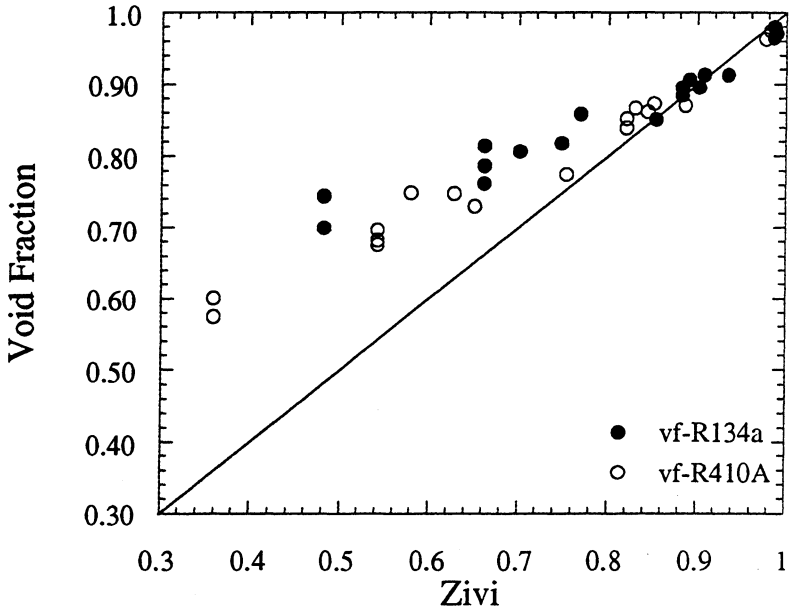

Figure 5.6 Void Fraction vs. Zivi correlation

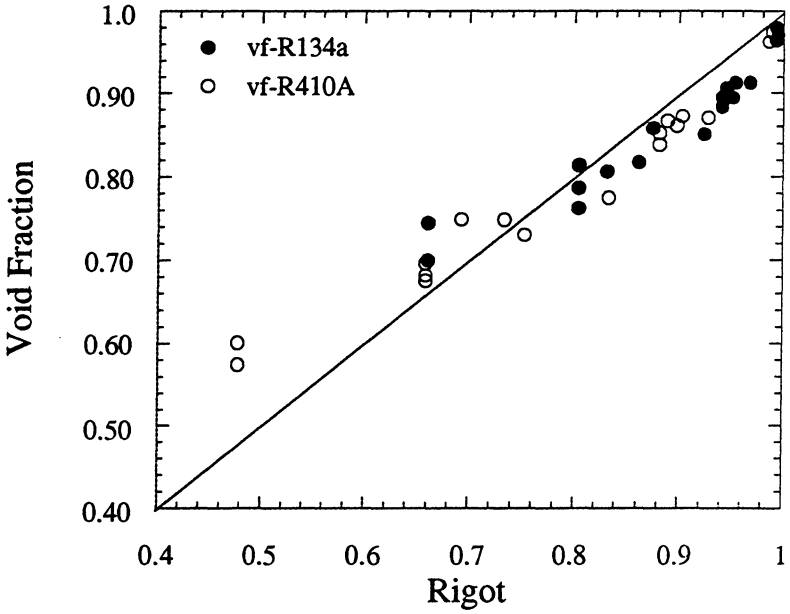

Figure 5.7 Void Fraction vs. Rigot correlation

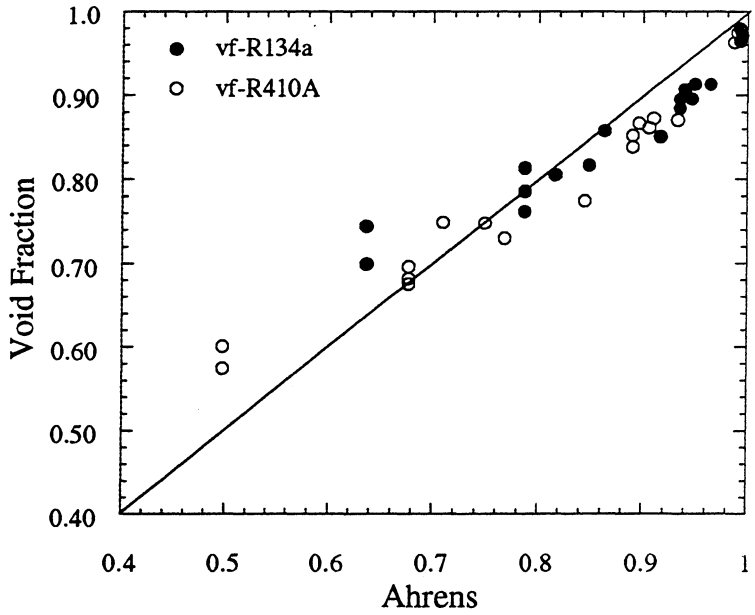

Figure 5.8 Void Fraction vs. Ahrens correlation

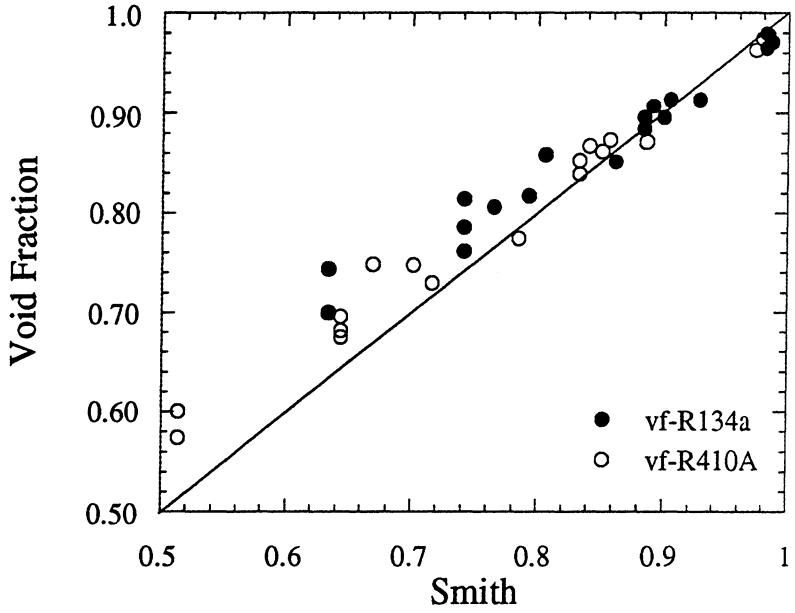

Figure 5.9 Void Fraction vs. Smith correlation

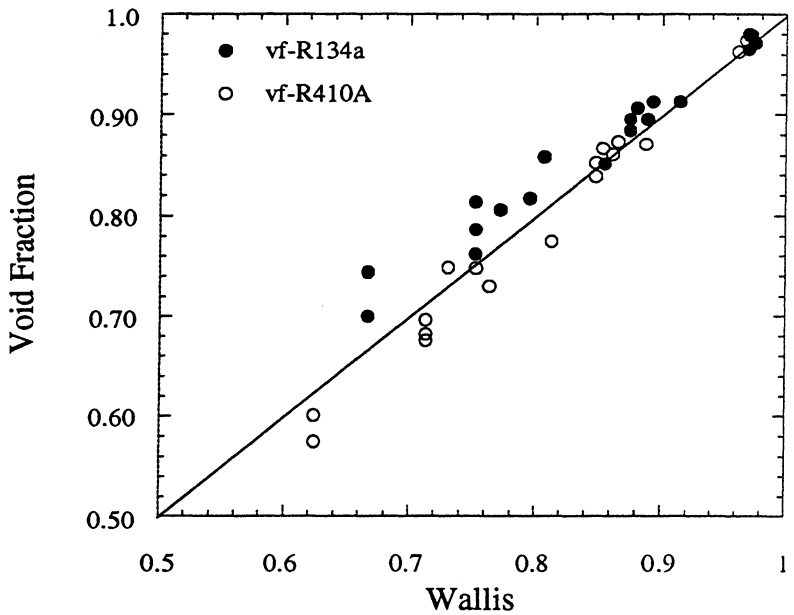

Figure 5.10 Void Fraction vs. Wallis correlation

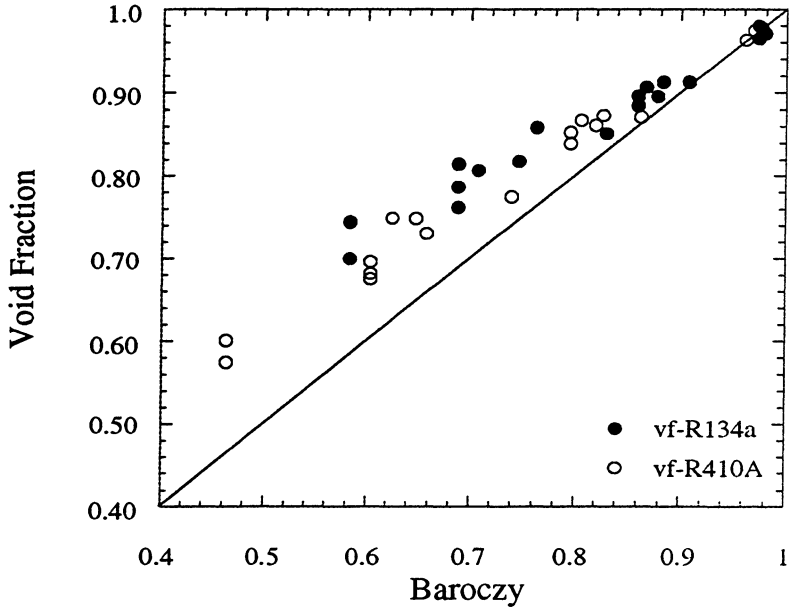

Figure 5.11 Void Fraction vs. Baroczy correlation

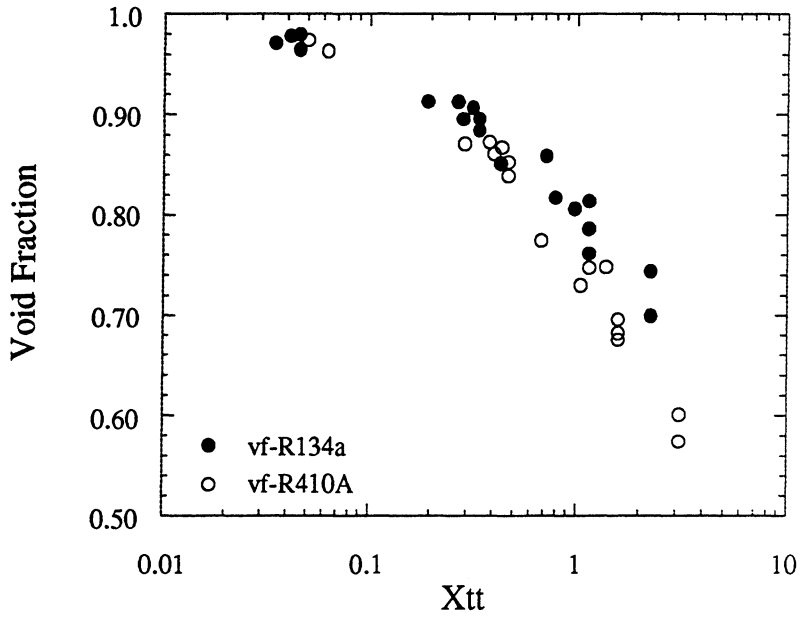

Figure 5.12 Void Fraction vs. the Lockhart-Martinelli Parameter

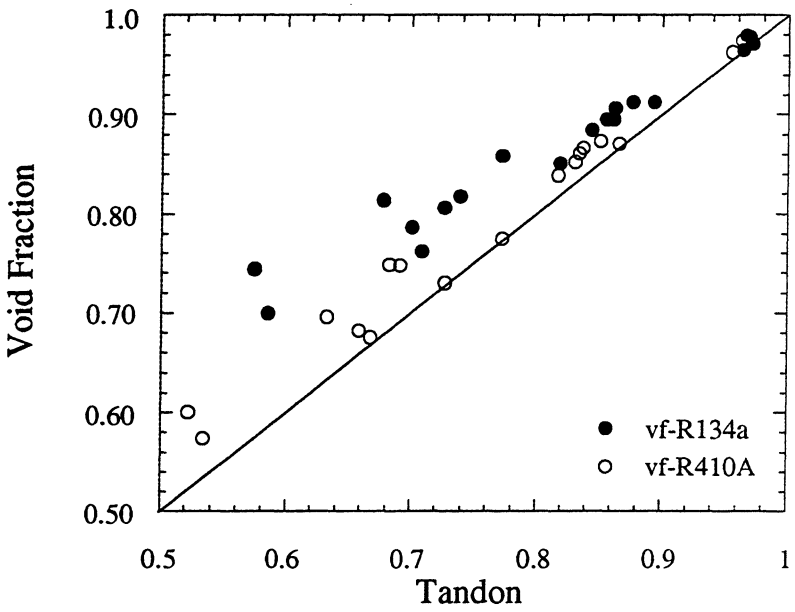

Figure 5.13 Void Fraction vs. Tandon correlation

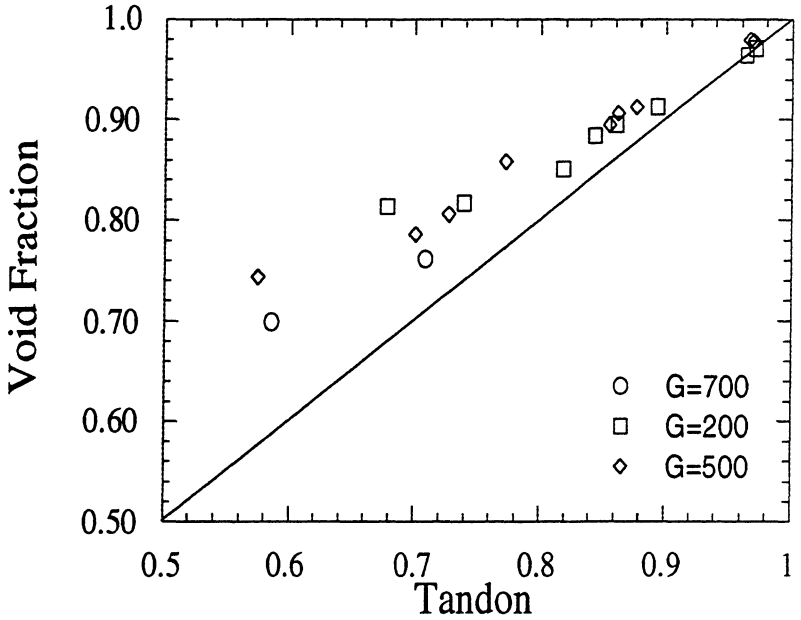

Figure 5.14 Void Fraction vs. Tandon correlation for R134a

(mass flux in $\frac{kg}{m^2 s}$)

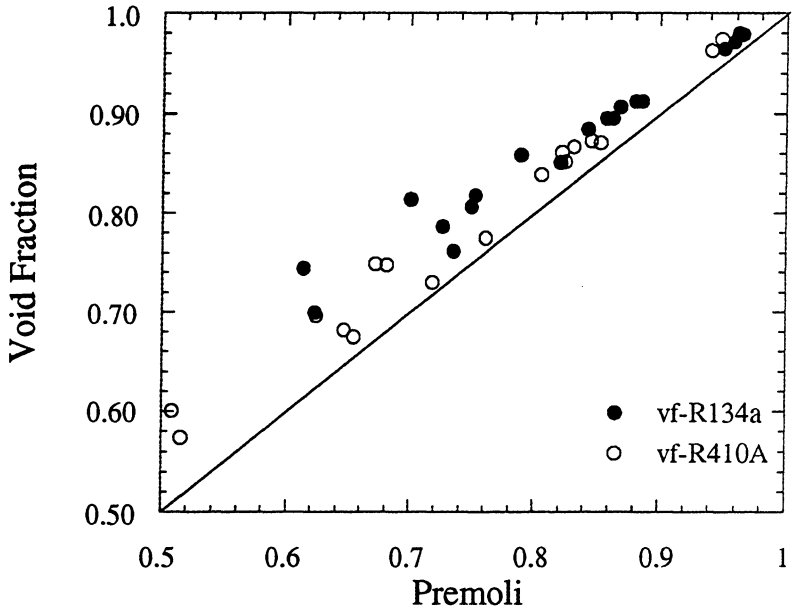

Figure 5.15 Void Fraction vs. Premoli correlation

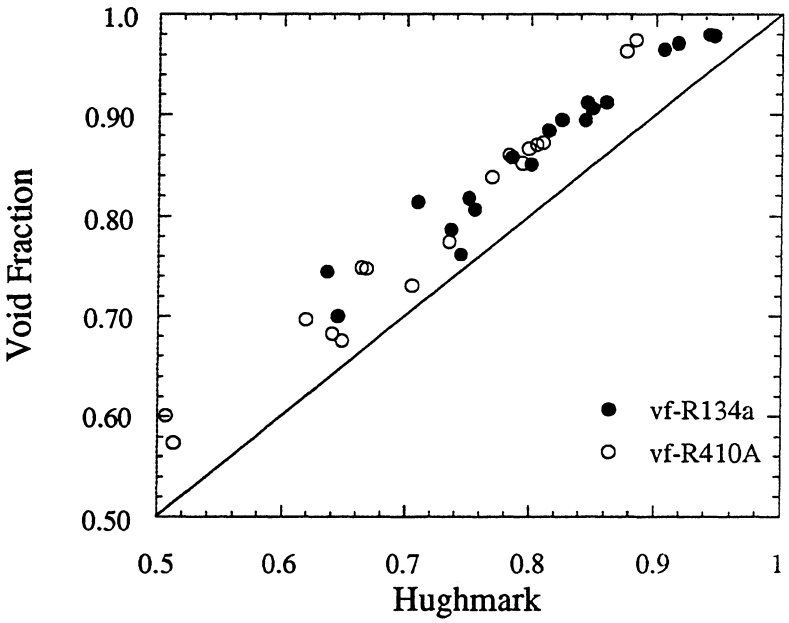

Figure 5.16 Void Fraction vs. Hughmark correlation

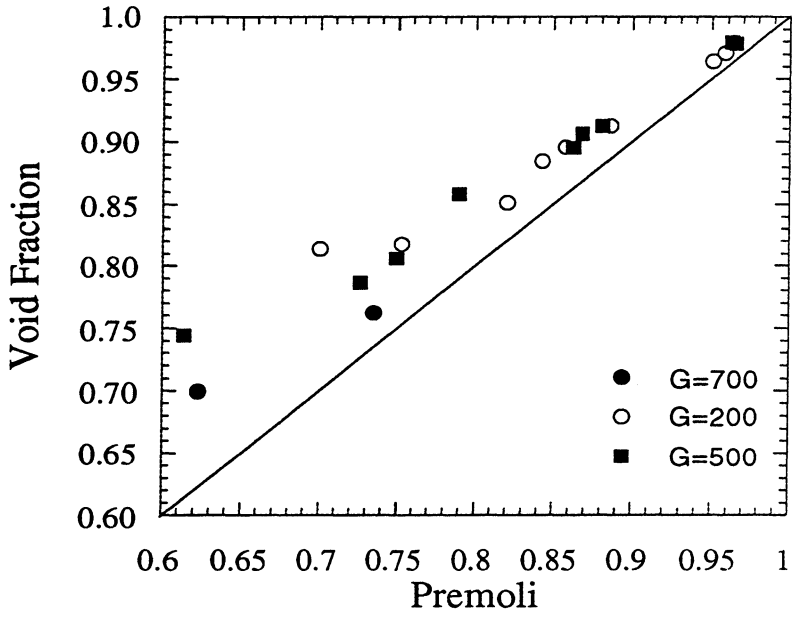

Figure 5.17 Void Fraction vs. Premoli correlation for R134a (mass flux in $\frac{kg}{m^2 s}$)

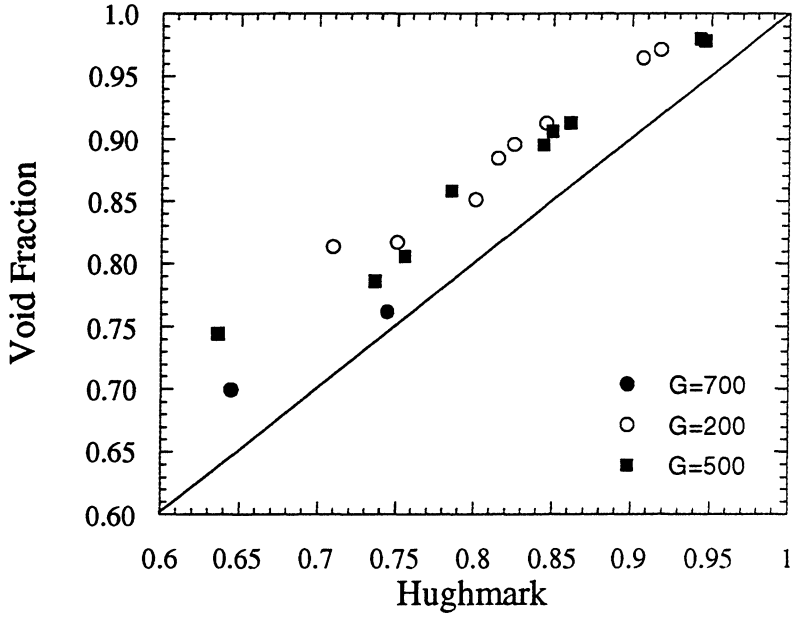

Figure 5.18 Void Fraction vs. Hughmark correlation for R134a (mass flux in $\frac{kg}{m^2 s}$)

Chapter 6
Axially Grooved Tube Results

This chapter discusses the results of the 7.25 mm base diameter axially grooved tube. The results will be examined for both R134a and R410A, the effect of heat addition into the test section, the effect of varying the quality of the fluid in the test section, and the mass flux of the fluid passing through the test section. Next, the data will be compared to the predictions of 10 different correlations and recommendations will be given as to which correlations work well for the axially grooved, heat transfer enhanced tube.

6.1 Void Fraction Results

This section examines the effects of refrigerant, heat addition, mass flux, and diameter on void fraction using the mass quality as the basis of comparison.

6.1.1 Effect of Refrigerant on Void Fraction

These tests were performed using refrigerants R134a and R410A. Figure 6.1 shows void fraction vs. quality for both R134a and R410A. It is easily seen from this graph that R410A consistently has a lower void fraction than R134a at any given quality. This was expected because R410A has a vapor density approximately twice that of R134a, while their liquid densities are relatively similar. Being that the vapor density to liquid density ratio of R410A is much greater than that of R134a, at a given mass quality, the denser vapor of R410A should take up a much smaller volume than R134a.

6.1.2 Effect of Heat Flux on Void Fraction

Figure 6.2 shows void fraction vs. quality for R134a at three different heat fluxes: $0\ \frac{kW}{m^2}$, $3\ \frac{kW}{m^2}$ and $10\ \frac{kW}{m^2}$. It should be noted that the heat flux was used to calculate the average quality of the refrigerant in the test section. The refrigerant R134a was arbitrarily chosen for this plot to demonstrate the effect of heat flux. This plot shows that heat flux has no effect on void fraction.

6.1.3 Effect of Mass Flux on Void Fraction

The effect of mass flux on void fraction was determined experimentally by running tests at four different mass fluxes: 75 $\frac{kg}{m^2s}$, 200 $\frac{kg}{m^2s}$, 500 $\frac{kg}{m^2s}$, and 700 $\frac{kg}{m^2s}$. Figure 6.3 shows void fraction vs. quality for R410A at four different mass fluxes. It is apparent from this plot that for this 7.25 mm base diameter, axially grooved tube, void fraction increases with higher mass fluxes. Smooth tube evaporation discussed earlier did not show mass flux dependency while data from companion studies on a condenser by Graham [1998] and Kopke [1998] show strong mass flux dependency.

6.1.4 Effect of Tube Diameter on Void Fraction

The effects of tube diameter on void fraction was determined by comparing data with that of Wilson. Wilson performed identical tests on the same apparatus using a test section that had a base diameter of 8.89 mm. Figure 6.4 shows void fraction vs. quality for the refrigerant R410A, for both the 7.25 mm tube and the 8.89 mm tube. This plot indicates that the void fraction at a given quality is higher for a larger diameter tube.

6.2 Comparison of Data with Correlations

This section discusses the trends found in the comparisons of the data taken for the 7.25 mm base diameter tube with the 10 existing correlations. Although these correlations were not intended for this particular geometry, it is useful to examine how they compare to these data.

6.2.1 Homogeneous Correlation

When compared to these data, the homogeneous correlation did not show much agreement. The average point over predicted the void fraction by more than 15%, with the maximum error being approximately 30%. The only major trend seen in this comparison is that the data falls in four bands separated by mass flux. This can be seen in Figure 6.5.

6.2.2 Slip-Ratio Correlations

All four of the slip-ratio correlations showed a similar trend. They all slightly over predicted the high void fractions and under predicted the low void fractions. One of the slip-ratio correlations, the Smith correlation, performed much better than the other three. The errors associated with these four correlations are shown in the following table:

	Rigot	Zivi	Smith	Ahrens
Ave. Error	7.484 %	7.171 %	3.3416 %	7.396 %
Max. Error	17.250 %	30.825 %	10.835 %	18.335 %

Table 6.1 Error associated with slip-ratio correlations

Figure 6.6 through Figure 6.9 show the comparisons to these correlations. It is noted that for all of these plots, the data are separated by mass flux. The Smith correlation, Figure 6.8, is the only slip-ratio correlation where the slope of the data matches the slope of the correlation. The data for the mass flux of 500 $\frac{kg}{m^2 s}$ all fell directly along the Smith prediction.

6.2.3 Lockhart-Martinelli Correlations

The two Lockhart-Martinelli parameter correlations both show segregation of the data by mass flux. They did, however, show different trends in that the Baroczy correlation slightly under predicted the low void fraction points whereas the Wallis correlation tended to over predict the low void fraction points. Figure 6.10 and Figure 6.11 show the plots of the data versus these two correlations. Overall, the Baroczy correlation predicted the data more accurately than the Wallis correlation, mainly at the lower void fractions. The percent error for these correlations are shown below.

	Wallis	Baroczy
Ave. Error	4.43 %	5.20 %
Max. Error	24.85 %	14.84 %

Table 6.2 Error associated with Lockhart-Martinelli correlations

6.2.4 Mass Flux Dependent Correlations

The three mass flux dependent correlations predicted the data fairly well. Since the data was observed to have a dependence on the mass flux, this was expected. The percent error for these correlations are shown below.

	Tandon	Premoli	Hughmark
Ave. Error	2.94 %	2.13 %	4.91 %
Max. Error	10.43 %	5.87 %	14.43 %

Table 6.3 Error associated with Mass Flux Dependent correlations

The Tandon correlation, shown in Figure 6.12, seems to have a systematic error that separates the data by refrigerant. The Hughmark correlation, Figure 6.13, does not show any segregation by refrigerant or mass flux; but it under predicts the void fraction, particularly at higher void fractions. The best fit for this set of data came from the Premoli correlation, which is shown in Figure 6.14. This plot shows a bit of segregation by refrigerants, however the data does collapse very close to the predictions.

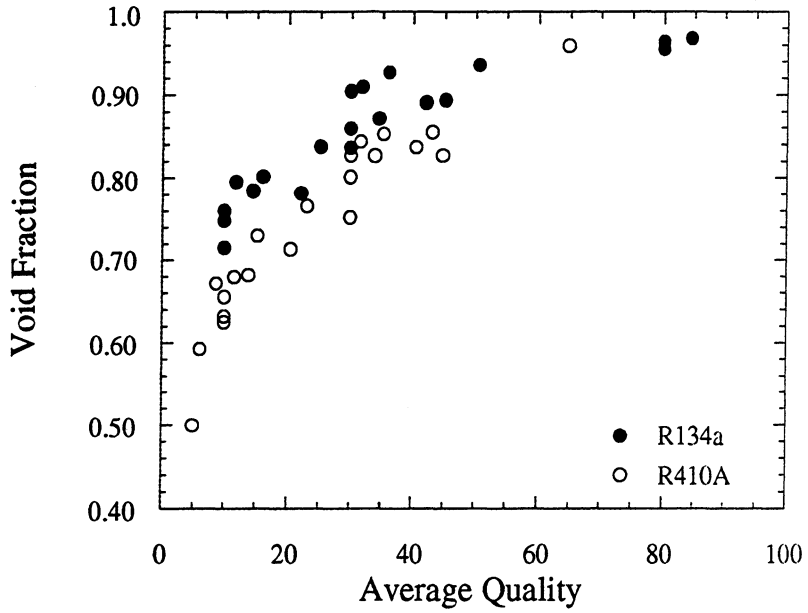

Figure 6.1 Void Fraction vs. Average Quality for R134a and R410A

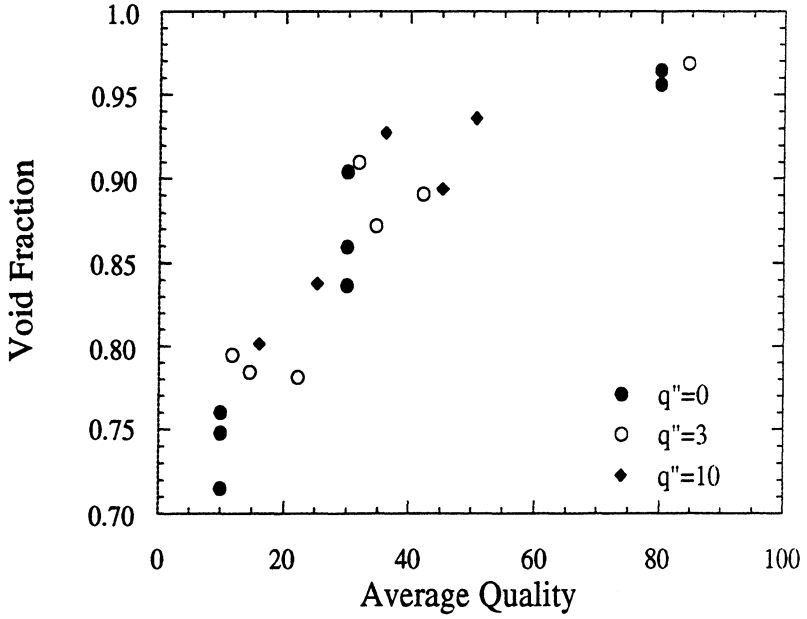

Figure 6.2 Void Fraction vs. Average Quality for R134a to show heat flux effect (heat flux in $\frac{kW}{m^2}$)

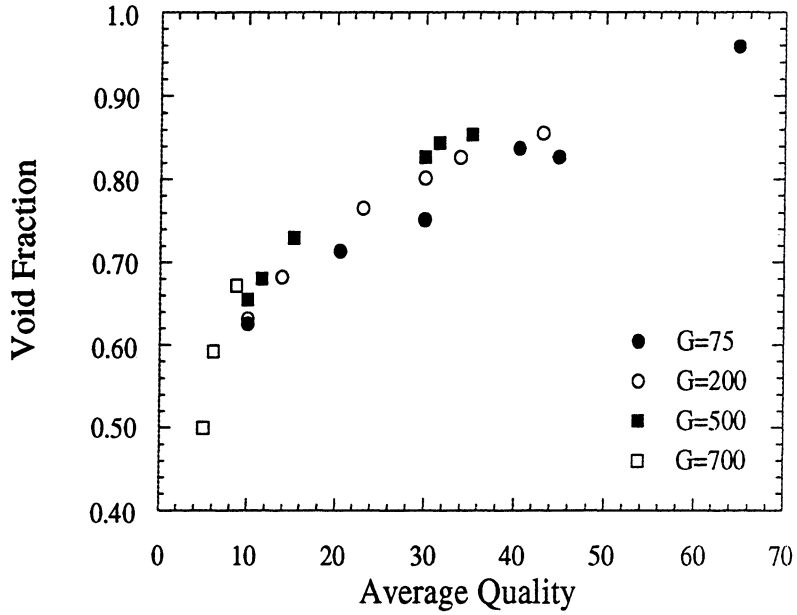

Figure 6.3 Void Fraction vs. Average Quality for R410A to show mass flux effect

(mass flux in $\frac{kg}{m^2 s}$)

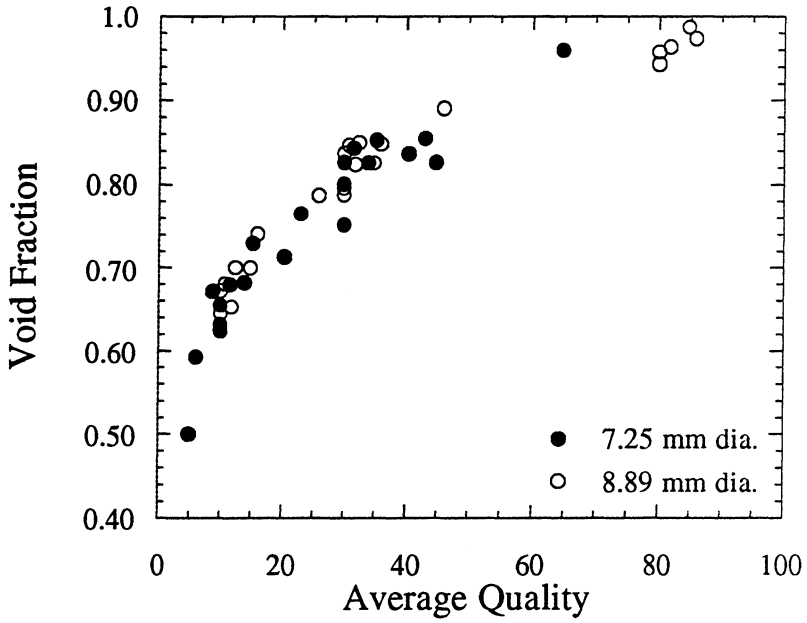

Figure 6.4 Void Fraction vs. Average Quality for R410A to show diameter effect

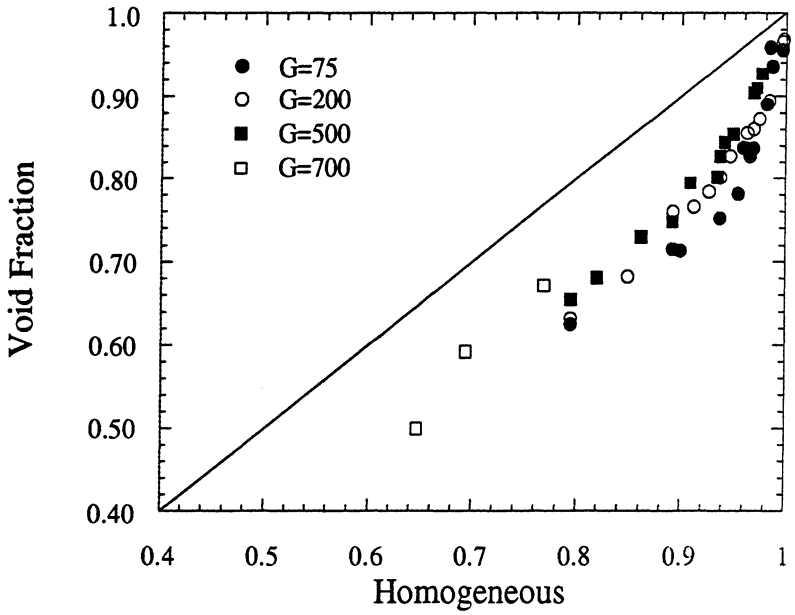

Figure 6.5 Void Fraction vs. Homogeneous correlation

(mass flux in $\frac{kg}{m^2 s}$)

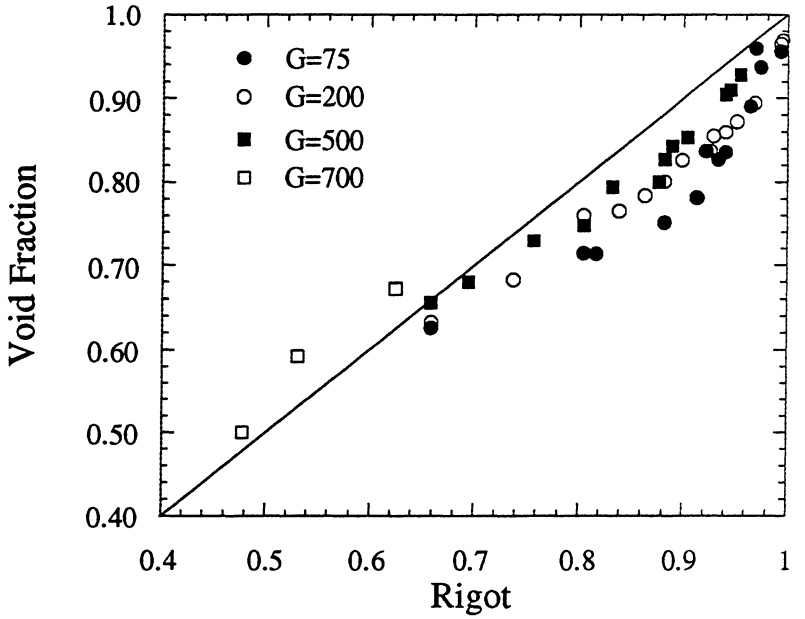

Figure 6.6 Void Fraction vs. Rigot correlation

(mass flux in $\frac{kg}{m^2 s}$)

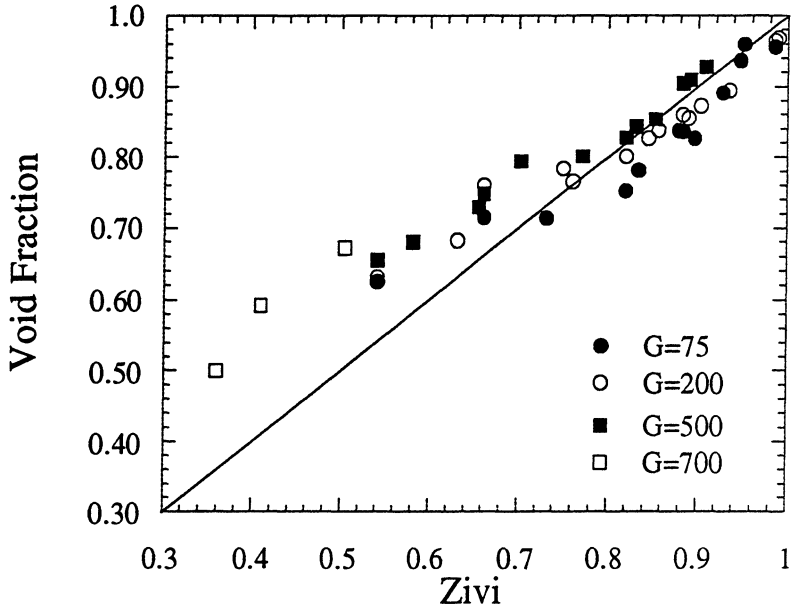

Figure 6.7 Void Fraction vs. Zivi correlation

(mass flux in $\frac{kg}{m^2 s}$)

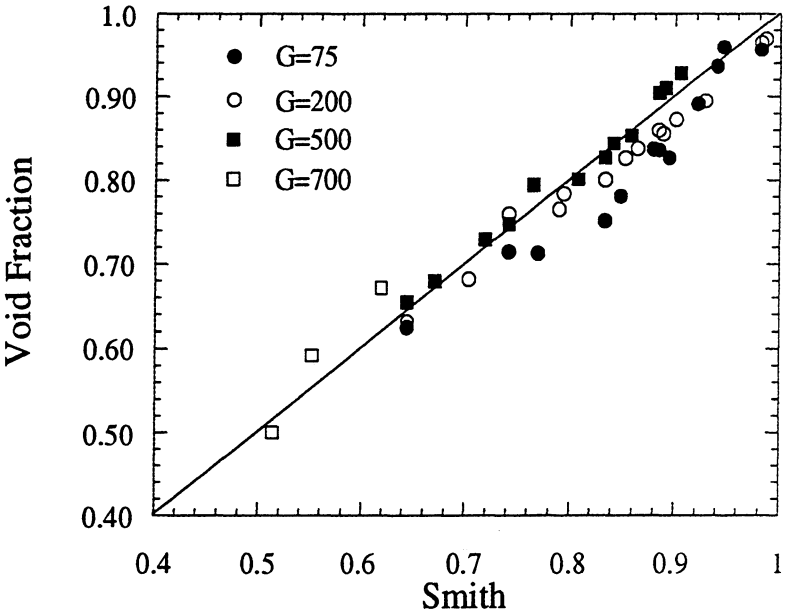

Figure 6.8 Void Fraction vs. Smith correlation

(mass flux in $\frac{kg}{m^2 s}$)

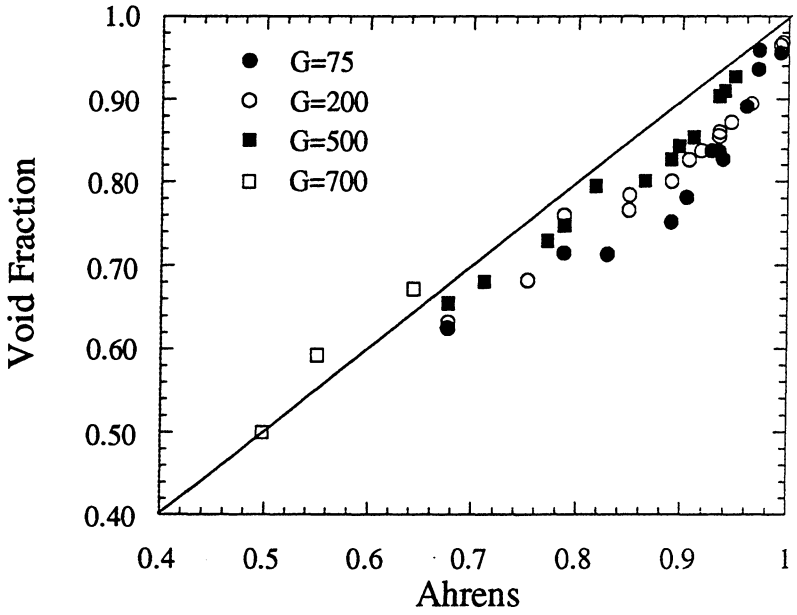

Figure 6.9 Void Fraction vs. Ahrens correlation

(mass flux in $\frac{kg}{m^2 s}$)

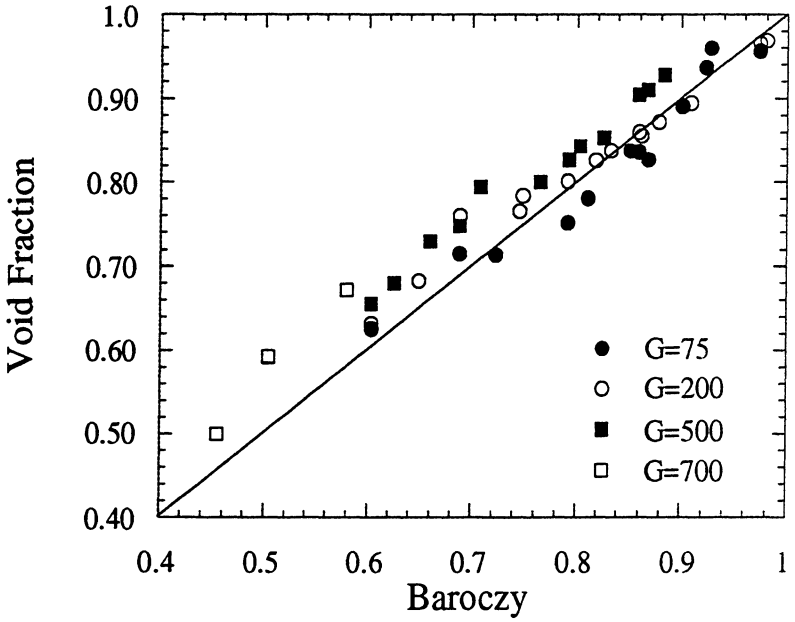

Figure 6.10 Void Fraction vs. Baroczy correlation

(mass flux in $\frac{kg}{m^2 s}$)

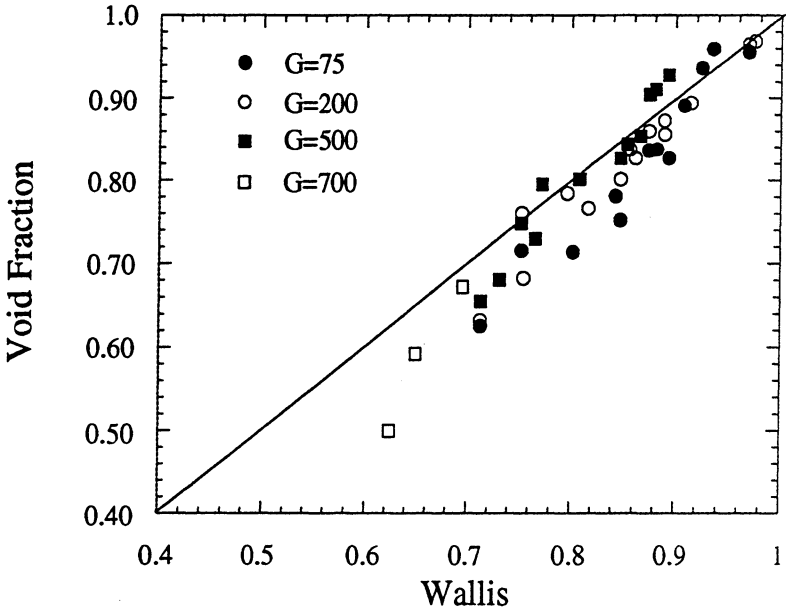

Figure 6.11 Void Fraction vs. Wallis correlation

(mass flux in $\frac{kg}{m^2 s}$)

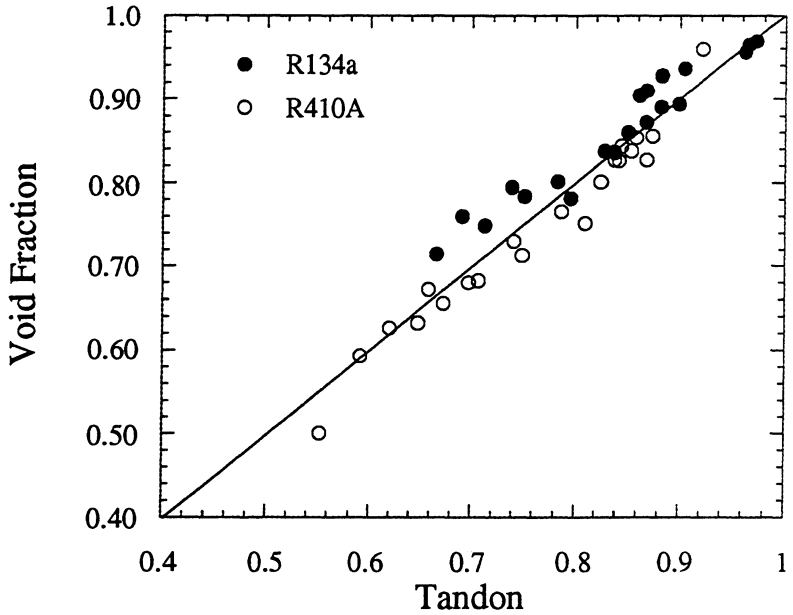

Figure 6.12 Void Fraction vs. Tandon correlation

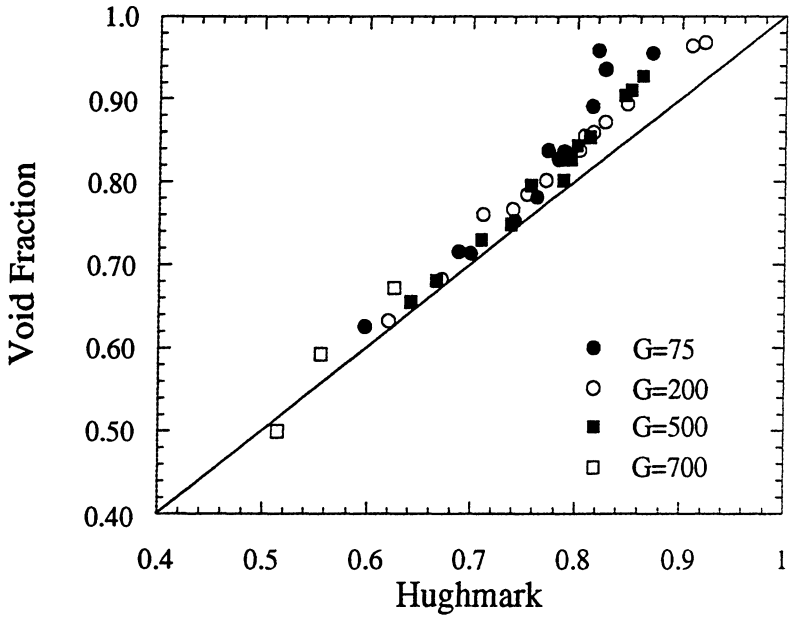

Figure 6.13 Void Fraction vs. Hughmark correlation

(mass flux in $\frac{kg}{m^2 s}$)

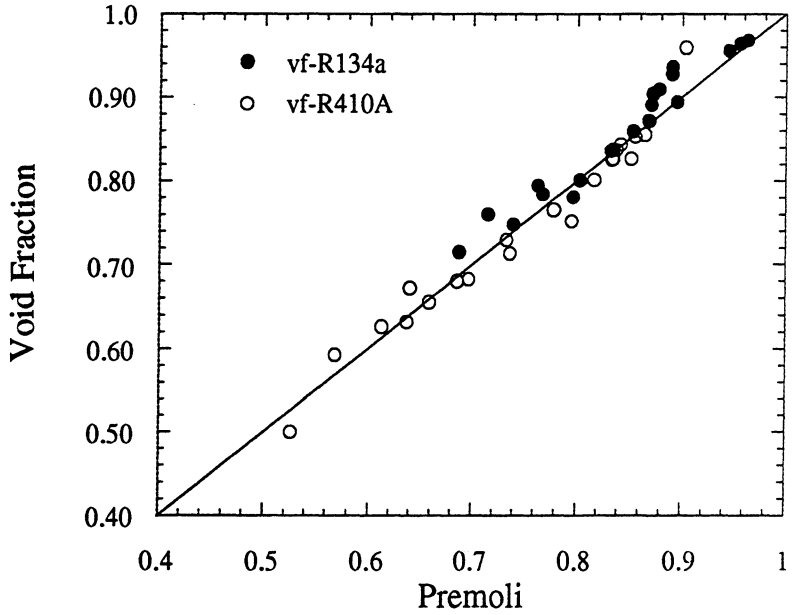

Figure 6.14 Void Fraction vs. Premoli correlation

Chapter 7
18° Helically Grooved Tube Results

This chapter discusses the results of the 7.26 mm base diameter 18° helically grooved tube. The results will be examined for both R134a and R410A, the effect of heat addition into the test section, the effect of varying the quality of the fluid in the test section, and the mass flux of the fluid passing through the test section. Next, the data will be compared to the predictions of 10 different correlations and recommendations will be given as to which correlations work well for the 18° helically grooved, heat transfer enhanced tube.

7.1 Void Fraction Results

This section examines the effects of refrigerant, heat addition, mass flux, and diameter on void fraction using the mass quality as the basis of comparison.

7.1.1 Effect of Refrigerant on Void Fraction

These tests were performed using refrigerants R134a and R410A. Figure 7.1 shows void fraction vs. quality for both R134a and R410A. It is easily seen from this graph that R410A consistently has a lower void fraction than R134a at any given quality. This was expected because R410A has a vapor density much higher than that of R134a, while their liquid densities are relatively similar. Being that the vapor density to liquid density ratio of R410A is much greater than that of R134a, at a given mass quality, the denser vapor of R410A should take up a much smaller volume than R134a.

7.1.2 Effect of Heat Flux on Void Fraction

Figure 7.2 shows void fraction versus quality for R134a at three different heat fluxes: $0\ \frac{kW}{m^2}$, $3\ \frac{kW}{m^2}$ and $10\ \frac{kW}{m^2}$. It should be noted that the heat flux was used to calculate the average quality of the refrigerant in the test section. The refrigerant R134a was chosen for this plot to demonstrate the effect of heat flux. This plot shows that heat flux has no effect on void fraction.

7.1.3 Effect of Mass Flux on Void Fraction

The effect of mass flux on void fraction was determined experimentally by running tests at four different mass fluxes: 75 $\frac{kg}{m^2s}$, 200 $\frac{kg}{m^2s}$, 500 $\frac{kg}{m^2s}$, and 700 $\frac{kg}{m^2s}$. Figure 7.3 shows void fraction vs. quality for R134a at four different mass fluxes. By examining this plot, it seems that for this 7.26 mm base diameter, helically grooved tube, void fraction mildly increases with higher mass fluxes.

7.1.4 Effect of Tube Diameter on Void Fraction

The effects of tube diameter on void fraction was determined by comparing data with that of Wilson [1998]. Wilson [1998] performed identical tests on the same apparatus using a test section that had a base diameter of 8.93 mm. Figure 7.4 shows void fraction vs. quality for the refrigerant R410A, for both the 7.26 mm tube and the 8.93 mm tube. This plot indicates that there is no dependence on tube diameter for the 18° helically grooved tube.

7.2 Comparison of Data with Correlations

This section discusses the trends found in the comparisons of the data taken for the 7.26 mm base diameter tube with the 10 existing correlations. Although these correlations were not intended for this particular geometry, it is useful to examine how they compare to this data.

7.2.1 Homogeneous Correlation

When compared to this data, the homogeneous correlation did not show much agreement. The average point over predicted the void fraction by almost 15%, with the maximum error being approximately 25%. The only major trend seen in this comparison is that the data shows a mild mass flux dependence. This can be seen in Figure 7.5.

7.2.2 Slip-Ratio Correlations

The four of the slip-ratio correlations showed some interesting results. The Ahrens correlation and the Rigot correlation both over predicted the higher void fractions with fairly good agreement on the lower void fractions. The Zivi correlation gave reasonable

values for the higher void fractions, but showed a lot of mass flux segregation and it under predicted the low void fraction. The Smith correlation performed much better than the other three, but there is a fair amount of segregation due to the mass flux effect. The errors associated with these four correlations are shown in the following table:

	Rigot	Zivi	Smith	Ahrens
Ave. Error	6.92 %	8.37 %	3.12 %	6.57 %
Max. Error	16.98 %	33.73 %	8.51 %	15.79 %

Table 7.1 Error associated with slip-ratio correlations

Figure 7.6 through Figure 7.9 show the comparisons to these correlations. It is noted that for all of these plots, the data is separated by mass flux. The Smith correlation, Figure 7.8, is the best slip-ratio correlation in that the slope of the data matches the slope of the correlation. The data for the mass fluxes of 200 $\frac{kg}{m^2s}$ and 500 $\frac{kg}{m^2s}$ all fell very close to the Smith prediction; with the 700 $\frac{kg}{m^2s}$ data falling above the line and the 75 $\frac{kg}{m^2s}$ data falling below the line.

7.2.3 Lockhart-Martinelli Correlations

The two Lockhart-Martinelli parameter correlations both show segregation of the data by refrigerant. Figure 7.10 and Figure 7.11 show the plots of the data versus these two correlations. The segregation is more dominant in the Wallis correlation, but is also seen in the Baroczy correlation . Also, they showed different trends in that the Baroczy correlation slightly under predicted the low void fraction points whereas the Wallis correlation tended to over predict the low void fraction points. Overall, the Wallis correlation predicted the data more accurately than the Baroczy correlation. The percent error for these correlations are shown below.

	Wallis	Baroczy
Ave. Error	3.49 %	6.12 %
Max. Error	15.19 %	16.08 %

Table 7.2 Error associated with Lockhart-Martinelli correlations

7.2.4 Mass Flux Dependent Correlations

The three mass flux dependent correlations predicted the data fairly well. Since the data was observed to have a dependence on the mass flux, this was expected. The percent error for these correlations are shown below.

	Tandon	Premoli	Hughmark
Ave. Error	3.58 %	2.83 %	5.70 %
Max. Error	12.03 %	9.36 %	11.53 %

Table 7.3 Error associated with Mass Flux Dependent correlations

The Tandon correlation, shown in Figure 7.12, seems to have a systematic error that separates the data by refrigerant. It shows good agreement with the R410A, but predicts low values for the R134a. The Hughmark correlation, Figure 7.13, does not show any segregation by refrigerant or mass flux; but it under predicts the void fraction, particularly at higher void fractions. The best fit for this set of data came from the Premoli correlation, which is shown in Figure 7.14.

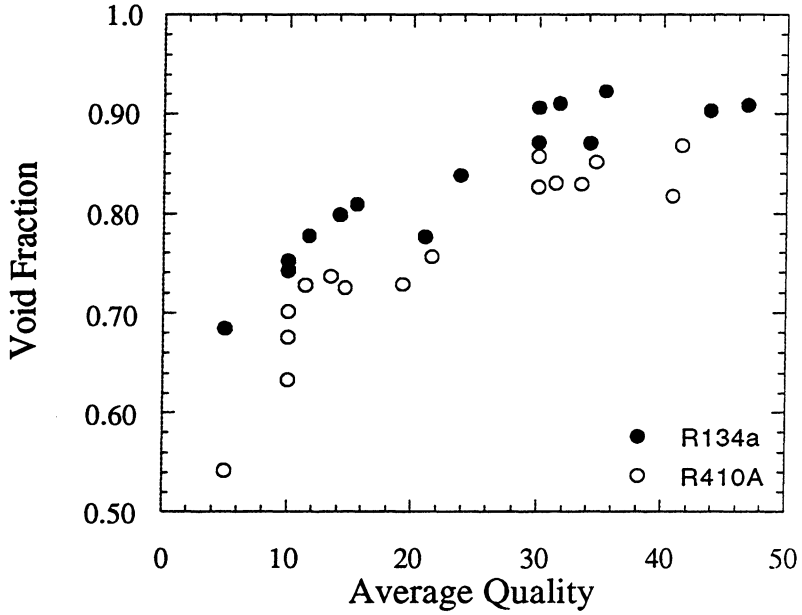

Figure 7.1 Void Fraction vs. Average Quality for R134a and R410A

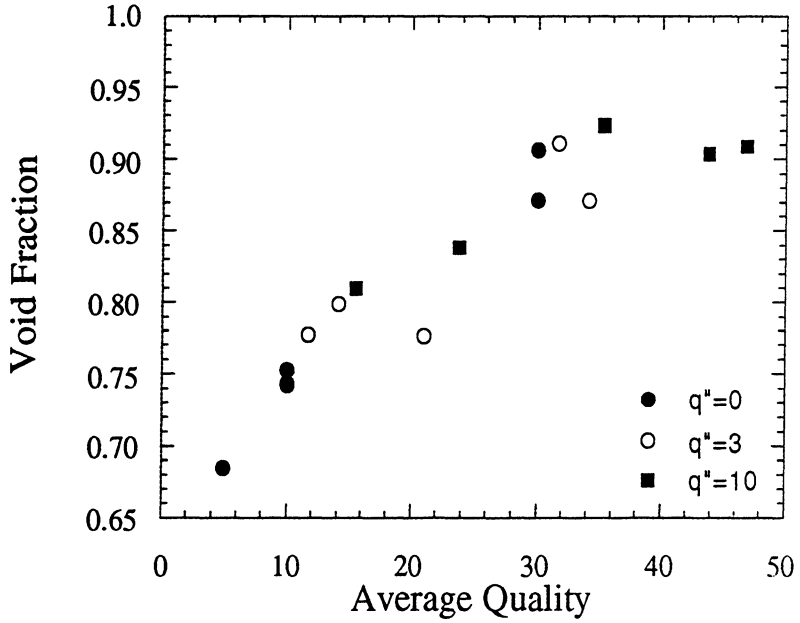

Figure 7.2 Void Fraction vs. Average Quality for R134a to show heat flux effect (heat flux in $\frac{kW}{m^2}$)

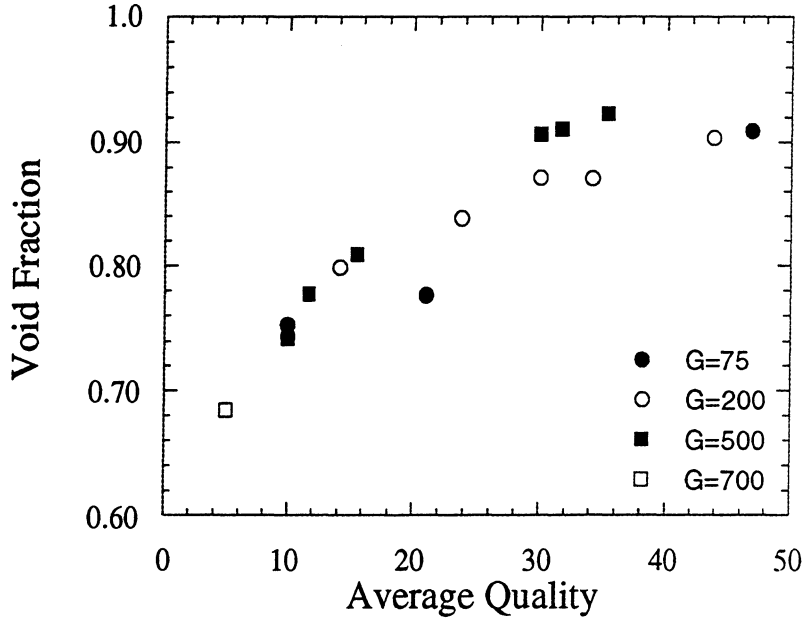

Figure 7.3 Void Fraction vs. Average Quality for R134a to show mass flux effect (mass flux in $\frac{kg}{m^2 s}$)

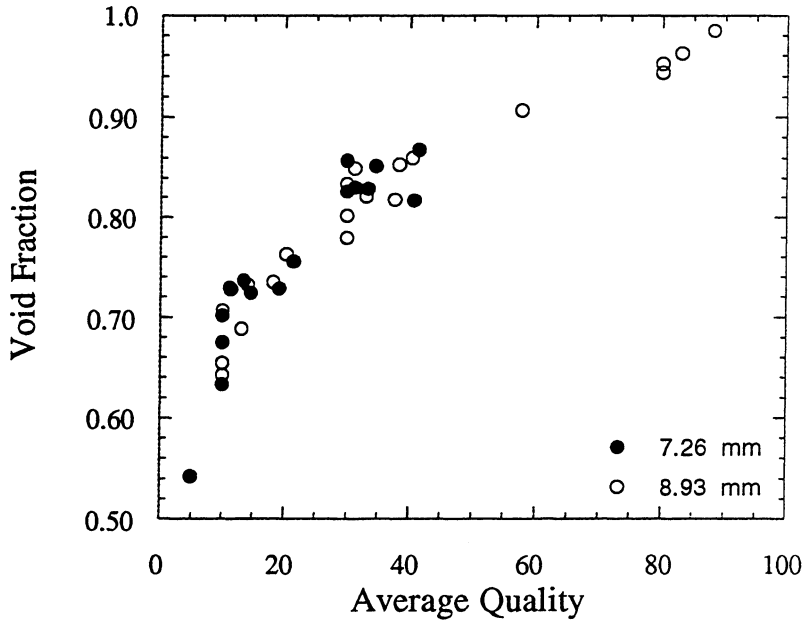

Figure 7.4 Void Fraction vs. Average Quality for R410A to show diameter effect

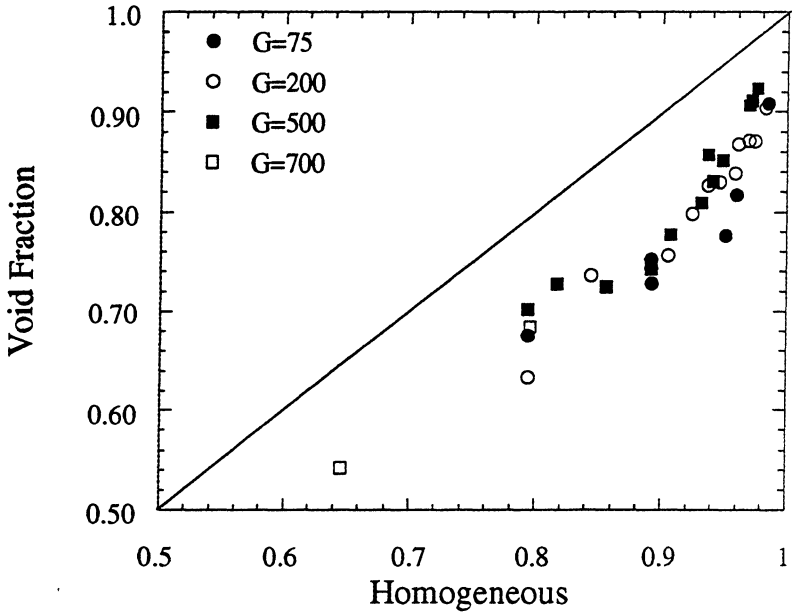

Figure 7.5 Void Fraction vs. Homogeneous correlation

(mass flux in $\frac{kg}{m^2 s}$)

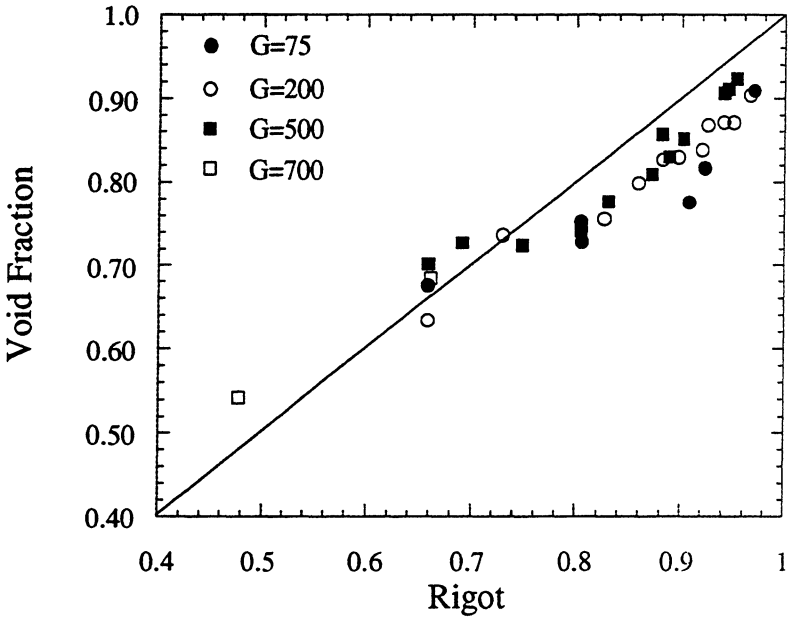

Figure 7.6 Void Fraction vs. Rigot correlation

(mass flux in $\frac{kg}{m^2 s}$)

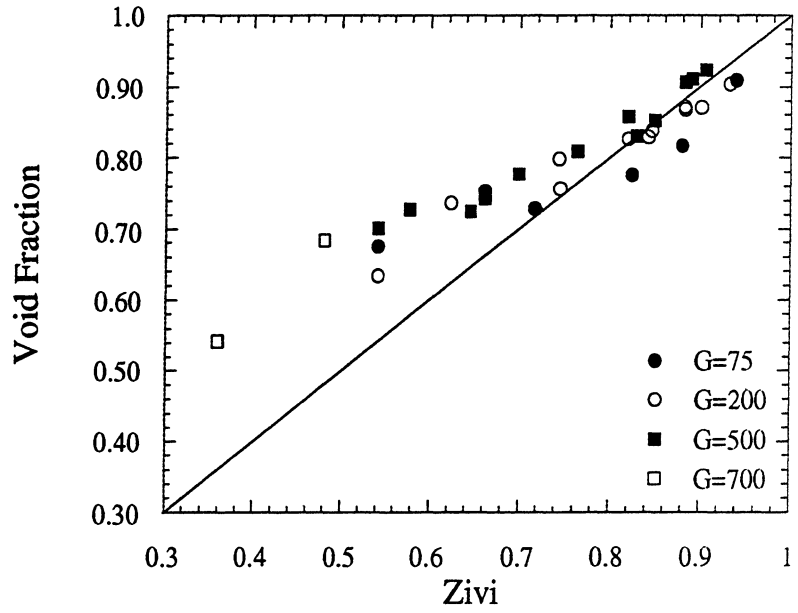

Figure 7.7 Void Fraction vs. Zivi correlation

(mass flux in $\frac{kg}{m^2 s}$)

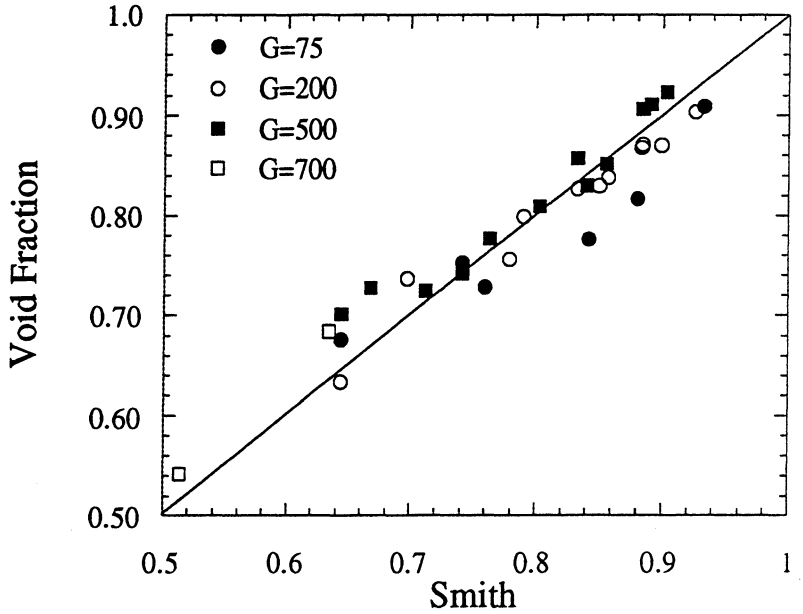

Figure 7.8 Void Fraction vs. Smith correlation

(mass flux in $\frac{kg}{m^2 s}$)

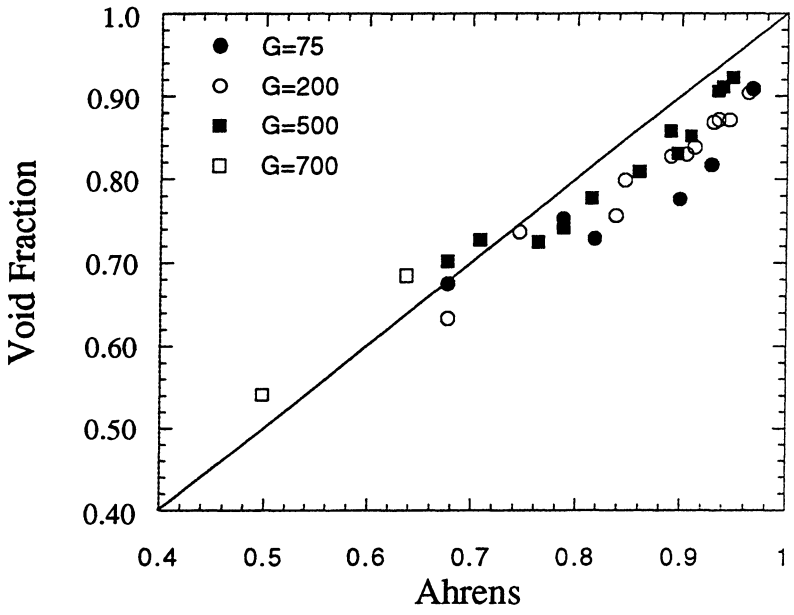

Figure 7.9 Void Fraction vs. Ahrens correlation

(mass flux in $\frac{kg}{m^2 s}$)

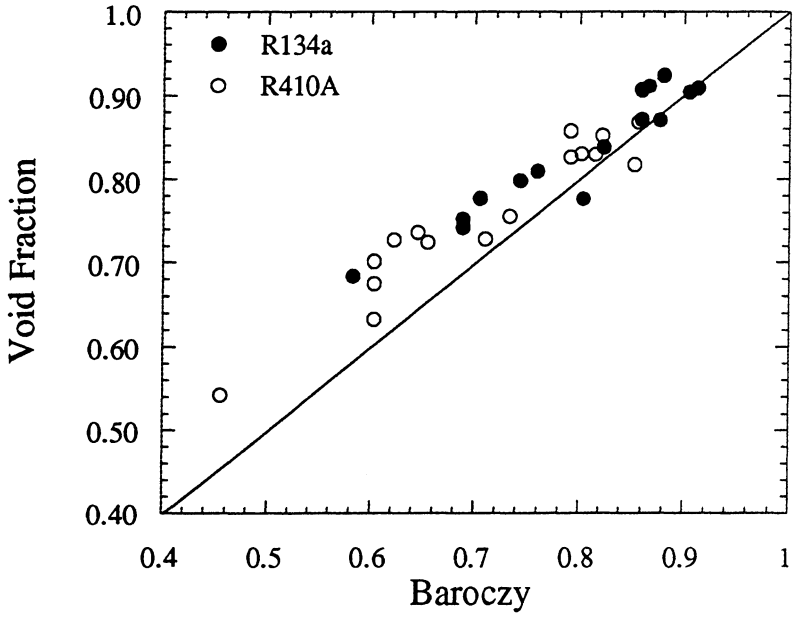

Figure 7.10 Void Fraction vs. Baroczy correlation

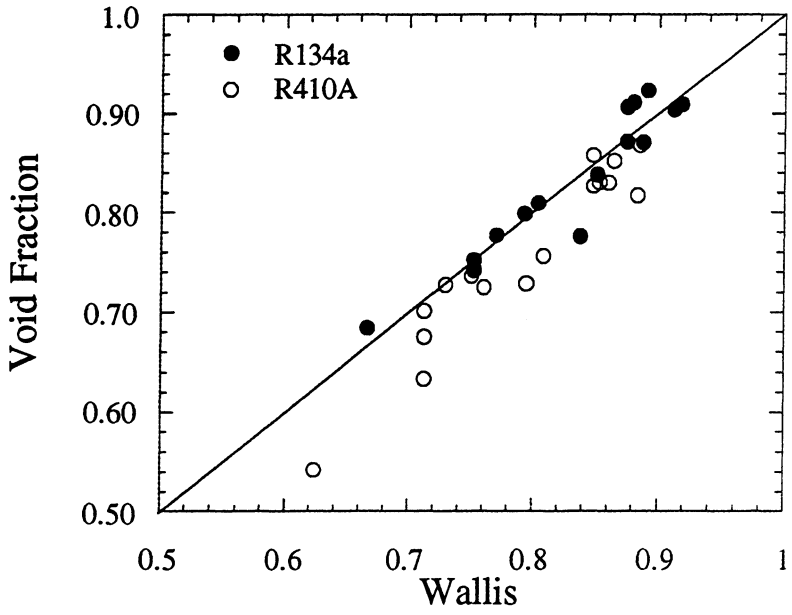

Figure 7.11 Void Fraction vs. Wallis correlation

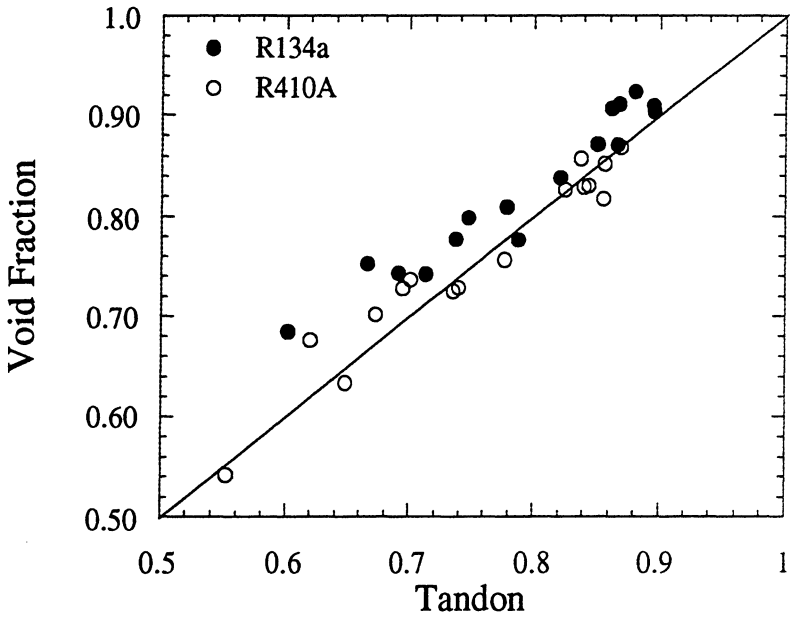

Figure 7.12 Void Fraction vs. Tandon correlation

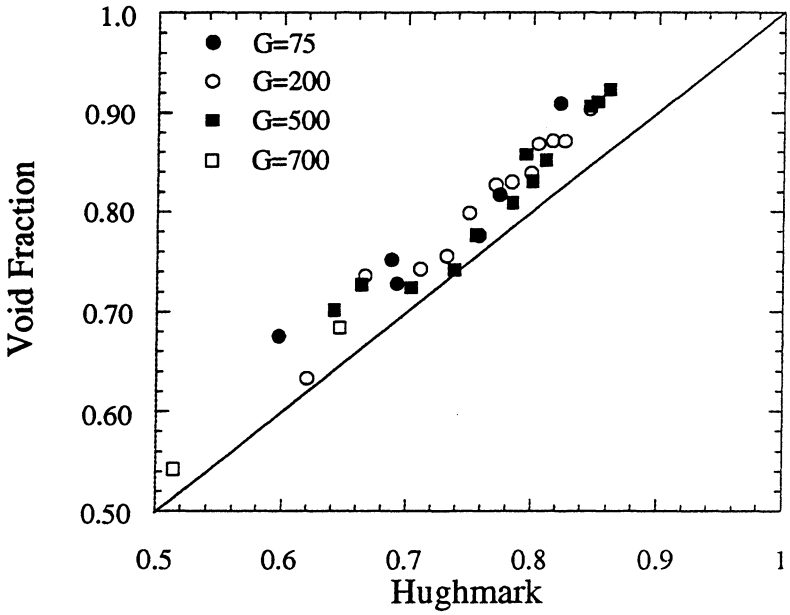

Figure 7.13 Void Fraction vs. Hughmark correlation

(mass flux in $\frac{kg}{m^2 s}$)

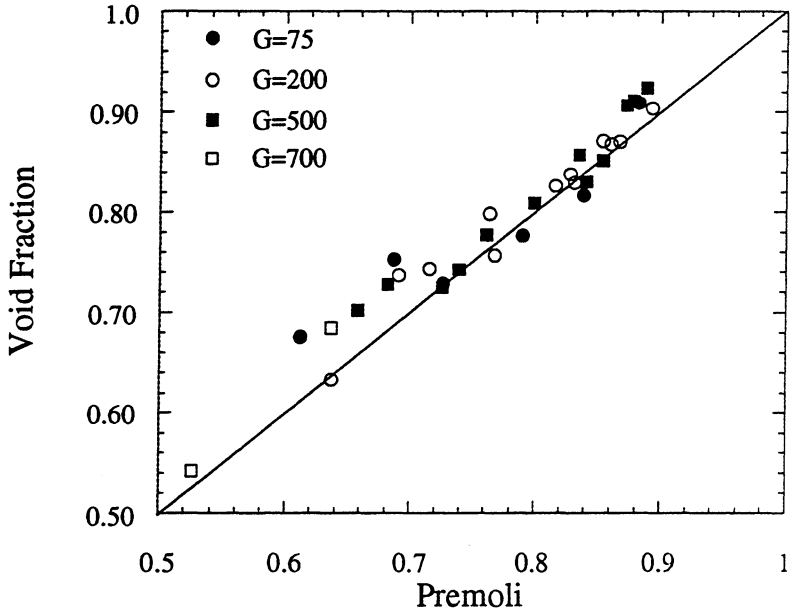

Figure 7.14 Void Fraction vs. Premoli correlation

(mass flux in $\frac{kg}{m^2 s}$)

Chapter 8
Recommendations

The purpose of this chapter is to analyze the results found in chapters 5, 6, and 7. Recommendations are also given as to which correlations are best suited for the particular situations.

8.1 4.26 mm Smooth Tube

The results from the 4.26 mm smooth tube, yielded some rather interesting results. The data were well fitted by many of the existing correlations for void fractions above 84%. For lower void fractions below this, none of the existing correlations were able to eliminate the segregation of the data by refrigerant.

8.1.1 Flow Regime Effects

It was noted in the discussion of the Wallis correlation that there seemed to be some sort of transition in the trend of the data for Lockhart-Martinelli parameters greater than 0.5. The formulation of the existing correlations, with the exception of Hughmark, all assumed annular flow. Based on this, it is useful to examine a flow regime map. Wattelet [1994] stated that the most accurate of these flow maps is the model generated by Taitel and Dukler [1976]. The data points for these tests are shown on a Taitel and Dukler map shown in Figure 8.1. Taitel and Dukler stated that there is a transition from annular to intermittent flow at a Lockhart-Martinelli parameter of 1.6. The transition in the pattern seen in this data occurs at $X_{tt} = 0.5$, however it is also stated that these transitions are not very well defined. Another flow map presented by Mandhane [1974] shows much closer agreement with the transition seen in this data. The Mandhane map is shown in Figure 8.2. This map shows the transition from annular to intermittent flow to occur at the exact value of X_{tt} where a transition was noticed in the data. It was also stated in Westwater [1988] that for smaller diameter tubes, the effects of surface tension may cause the flow to favor slug flow over annular flow, which would help explain how the transition would occur at a value of X_{tt} of 0.5.

8.1.2 Recommendations

Since it seems as though the data taken for this experiment crosses into a flow regime where the existing correlations all fail due to a systematic error involving the liquid to vapor density ratio, a correlation should be developed to predict void fraction in this flow regime. The first recommendation is that the Wallis correlation be used for X_{tt} less than 0.5 for this particular tube diameter. The Wallis correlation is chosen due to the accuracy and the ease in which it may be calculated.

At the present time, there are only 17 data points that lie in this flow regime. The second recommendation is that more data be taken to curve fit this flow regime as well as more accurately predict the transition to this flow regime. Since the homogeneous correlation and the Rigot correlation were the only two that did not show a systematic error by refrigerants, the volumetric quality (defined in chapter 2), β, should be examined as an independent variable. Figure 8.3 is a plot of the data points in the intermittent flow regime versus the volumetric quality. This set of data points yielded the following curve fit:

$$\alpha = 0.4428 - 0.1987\beta + 0.6558\beta^2 \qquad (8.1)$$

This curve fit has an average deviation on 4%; however this is only a preliminary curve fit and by introducing more data, a more accurate correlation may be developed.

8.2 7.25 mm Base Diameter Axially Grooved Tube

The results of the 7.25 mm base diameter axially grooved tube showed that the void fraction was strongly dependent on the mass flux. The three mass flux dependent correlations provided fairly good predictions of the data. The Hughmark correlation provided a good collapse for the data, but tended to predict the void fractions to be lower than they were. Some segregation of the data by refrigerant was noted for the Tandon correlation, and mildly in the Premoli correlation. Overall, the Premoli correlation was well suited for the 4.25 mm base diameter axially grooved tube.

The main problem in using the Premoli correlation is that it is mildly dependent on the Weber number which is a function of surface tension. Surface tension is a property that is rather difficult to measure and one for which little data exists. The Weber number is used to calculate the parameter F_2. The values of F_2 are very small, the largest value in this data set being 0.0036, mainly due to the small coefficient in front of the equation for F_2. Since this parameter is generally very small and considering the order of magnitude of

its influence on the void fraction, the values of the Premoli predictions were calculated assuming the value of F_2 to be equal to zero. The accuracy of this model is to within 5 one hundredths of one percent of the Premoli correlation. A plot of the void fraction vs. this F_2 adjusted Premoli correlation is shown in Figure 8.4. Once again, it is observed that there is a bit of segregation by refrigerants; but overall, there is good agreement.

8.3 7.26 mm Base Diameter 18° Helically Grooved Tube

The 7.26 mm base diameter 18° helically grooved tube showed reasonable agreement with many of the existing correlations. The best overall correlation was the Premoli, however it tended to under predict the void fraction for all of the data. Once again, the $F_2 = 0$ argument was made and the accuracy of this model was preserved to within 7 one hundredths of one percent. To eliminate the tendency to under predict the void fraction, the coefficient of F_1 was adjusted. For this adjusted correlation, the parameter F_1 should be calculated in the following manner:

$$F_1 = 1.3 \bullet Re_L^{-0.19}\left(\frac{\rho_l}{\rho_g}\right)^{0.22} \tag{8.2}$$

Figure 8.5 shows a plot of the adjusted Premoli correlation. This model has an average error of 2.37 % with a maximum error of 5.54 %.

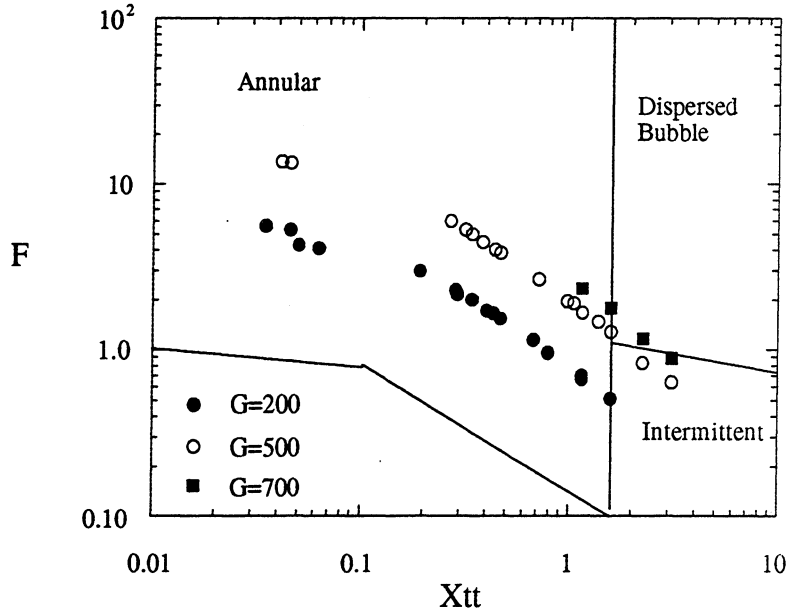

Figure 8.1 Taitel and Dukler flow regime map for the 4.26 mm smooth tube (mass flux in $\frac{kg}{m^2 s}$)

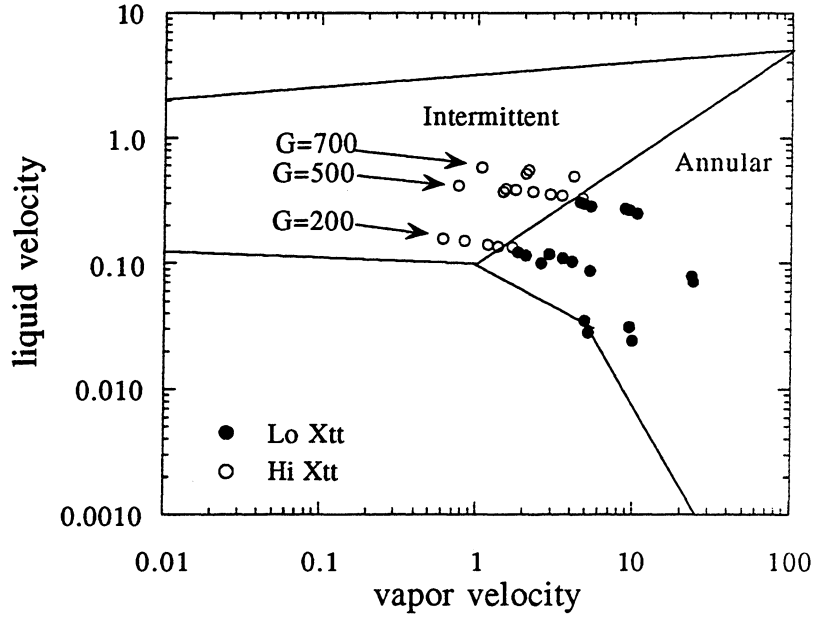

Figure 8.2 Flow regime map by Mandhane for the 4.26 mm smooth tube (mass flux in $\frac{kg}{m^2 s}$)

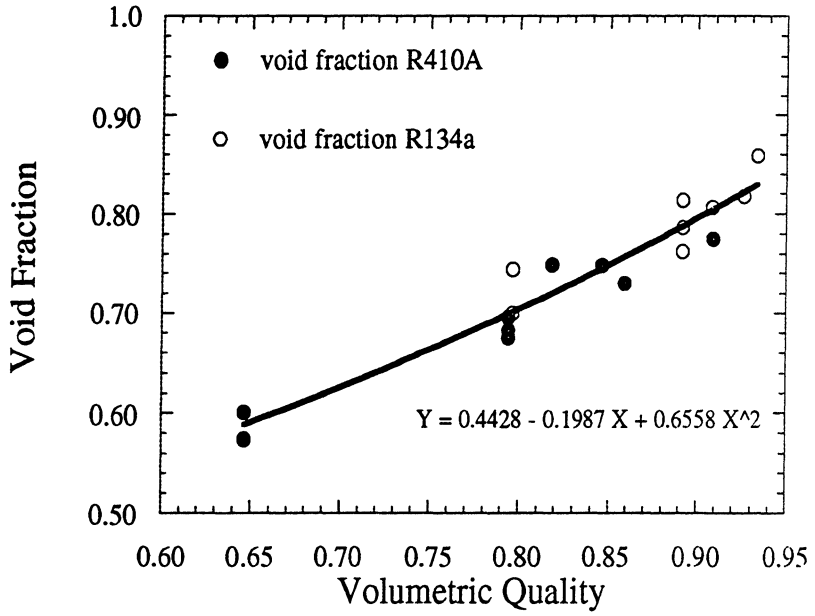

Figure 8.3 Void Fraction vs. Volumetric Quality
for data in the Intermittent Flow Regime

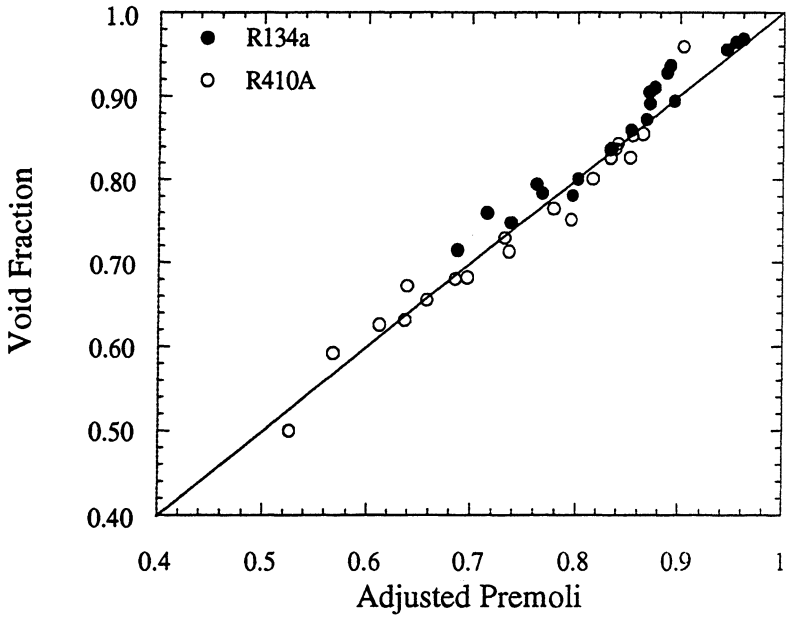

Figure 8.4 Void Fraction vs. Adjusted Premoli correlation for 7.25 mm base diameter axially grooved tube

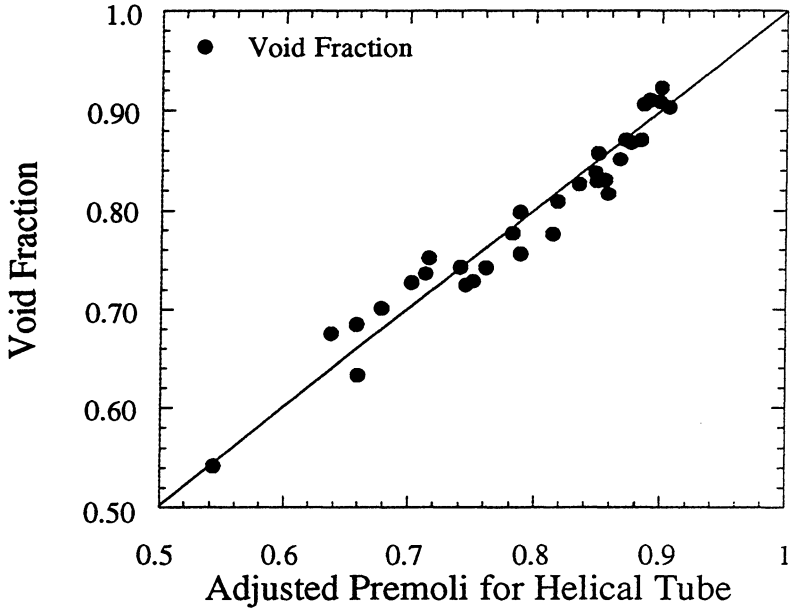

Figure 8.5 Void Fraction vs. Adjusted Premoli correlation for 7.26 mm base diameter 18° helically grooved tube

Bibliography

Ahrens, F. W. 1983. "Heat pump modeling, simulation and design." *Heat Pump Fundamentals. Proceedings of the NATO Advanced Study Institute on Heat Pump Fundamentals, Espinho, Spain, 1980.* J. Berghmans, ed. The Hague, Netherlands: Martinus Nijhoff Publishers.

Anderson, G. H. and B. G. Mantzouranis. 1960. "Liquid entrainment; measuring local mass flow density of liquid drops and their velocity." *Chem. Engrng Sci.*

Bankoff, S. G. 1960. "A variable density single-fluid model for two-phase flow with particular reference to steam-water flow." *Transactions ASME, Journal of Heat Transfer,* Vol. 82, pp. 265-272.

Baroczy, C. J. 1965. "Correlation of liquid fraction in two-phase flow with application to liquid metals." *Chemical Engineering Progress Symposium Series*, Vol. 61, No. 57, pp. 179-191.

Dobson, M. K. 1994. "Heat transfer and flow regimes during condensation in a horizontal tube." Ph.D. Dissertation, University of Illinois.

Domanski, P., and D. Didion. 1983. *Computer Modeling of the Vapor Compression Cycle with Constant Flow Area Expansion Device*. NBS Building Science Series 155.

Gaibel, J. A., et al. 1994. "Condensation of a 50/50 blend of R-32/R-125 in horizontal tubes with and without oil." *University of Illinois Air Conditioning and Refrigeration Center Technical Report* , 56.

Graham, D. M. 1998. "Experimental investigation of void fraction during refrigerant condensation." M.S. Thesis, University of Illinois.

Haywood, R. W., Knights, G. A., Middleton, G. E. and J. R. S. Thom. 1961. "Experimental study of the flow conditions and pressure drop of steam-water mixtures at high pressures in heated and unheated tubes." *Proc. Instn. Mech. Engrs.*

Hinde, D. K., M. K. Dobson, J. C. Chato, M. E. Mainland and N. L. Rhines. 1992 "Condensation of refrigerants 12 and 134a in horizontal tubes with and without oils." *University of Illinois Air Conditioning and Refrigeration Center Technical Report* , 26.

Hughmark, G. A. 1962. "Holdup in gas-liquid flow." *Chemical Engineering Progress*, Vol. 58, No. 4, pp. 62-65.

Hurlburt, E. T. and T. A. Newell. 1997. "Prediction of the circumferential film thickness distribution in horizontal annular gas-liquid flow." Submitted to Int. J. Multiphase Flow.

Isbin, H. S., Shear, N. C. and K. C. Eddy. 1957. "Void fractions in two-phase steam water flow." *A.I.Ch.E. Jl*, Vol. 3, pp. 136-142.

Kenney, P. J., et al. 1994, "Condensation of a zeotropic refrigerant R-32/R-125/R-134a (23% / 25% / 52%) in a horizontal tube." *University of Illinois Air Conditioning*

and Refrigeration Center Technical Report, 62.

Kopke, H. R. 1998. "Experimental investigation of void fraction during refrigerant condensation." M.S. Thesis, University of Illinois.

Larson, H. C. 1957. "Void fractions of two-phase steam water mixtures." M.S. Thesis, University of Minnesota.

Lockhart, R. W. and R. C. Martinelli. 1949. "Proposed correlation of data for isothermal two-phase, two-component flow in pipes." *Chemical Engineering Progress*, Vol. 45, No. 1, pp. 39-48.

Maurer, G. 1960. "A method for predicting steady-state boiling vapor fractions in reactor coolant channels." Bettis Technical Review, WAPD-BT-19.

Martinelli, R. C., and D. B. Nelson. 1948. "Prediction of pressure drop during forced circulation boiling of water." *Transactions ASME*, Vol. 70, pp. 695-702.

Ponchner, M. 1995. "Condensation of HFC-134a in an 18° helix angle micro-finned tube." M.S. Thesis, University of Illinois.

Polaski, M. 1993. "Comparison of the accuracy of thermocouple mounting techniques on concentric tube heat exchangers." Independent Study Project, University of Illinois.

Premoli, A., D. Francesco, and A. Prina. 1971. "A dimensional correlation for evaluating two-phase mixture density." *La Termotecnica*, Vol. 25, No. 1, pp. 17-26.

Rice, C.K. 1987. "The effect of void fraction correlation and heat flux assumption on refrigerant charge inventory predictions." *ASHRAE Transactions*, Vol. 93, Part 1, pp. 341-367.

Rouhani, S.Z. and K.M. Becker. 1963. "Measurements of void fraction for flow of boiling heavy water in vertical round duct." *Aktebolaget Atomenergie Rep.*, No. AE-106.

Sacks, P.S. 1975. "Measured characteristics of adiabtic and condensing single component two-phase flow of refrigerant in a 0.377-In. diameter horizontal tube." ASME Winter Annual Meeting, Houston, TX, 75-WA/HT-24.

Smith, S. L. 1969. "Void fractions in two-phase flow: a correlation based upon an equal velocity head model." *Proc. Instn. Mech Engrs.*, London, Vol. 184, Pt. 1, No. 36, pp. 647-664.

Sweeney, K. A. 1996. "The heat transfer and pressure drop behavior of a zeotropic refrigerant mixture in a microfinned tube." M.S. Thesis, University of Illinois.

Tandon, T. N., H. K. Varma, and C. P. Gupta. 1985. "A void fraction model for annular two-phase flow." *International Journal of Heat and Mass Transfer*, Vol. 28, No. 1, pp. 191-198.

Thom, J. R. S. 1964. "Prediction of pressure drop during forced circulation boiling of water." *International Journal of Heat and Mass Transfer*, Vol. 7, pp. 709-724.

Wallis, G. B. 1969. *One-Dimensional Two-Phase Flow*. New York: McGraw-Hill,

pp.51-54.

Wilson, M. J. 1998. "Experimental investigation of void fraction during horizontal flow in larger diameter applications." M.S. Thesis, University of Illinois.

Zivi, S. M. 1964. "Estimation of steady-state steam void-fraction by means of the principle of minimum entropy production." *Transactions ASME, Journal of Heat Transfer*, Series C, Vol. 86, May, pp. 247-252.

Appendix A
Experimental Data

This appendix contains the void fraction data for all three of the test sections. For this section the units of G, the refrigerant mass flux, are given in $\frac{kg}{m^2 s}$, and q", the test section heat flux are given in $\frac{kW}{m^2}$. The average quality, X_{av}, is the average quality in the test section during operation and is in percent.

Table A.1 Experimental Data for 4.26 mm Smooth Tube

Refrigerant	G	X_{av}	q"	Void Fraction
R134a	200.00	10.000	0.0000	0.81370
R134a	200.00	30.000	0.0000	0.88420
R134a	200.00	80.000	0.0000	0.96450
R134a	500.00	10.000	0.0000	0.78620
R134a	500.00	30.000	0.0000	0.89520
R134a	500.00	80.000	0.0000	0.97950
R134a	200.00	14.420	3.0000	0.81740
R134a	200.00	34.420	3.0000	0.89530
R134a	200.00	84.420	3.0000	0.97090
R134a	500.00	11.770	3.0000	0.80610
R134a	500.00	31.770	3.0000	0.90630
R134a	500.00	81.770	3.0000	0.97830
R134a	200.00	24.750	10.000	0.85100
R134a	200.00	44.750	10.000	0.91260
R134a	500.00	15.900	10.000	0.85820
R134a	500.00	35.900	10.000	0.91250
R134a	500.00	5.0000	0.0000	0.74400
R134a	700.00	10.000	0.0000	0.76180
R134a	700.00	5.0000	0.0000	0.69950
R410A	200.00	10.000	0.0000	0.69590
R410A	200.00	30.000	0.0000	0.83850
R410A	200.00	80.000	0.0000	0.96250
R410A	500.00	10.000	0.0000	0.68200
R410A	500.00	30.000	0.0000	0.85200
R410A	200.00	13.700	3.0000	0.74770
R410A	200.00	33.700	3.0000	0.86100
R410A	200.00	83.700	3.0000	0.97400
R410A	500.00	11.480	3.0000	0.74850
R410A	500.00	31.480	3.0000	0.86650
R410A	200.00	22.330	10.000	0.77450
R410A	200.00	42.330	10.000	0.87050
R410A	500.00	14.930	10.000	0.73000
R410A	500.00	34.930	10.000	0.87270
R410A	700.00	5.0000	0.0000	0.57400
R410A	700.00	10.000	0.0000	0.67500
R410A	500.00	5.0000	0.0000	0.60050

Table A.2 Experimental Data for 7.25 mm Base Diameter Axially Grooved Tube

Refrigerant	G	X_{av}	q"	Void Fraction
R134a	200.00	10.000	0.0000	0.76000
R134a	200.00	30.000	0.0000	0.85970
R134a	200.00	80.000	0.0000	0.96440
R134a	500.00	10.000	0.0000	0.74800
R134a	500.00	30.000	0.0000	0.90430
R134a	75.000	10.000	0.0000	0.71500
R134a	75.000	30.000	0.0000	0.83640
R134a	75.000	80.000	0.0000	0.95570
R134a	200.00	14.560	3.0000	0.78400
R134a	200.00	34.560	3.0000	0.87220
R134a	200.00	84.560	3.0000	0.96820
R134a	500.00	11.820	3.0000	0.79460
R134a	500.00	31.820	3.0000	0.90980
R134a	75.000	22.160	3.0000	0.78110
R134a	75.000	42.160	3.0000	0.89080
R134a	200.00	25.200	10.000	0.83770
R134a	200.00	45.200	10.000	0.89410
R134a	500.00	16.080	10.000	0.80110
R134a	500.00	36.080	10.000	0.92750
R134a	75.000	50.540	10.000	0.93600
R410A	200.00	10.000	0.0000	0.63160
R410A	200.00	30.000	0.0000	0.80090
R410A	500.00	10.000	0.0000	0.65520
R410A	500.00	30.000	0.0000	0.82700
R410A	75.000	10.000	0.0000	0.62540
R410A	75.000	30.000	0.0000	0.75190
R410A	200.00	13.910	3.0000	0.68220
R410A	200.00	33.910	3.0000	0.82640
R410A	500.00	11.570	3.0000	0.68010
R410A	500.00	31.570	3.0000	0.84360
R410A	75.000	20.440	3.0000	0.71340
R410A	75.000	40.440	3.0000	0.83740
R410A	200.00	23.050	10.000	0.76530
R410A	200.00	43.050	10.000	0.85540
R410A	500.00	15.220	10.000	0.72970
R410A	500.00	35.220	10.000	0.85350
R410A	75.000	44.790	10.000	0.82690
R410A	75.000	64.790	10.000	0.95910
R410A	700.00	5.0000	0.0000	0.50000
R410A	700.00	6.1180	3.0000	0.59220
R410A	700.00	8.7280	10.000	0.67200

Table A.3 Experimental Data for 7.26 mm Base Diameter 18° Helically Grooved Tube

Refrigerant	G	X_{av}	q"	Void Fraction
R134a	75.000	10.000	0.0000	0.75235
R134a	75.000	21.050	3.0000	0.77625
R134a	75.000	46.850	10.000	0.90890
R134a	200.00	10.000	0.0000	0.74290
R134a	200.00	14.150	3.0000	0.79850
R134a	200.00	23.820	10.000	0.83820
R134a	200.00	30.000	0.0000	0.87110
R134a	200.00	34.150	3.0000	0.87055
R134a	200.00	43.820	10.000	0.90360
R134a	500.00	10.000	0.0000	0.74205
R134a	500.00	11.660	3.0000	0.77700
R134a	500.00	15.530	10.000	0.80925
R134a	500.00	30.000	0.0000	0.90640
R134a	500.00	31.660	3.0000	0.91100
R134a	500.00	35.330	10.000	0.92320
R134a	700.00	5.0000	0.0000	0.68430
R410A	75.000	10.000	0.0000	0.67530
R410A	75.000	19.240	3.0000	0.72845
R410A	75.000	40.800	10.000	0.81690
R410A	200.00	10.000	0.0000	0.63300
R410A	200.00	13.460	3.0000	0.73645
R410A	200.00	21.550	10.000	0.75600
R410A	200.00	30.000	0.0000	0.82660
R410A	200.00	33.460	3.0000	0.82950
R410A	200.00	41.550	10.000	0.86790
R410A	500.00	10.000	0.0000	0.70145
R410A	500.00	11.390	3.0000	0.72750
R410A	500.00	14.620	10.000	0.72455
R410A	500.00	30.000	0.0000	0.85740
R410A	500.00	31.390	3.0000	0.83040
R410A	500.00	34.620	10.000	0.85165
R410A	700.00	5.0000	0.0000	0.54195

Appendix B
Additional Figures for 4.26 mm Smooth Tube

This Appendix contains the graphical representation of the experimental data. Graphs here include void fraction versus average quality for R134a and R410A, as well as the predictions of the ten correlations that were compared to the data.

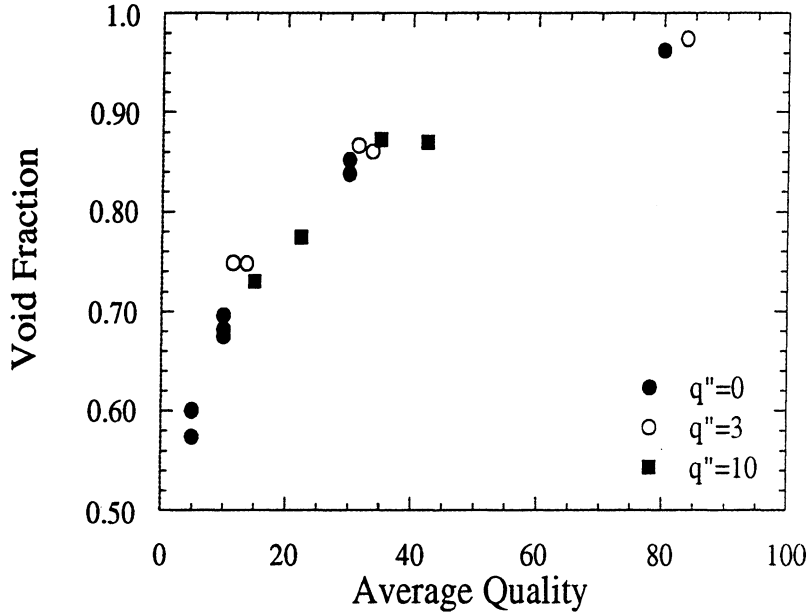

Figure B.1 Void Fraction vs. Average Quality for R410A to show heat flux effect (heat flux in $\frac{kW}{m^2}$)

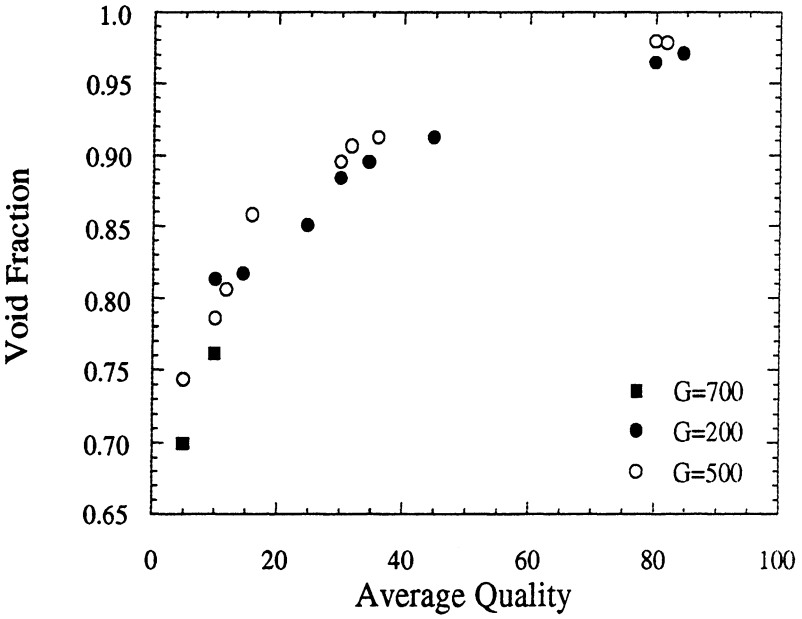

Figure B.2 Void Fraction vs. Average Quality for R134a to show mass flux effect (mass flux in $\frac{kg}{m^2 s}$)

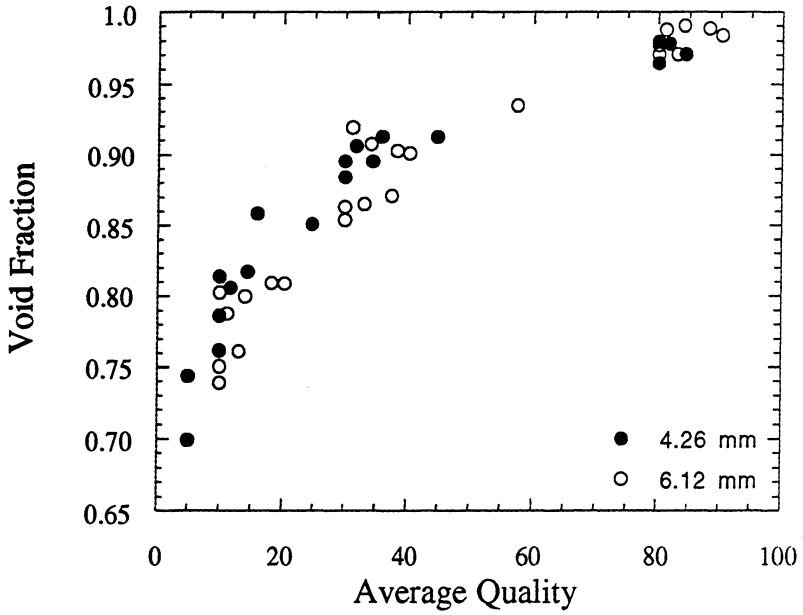

Figure B.3 Void Fraction vs. Average Quality for R134a to show diameter effect

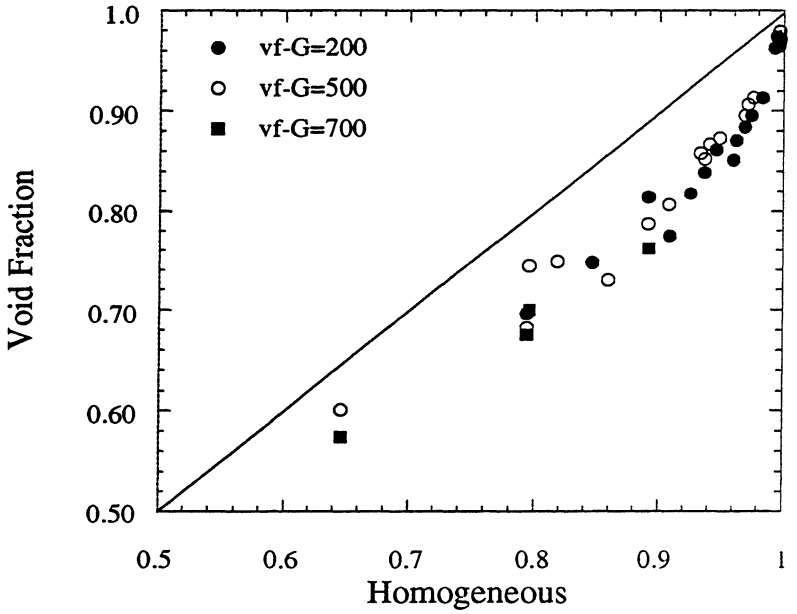

Figure B.4 Void Fraction vs. Homogeneous Correlation

(mass flux in $\frac{kg}{m^2 s}$)

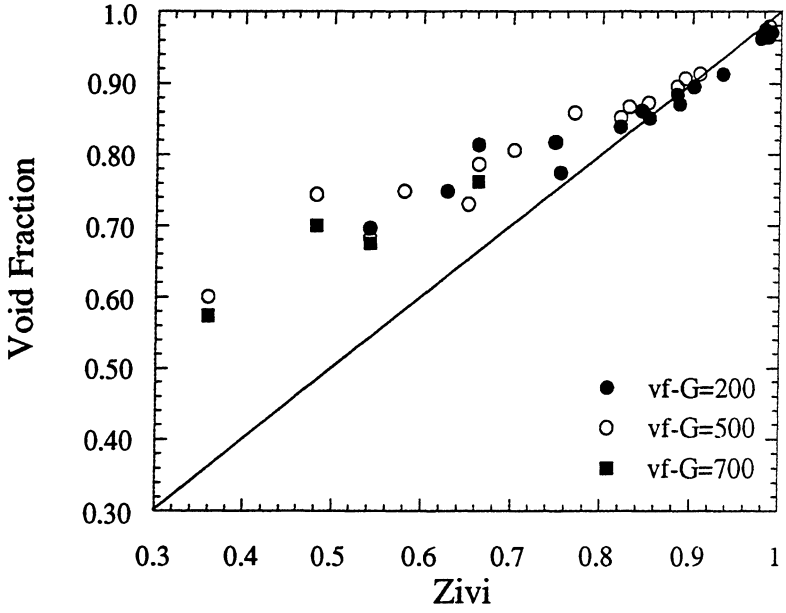

Figure B.5 Void Fraction vs. Zivi Correlation

(mass flux in $\frac{kg}{m^2 s}$)

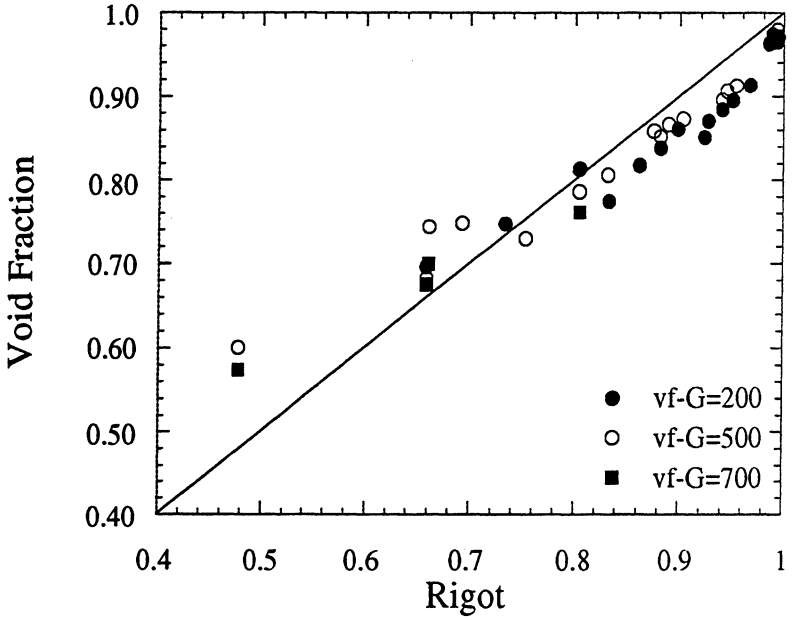

Figure B.6 Void Fraction vs. Rigot Correlation

(mass flux in $\frac{kg}{m^2 s}$)

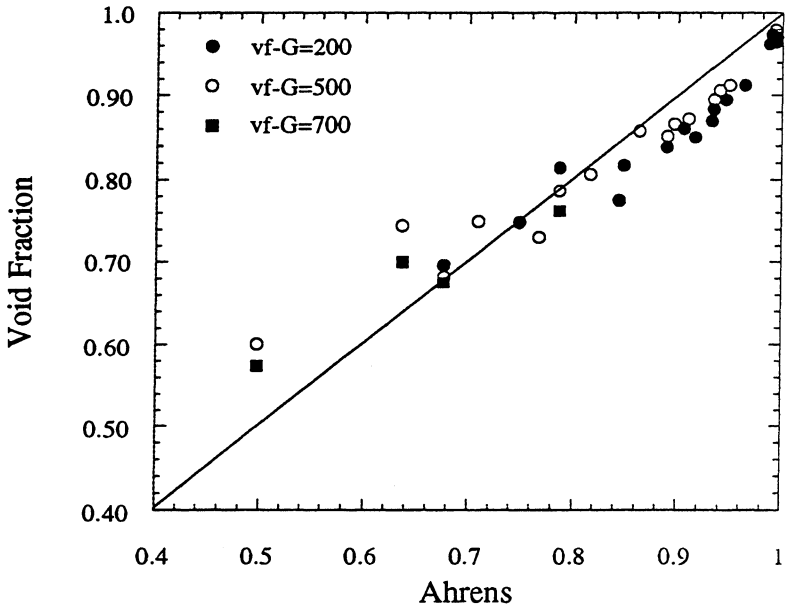

Figure B.7 Void Fraction vs. Ahrens Correlation

(mass flux in $\frac{kg}{m^2 s}$)

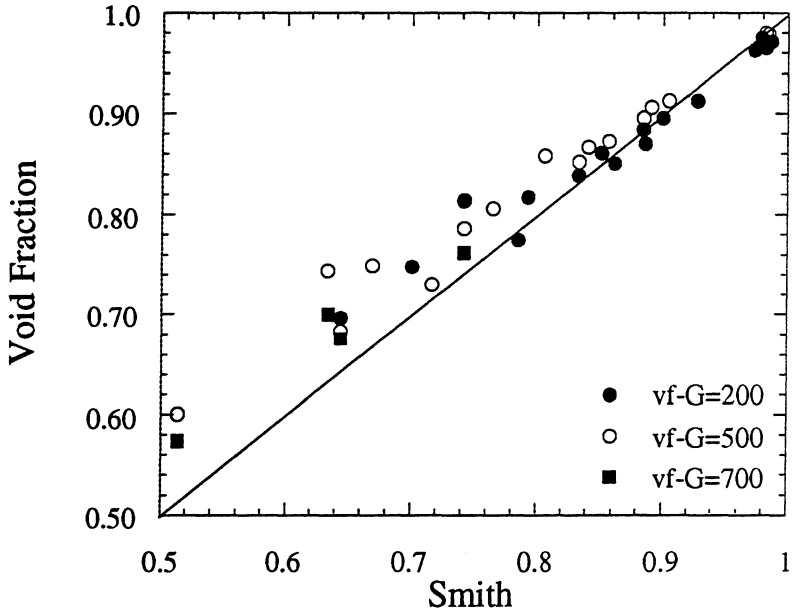

Figure B.8 Void Fraction vs. Smith Correlation

(mass flux in $\frac{kg}{m^2 s}$)

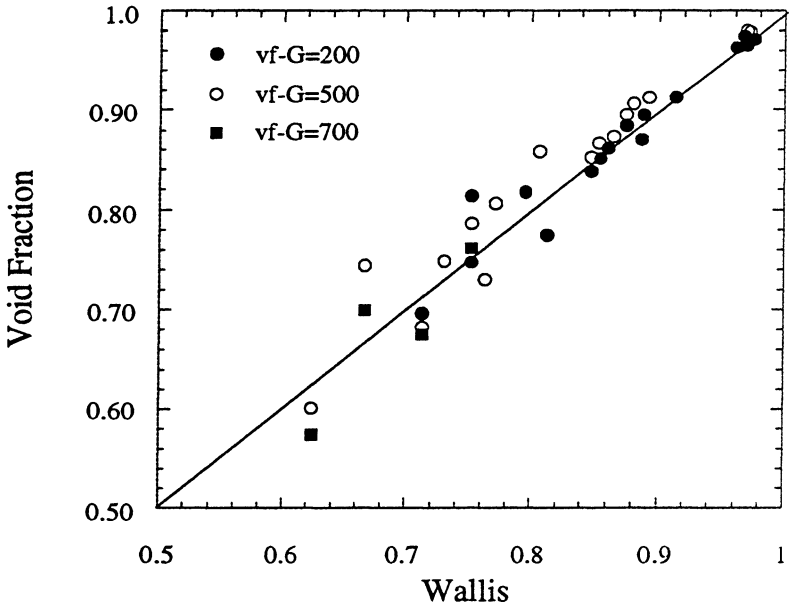

Figure B.9 Void Fraction vs. Wallis Correlation

(mass flux in $\frac{kg}{m^2 s}$)

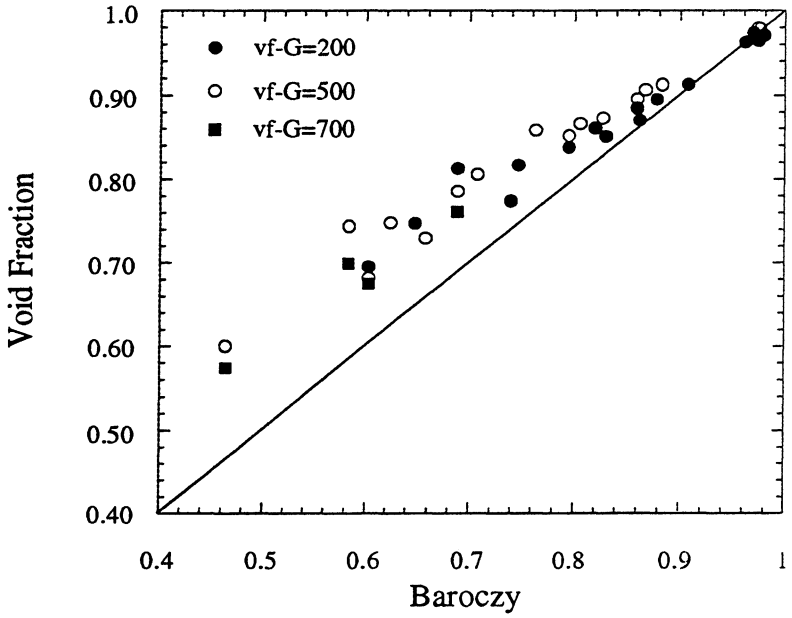

Figure B.10 Void Fraction vs. Baroczy Correlation

(mass flux in $\frac{kg}{m^2 s}$)

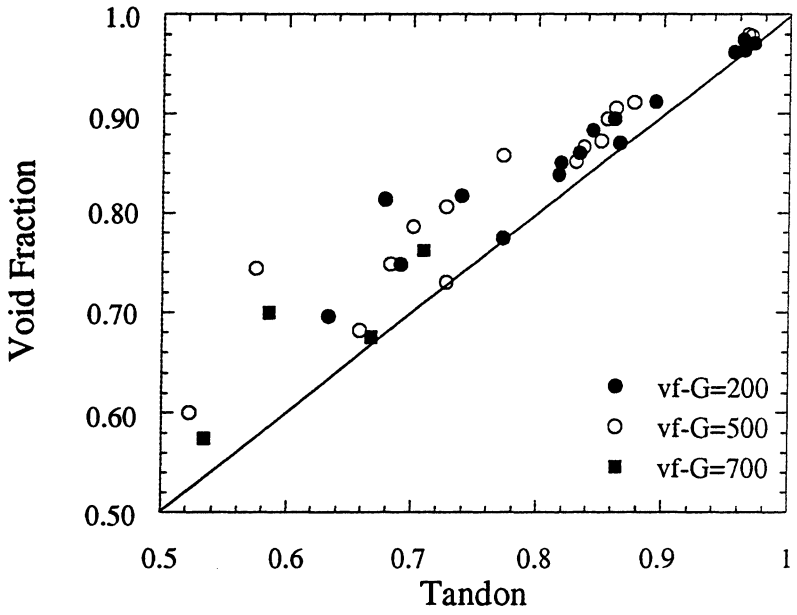

Figure B.11 Void Fraction vs. Tandon Correlation

(mass flux in $\frac{kg}{m^2 s}$)

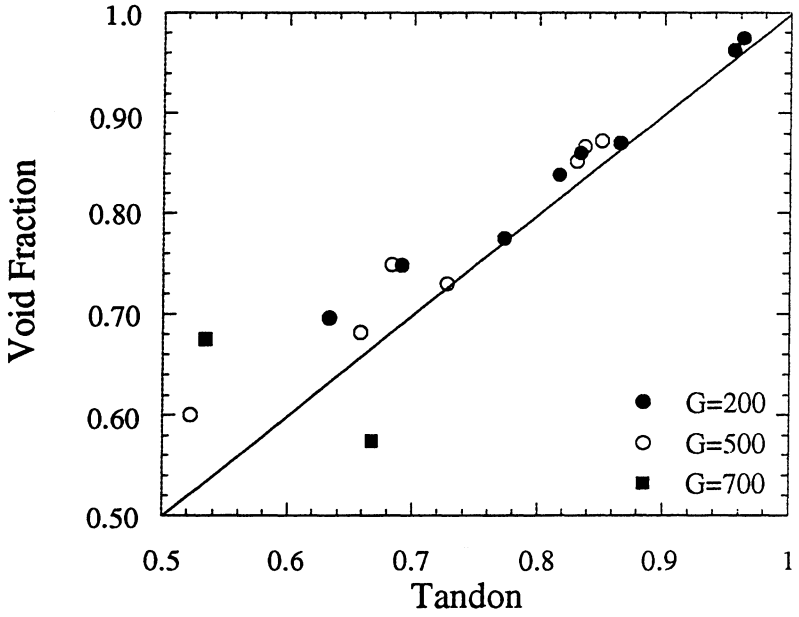

Figure B.12 Void Fraction vs. Tandon Correlation for R410A

(mass flux in $\frac{kg}{m^2 s}$)

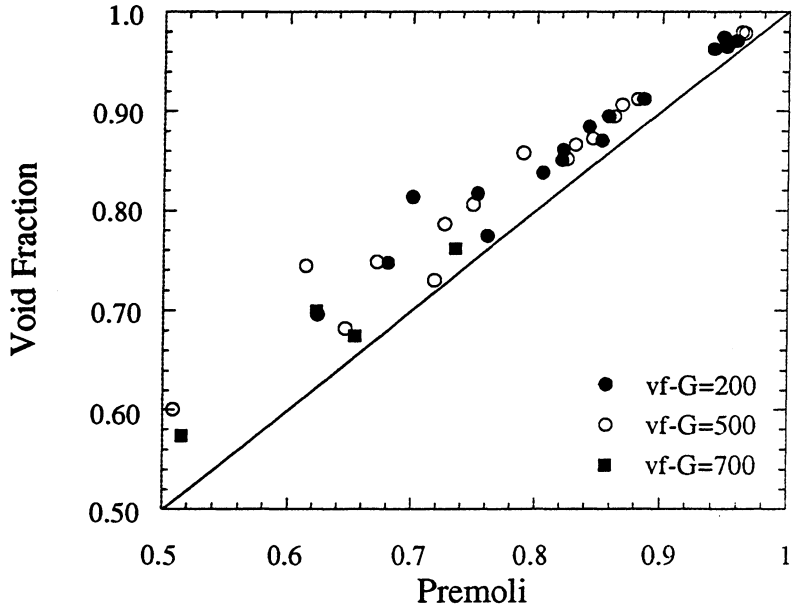

Figure B.13 Void Fraction vs. Premoli Correlation

(mass flux in $\frac{kg}{m^2 s}$)

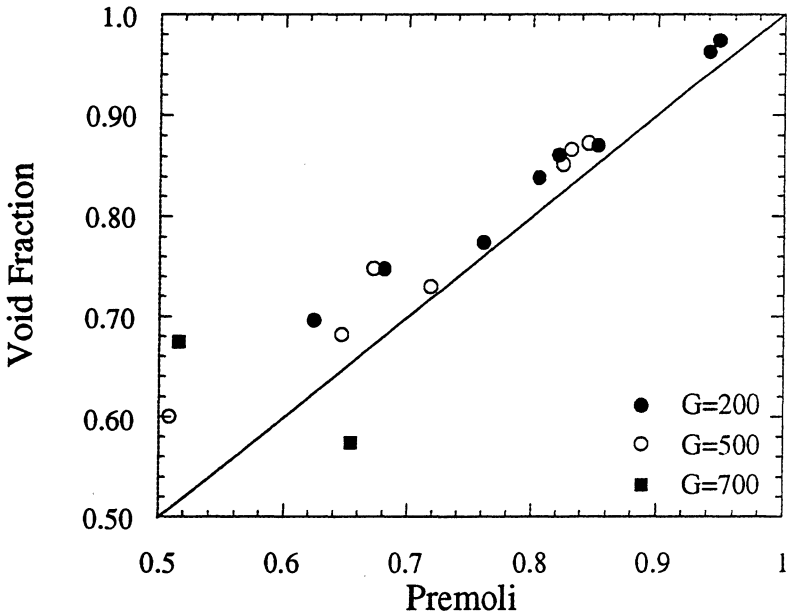

Figure B.14 Void Fraction vs. Premoli Correlation for R410A

(mass flux in $\frac{kg}{m^2 s}$)

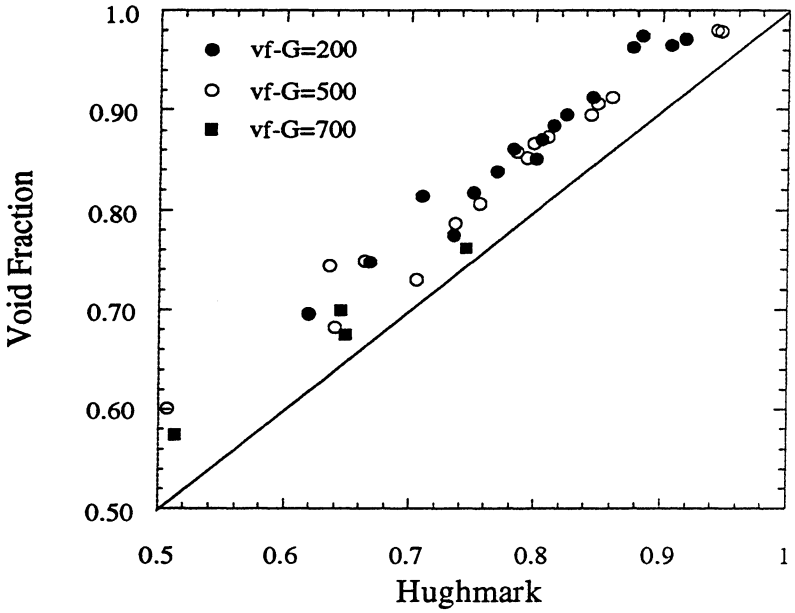

Figure B.15 Void Fraction vs. Hughmark Correlation

(mass flux in $\frac{kg}{m^2 s}$)

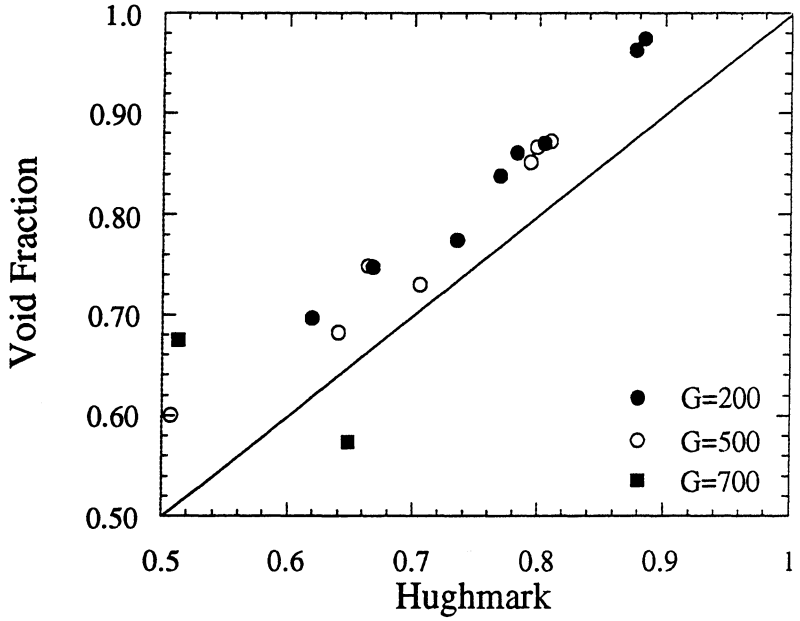

Figure B.16 Void Fraction vs. Hughmark Correlation for R410A

(mass flux in $\frac{kg}{m^2 s}$)

Appendix C
Additional Figures for 7.25 mm Base Diameter Axially Grooved Tube

This Appendix contains the graphical representation of the experimental data. Graphs here include void fraction versus average quality for R134a and R410A, as well as the predictions of the ten correlations that were compared to the data.

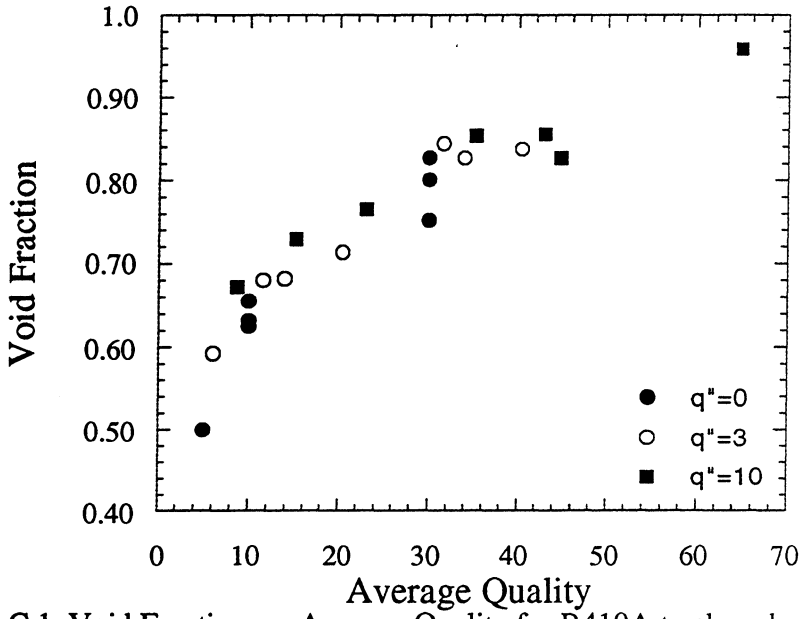

Figure C.1 Void Fraction vs. Average Quality for R410A to show heat flux effect

(heat flux in $\frac{kW}{m^2}$)

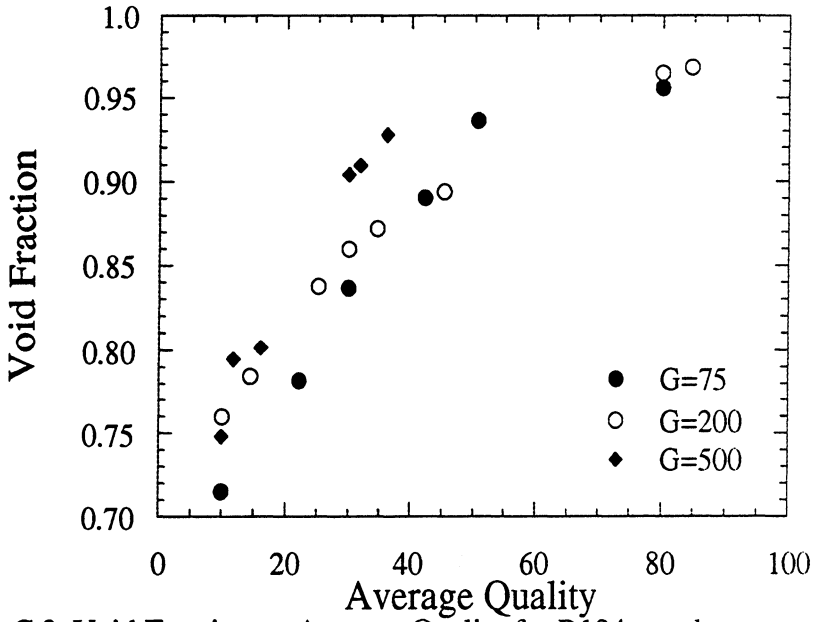

Figure C.2 Void Fraction vs Average Quality for R134a to show mass flux effect

(mass flux in $\frac{kg}{m^2 s}$)

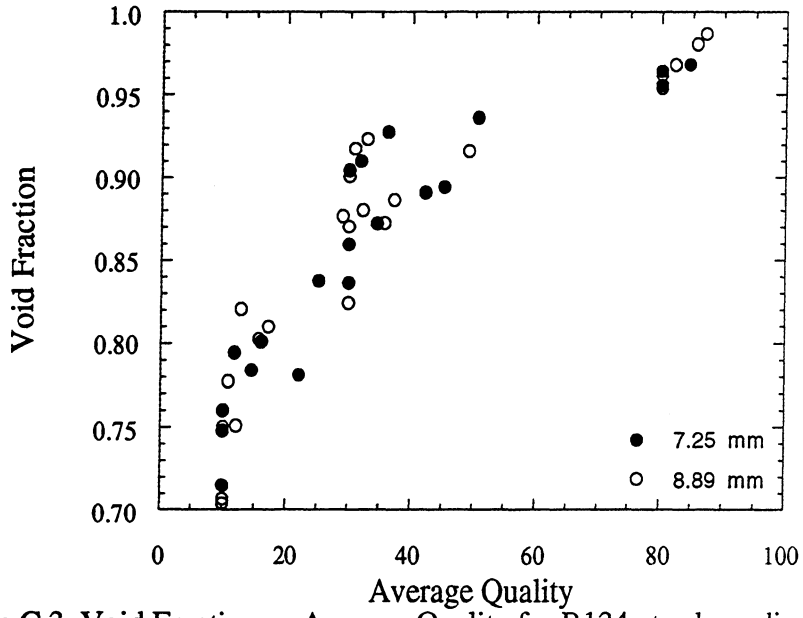

Figure C.3 Void Fraction vs Average Quality for R134a to show diameter effect

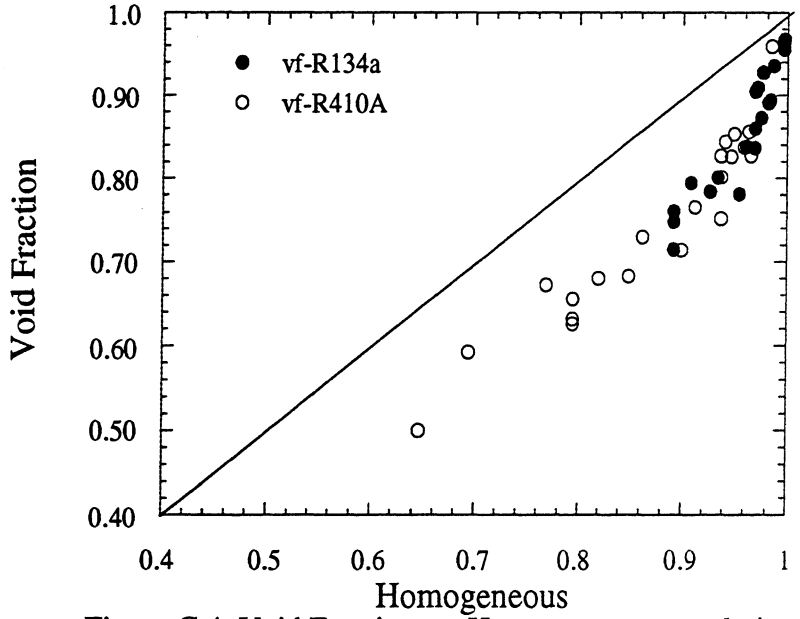

Figure C.4 Void Fraction vs. Homogeneous correlation

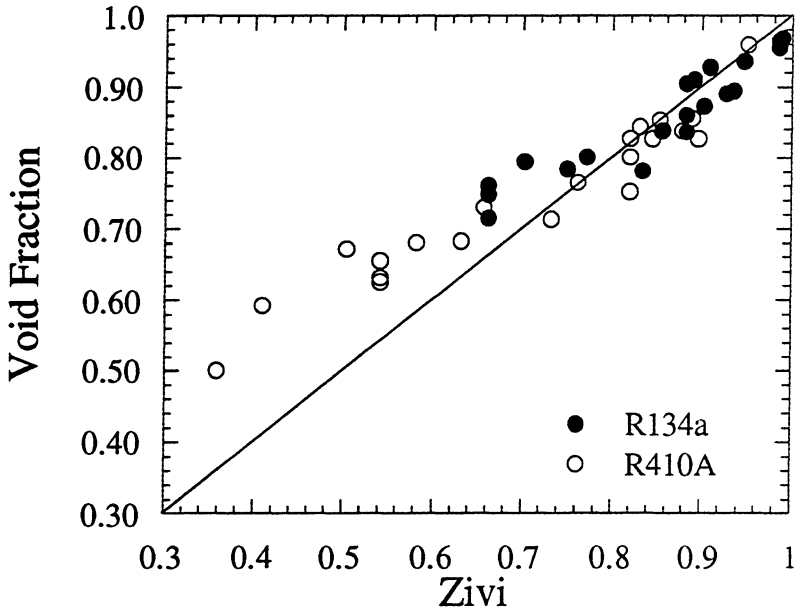

Figure C.5 Void Fraction vs. Zivi correlation

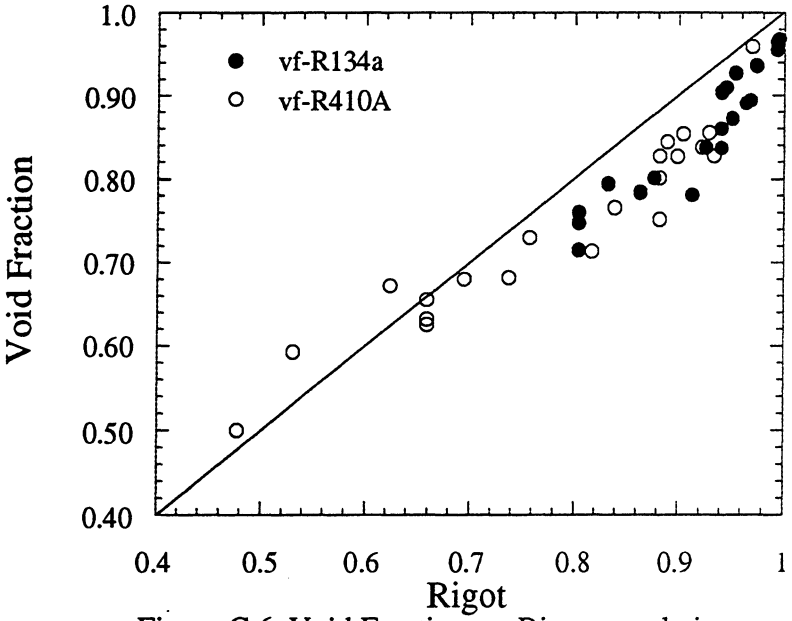

Figure C.6 Void Fraction vs. Rigot correlation

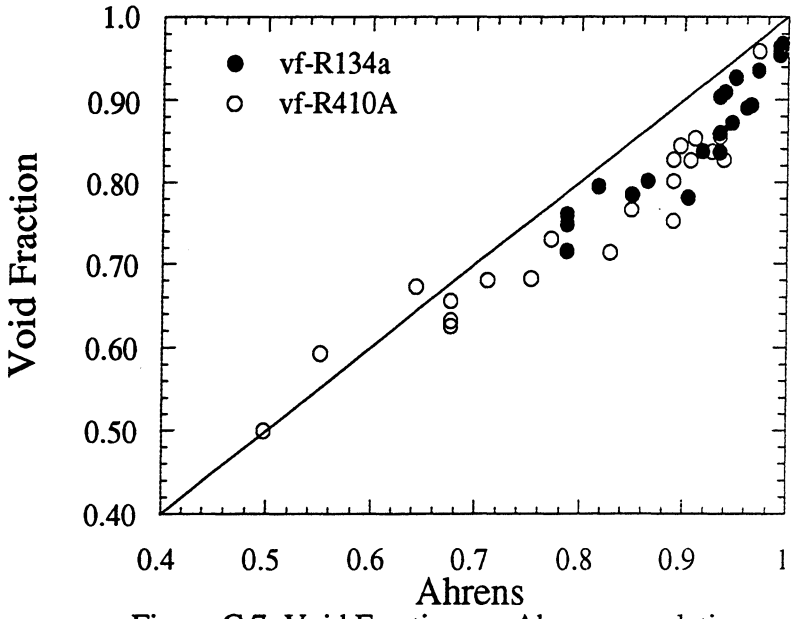

Figure C.7 Void Fraction vs. Ahrens correlation

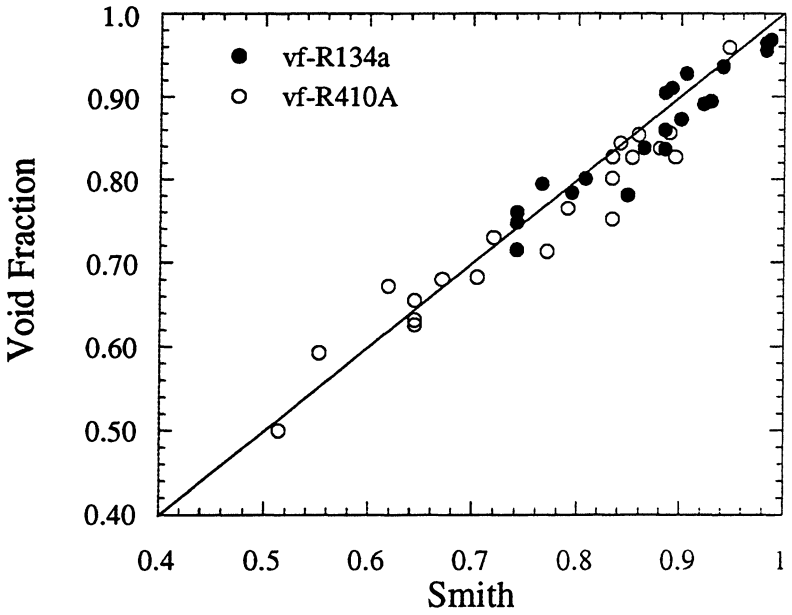

Figure C.8 Void Fraction vs. Smith correlation

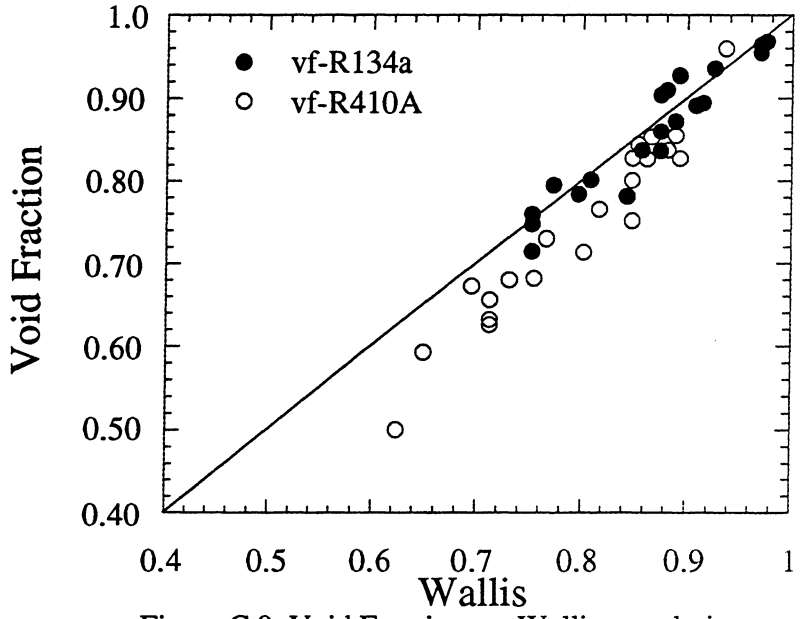

Figure C.9 Void Fraction vs. Wallis correlation

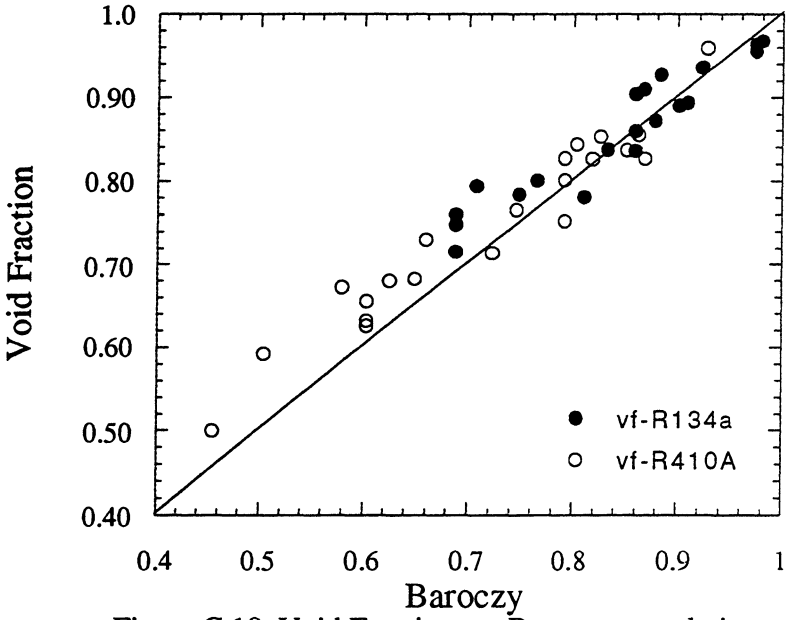

Figure C.10 Void Fraction vs. Baroczy correlation

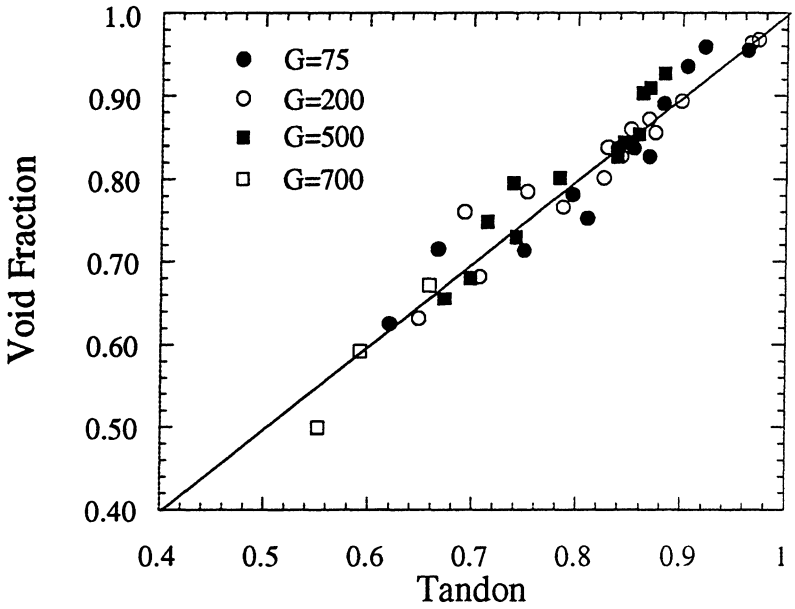

Figure C.11 Void Fraction vs. Tandon correlation

(mass flux in $\frac{kg}{m^2 s}$)

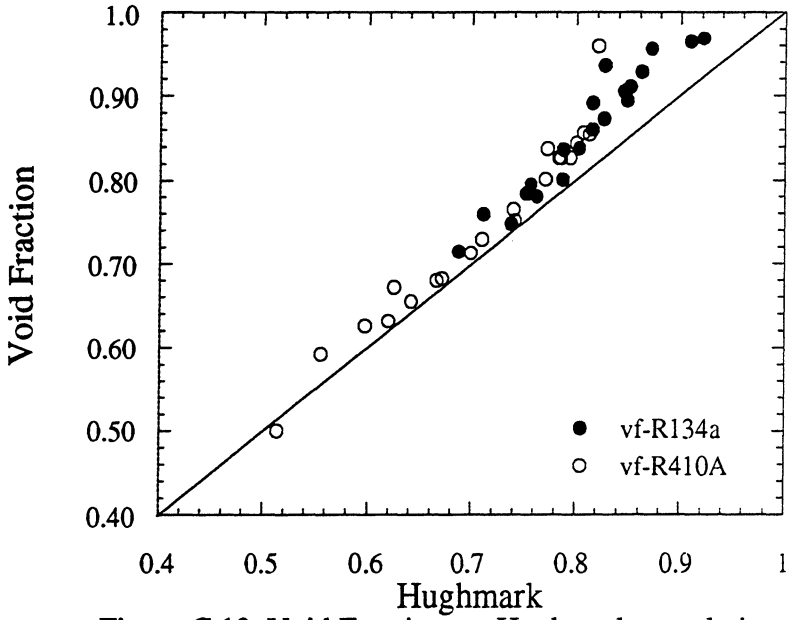

Figure C.12 Void Fraction vs. Hughmark correlation

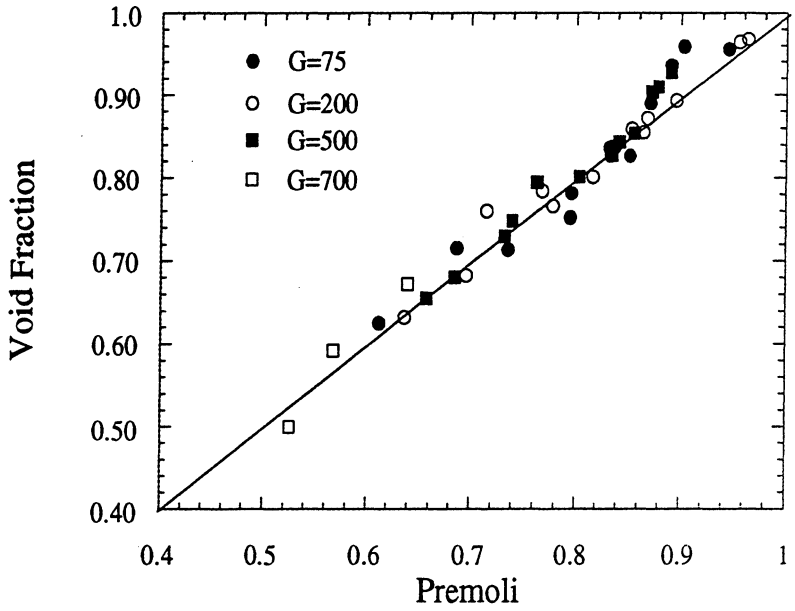

Figure C.13 Void Fraction vs. Premoli correlation

(mass flux in $\frac{kg}{m^2 s}$)

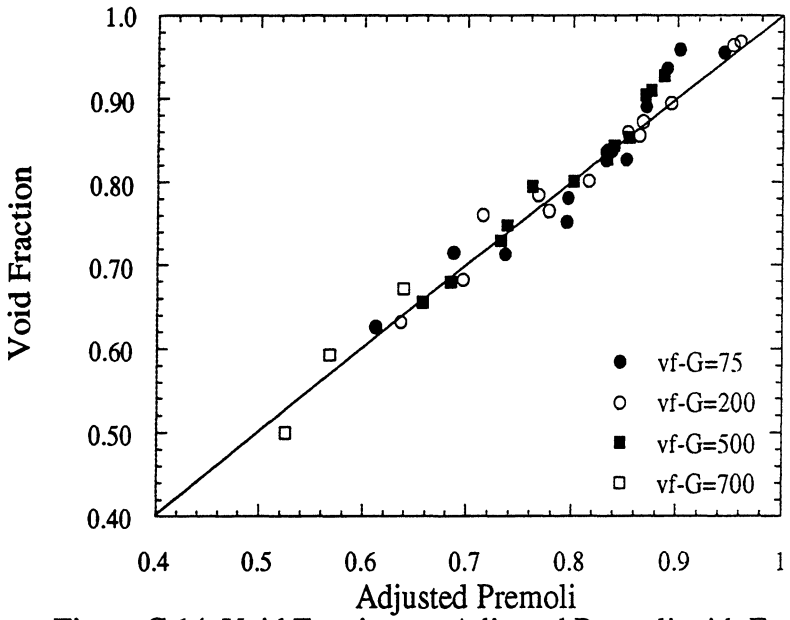

Figure C.14 Void Fraction vs. Adjusted Premoli with F_2=0

(mass flux in $\frac{kg}{m^2 s}$)

Appendix D
Additional Figures for 7.26 mm Base Diameter 18° Helically Grooved Tube

This Appendix contains the graphical representation of the experimental data. Graphs here include void fraction versus average quality for R134a and R410A, as well as the predictions of the ten correlations that were compared to the data.

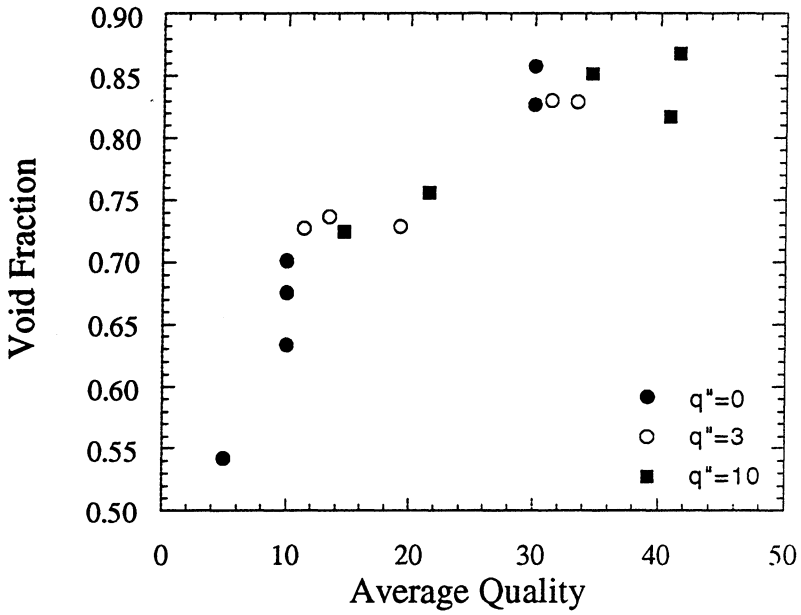

Figure D.1 Void Fraction vs. Average Quality for R410A to show heat flux effect (heat flux in $\frac{kW}{m^2}$)

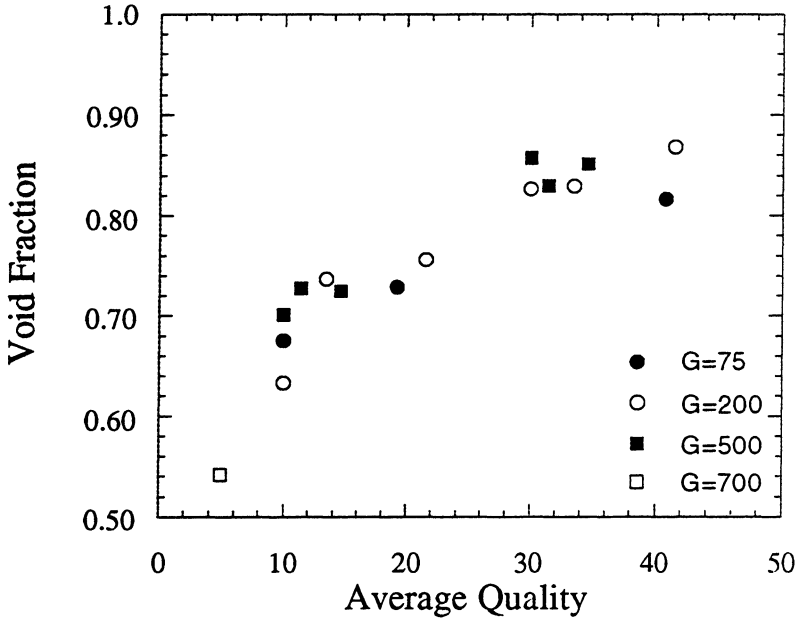

Figure D.2 Void Fraction vs. Average Quality for R410A to show mass flux effect (mass flux in $\frac{kg}{m^2 s}$)

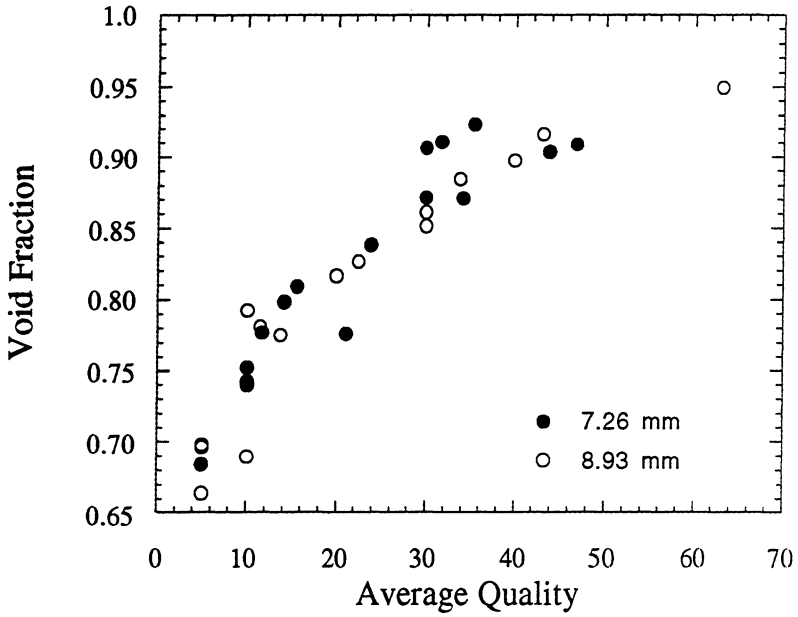

Figure D.3 Void Fraction vs. Average Quality for R134a to show diameter effect

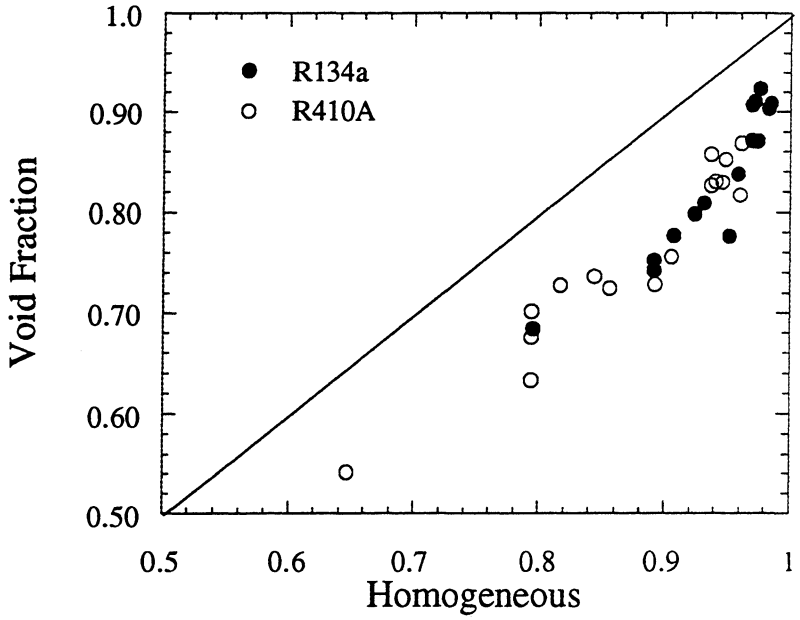

Figure D.4 Void Fraction vs. Homogeneous correlation

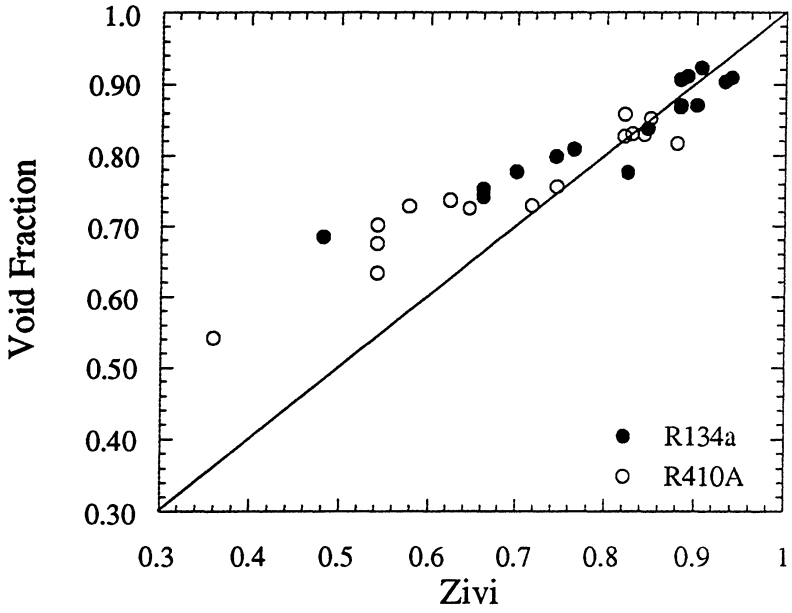

Figure D.5 Void Fraction vs. Zivi correlation

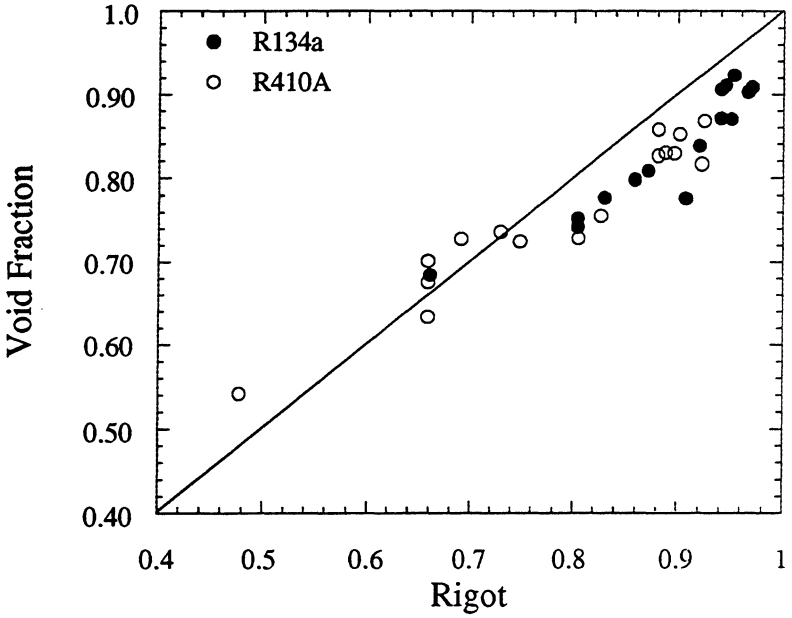

Figure D.6 Void Fraction vs. Rigot correlation

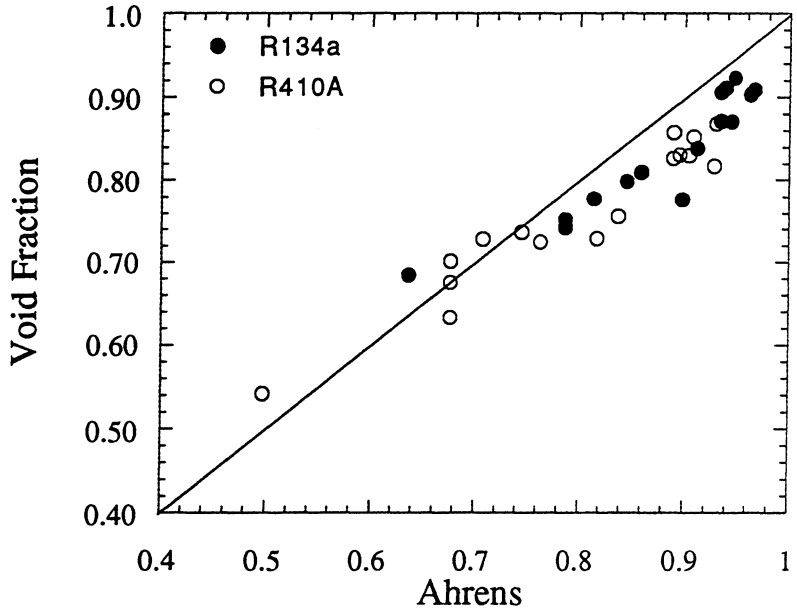

Figure D.7 Void Fraction vs. Ahrens correlation

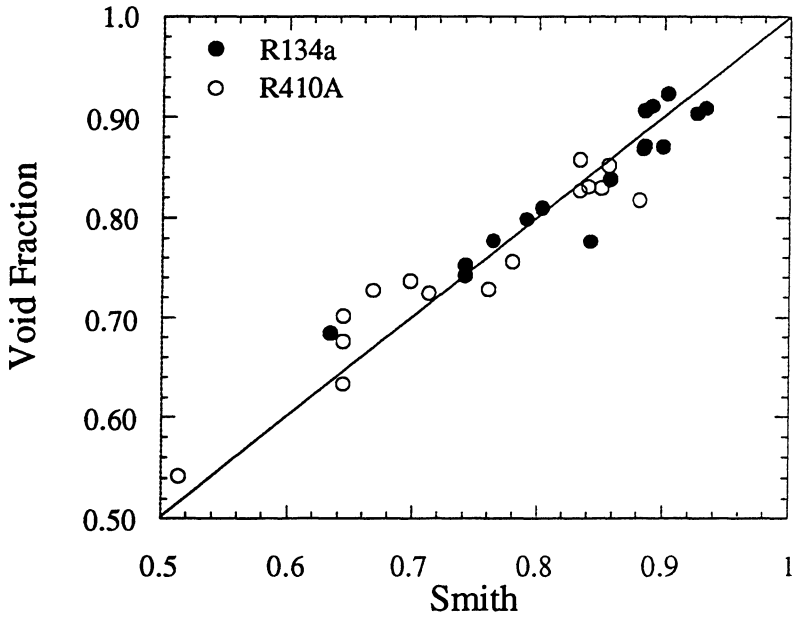

Figure D.8 Void Fraction vs. Smith correlation

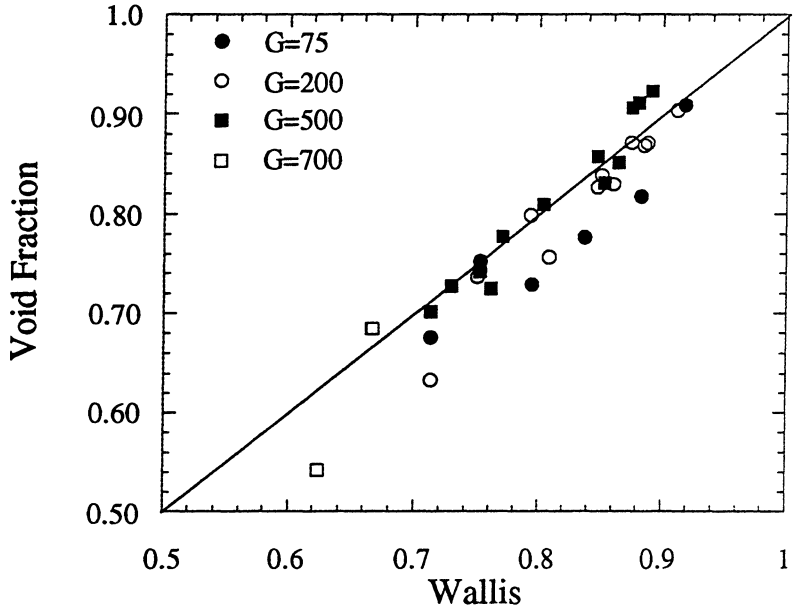

Figure D.9 Void Fraction vs. Wallis correlation

(mass flux in $\frac{kg}{m^2 s}$)

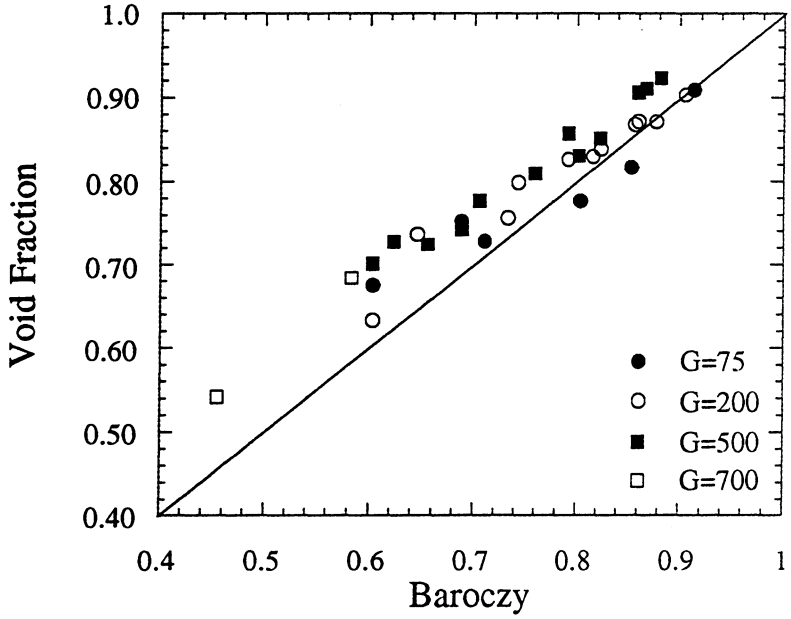

Figure D.10 Void Fraction vs. Baroczy correlation

(mass flux in $\frac{kg}{m^2 s}$)

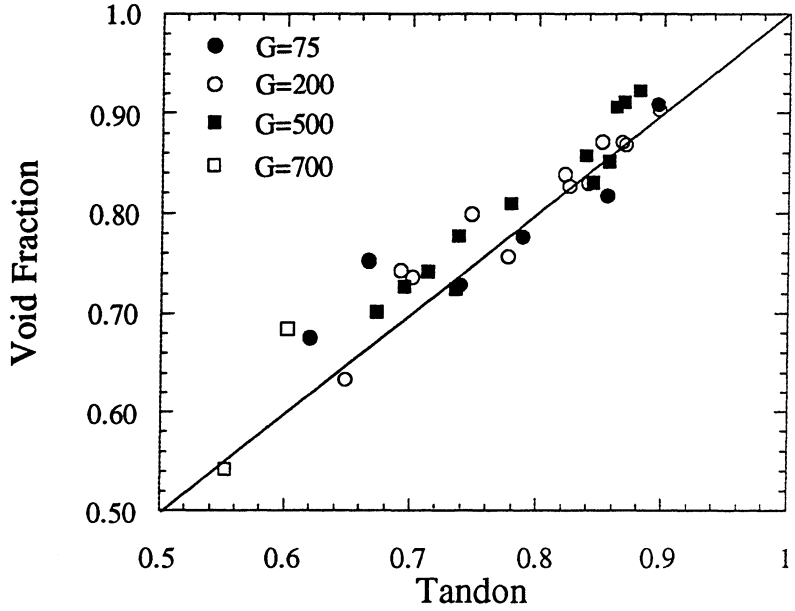

Figure D.11 Void Fraction vs. Tandon correlation

(mass flux in $\frac{kg}{m^2 s}$)

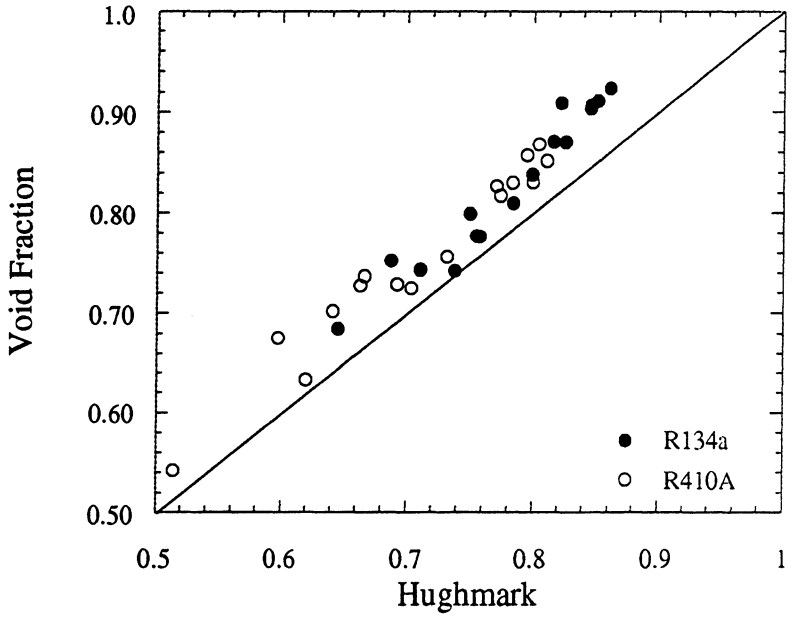

Figure D.12 Void Fraction vs. Hughmark correlation

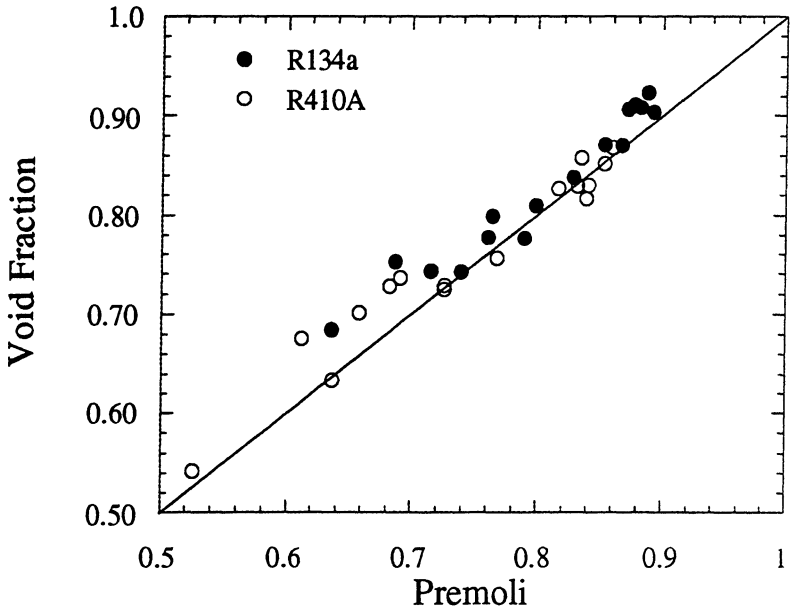

Figure D.13 Void Fraction vs. Premoli correlation

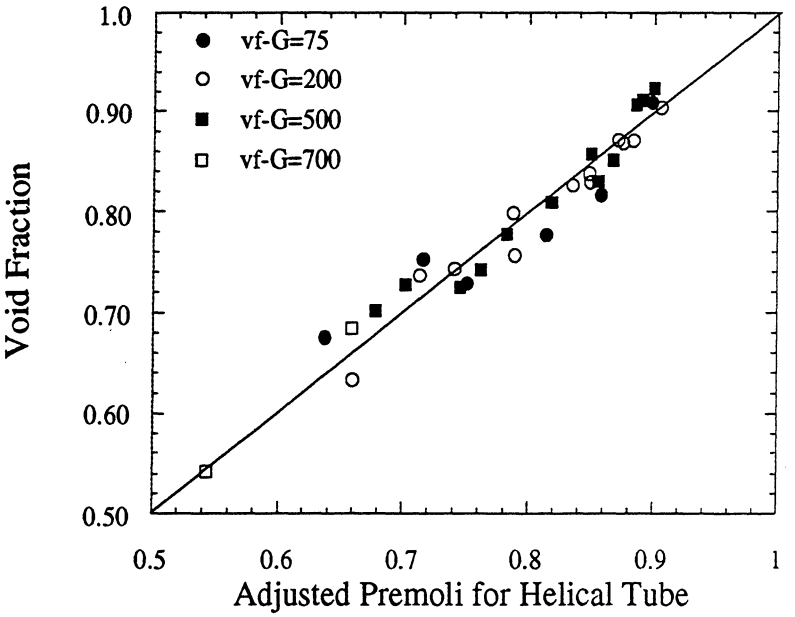

Figure D.14 Void Fraction vs. Premoli Correlation with adjusted F_1 equation

(mass flux in $\frac{kg}{m^2 s}$)